FINAL REPORT

Project Title: Nye County Ventilation Modeling

Author and PI: George Danko, Ph.D.

Report Period: April 1, 2003-March 31, 2004

Date of Report: May 4, 2004

Description of Activities

1. MULTIFLUX3.0 (MF3.0) was configured for ventilation simulations for the most recent conceptual DOE repository design in 2003. Five different air flow resistances were assumed, including the one that most likely would be the representative value for Yucca Mountain based on USGS permeability measurements.
2. Ventilation simulations were conducted with the MF3.0 model and software. The climate model was carefully selected from literature, representing the most recent results used for Yucca Mountain. Temperature and relative humidity variations were calculated along a representative emplacement drift for a period of 12,500 years.
3. A baseline simulation was also conducted assuming pre-closure ventilation but no air movement during the post-closure time period. The temperature field was compared with those obtained at five different air infiltrations according to Activities 1 and 2. It was concluded that the temperature field is robust, changing very little (within a few ^{o}C) with respect to the temperatures obtained with five different rates of air infiltration.
4. Three papers were published summarizing the results. The papers were submitted for technical review as well as for providing information to Nye County experts Drs. D. Hammermeister and J. Walton.
5. The hydrologic conceptual model of the repository was refined based on the simulation results. A draft description of the model was sent to Nye County experts Drs. D. Hammermeister and J. Walton.
6. The model, due to the robustness of the temperature field, appears to be insensitive to flow reversals. This means that very similar relative humidity and condensate formation may be expected at the exit section of the drift if air infiltrates through the emplacement area from either direction. The effects of short-time, seasonal or weekly reversals, as well as barometric pressure pumping will be studied in FY 2004 as follow-up exercises.
7. The results have been discussed with Nye County experts Drs. D. Hammermeister and J. Walton
8. All NWTRB meetings held during the reported period was attended.

Appendices.

References of three papers (slightly re-formatted from the original format) and a NWTRB presentation:

[1] Danko, G., Bahrami, D., 2004. “Coupled, Multi-Scale Thermohydrologic-Ventilation Modeling with MULTIFLUX”
[2] Danko, G., 2004. “Numerical Transport Code Functionalization Procedure and Software Functions.”
[3] Danko, G., Bahrami, D., 2004. “Heat and Moisture Flow Simulation with MULTIFLUX.”
[4] Danko, G., Bahrami, D., Walton, J., (presenter), 2004. “Nuclear Waste Technical Review Board: Status of Nye County Ventilation Studies”

Proceedings of ASME
Heat Transfer/Fluid Engineering
July 11-15, 2004, Charlotte, North Carolina, USA

HT-FED2004-56048

HEAT AND MOISTURE FLOW SIMULATION WITH MULTIFLUX

G. Danko
University of Nevada, Reno
Email: Danko@unr.edu
(775) 784-4284

D. Bahrami
University of Nevada, Reno
Email: Davood@unr.nevada.edu
(775) 784-4210

ABSTRACT

The paper describes the results of a ventilation study involving subsurface heat and moisture flow at Yucca Mountain (YM), Nevada. MULTIFLUX[1] (MF), a fully-coupled, hydrothermal-ventilation model and software code is used to model the flow of heat, moisture, and air in a subsurface airway within the conceptual, high-level nuclear waste repository proposed to be built at YM. The hydrothermal-ventilation/heat flow model and software MF is a universal coupler that connects the heat and moisture transport calculations in two different domains: (1) the rockmass, with a NUFT[2]-based NTCF[3] model, and (2) the airway with the heat-generating nuclear waste packages, using a CFD[4] model. Temperature, relative humidity and water condensate variations are analyzed in the emplacement drift, assuming air movement, to determine the conditions of the psychometric corrosion environment in the emplacement area. The calculation results show condensate formation in the cold drift section, and are found to be sensitive to choosing from two different CFD model configurations.

Keywords: ventilation, heat, moisture, MULTIFLUX, cold-trap condensates, Yucca Mountain

INTRODUCTION

Ventilation calculations are part of the thermal and hydrologic studies necessary for supporting the design of a high-level nuclear waste repository. In general, there are three main purposes for ventilation calculations: (1) to predict temperature variation with time in the emplacement airways, called drifts, during the pre-closure time period of construction and waste emplacement; (2) to determine the initial conditions, both in rockmass temperature and humidity distributions, for the thermohydrologic analysis for the post-closure time period; and (3) to analyze the evolution of the temperature, humidity and potential water condensate distributions with the effect of air infiltration through the repository system during the most critical, first few thousands of years of the post-closure time period. A complete ventilation analysis, directed at the three main purposes, was successfully completed using the coupled thermohydrologic-ventilation model and software MF, for a conceptual repository design at YM [1,2].

[1] MULTIFLUX is developed at the University of Nevada, Reno (UNR).
[2] NUFT (Non-equilibrium, saturated-Unsaturated Flow and Transport model) is developed at the Lawrence Livermore National Laboratory.
[3] Numerical Transport Code Functionalization, a MULTIFLUX function.
[4] Simple Computaional Fluid Dynamics sub-models are built-in functions in MULTIFLUX

DESCRIPTION OF THE THERMOHYDROLOGIC VENTILATION MODEL

The Integrated Pre- and Post-Closure Task

Temperature and relative humidity variations are analyzed from the beginning of waste emplacement for a 5,000-year period that includes two distinct thermal cycles, one during the pre-closure, and one during the post-closure time periods. The following ventilation conditions are specified:

- The drift is mechanically ventilated with a forced, constant airflow rate of 15 m^3/s for 50 years, using fan(s),
- With the access shafts and connecting tunnels backfilled and sealed, the emplacement drifts are exposed to natural air infiltration during post-closure through the fracture system of YM until the end of the study time period. It is assumed that the emplacement drifts are not backfilled, and that the gradual collapse of the drifts over time will not prevent the slow flow of air through the drifts in axial direction.

The Conceptual Repository Arrangement and Model

The arrangement follows the conceptual design developed by the US Department of Energy (DOE) [3] using five emplacement panels at YM, shown in Fig. 1. One emplacement drift at the center location of Panel 2, previously referred to as Panel 5 in [4], is selected for the present analysis. Panel 2 is surrounded by unheated edges and, therefore, will develop a temperature field colder around the edges than in the center.

An airflow across such a temperature distribution in any direction may give rise to moisture condensation along the relatively cold exit edge sections. This edge-cooling effect phenomenon will affect all the panels shown in Fig. 1, but Panel 2 is selected for modeling simplicity.

A post-closure airflow in the drift in any direction may develop since both ends of each drift are connected to the atmosphere through the natural fracture system at YM. A small airflow may not affect the temperature field significantly; however, it may carry heat-driven moisture from the relatively hot, middle section of the emplacement drift toward the cooler exit section. Under certain conditions, condensation may occur, generating liquid-phase water in the emplacement area. The thermohydrologic model configured in MF includes model-elements that describe the large-scale air movement and related psychrometric processes in the in the emplacement drift.

In a previous study [4], the effect of variation in air mass flow rate was studied. The likely air infiltration rate was determined from the balancing iterations equating the buoyancy pressure driving force with the airflow pressure loss in each emplacement drift. The same infiltration flow rate was used in the present study.

The geometry of the rockmass surrounding the center drift in Panel 2 is shown in Fig. 3. Two peripheral drifts located perpendicular to emplacement drifts act as manifolds to distribute and collect airflows for the emplacement drifts in Panel 2. The two vertical shafts, an intake and an exhaust, are used to connect the peripheral drifts to the atmosphere for pre-closure ventilation, also shown in Fig. 3. The peripheral drifts and the shafts, however, are assumed to be backfilled and completely sealed during the assumed repository closure at year 50.

THE MODELS OF THE ROCK DOMAIN

The heat and moisture flow models of the rock domain are generated in MF using NUFT [5]. The geometrical domain, shown in Fig. 3, is simplified for the NUFT runs for reducing the computational capacity and runtime. First, it is halved by the vertical symmetry plane along the drift centerline. Second, the rockmass is further halved along the length of the drift. The symmetry assumed between i=4 and i=5, bounded with an adiabatic surface, divides the entire rock domain into two mirrored halves, an entrance and an exit drift section area. These simplifications reduce the computational rock domain to a quarter of that in Fig. 3, however, two consecutive NUFT models are needed to deal with asymmetries. The reduced rock cell with its internal grids is shown in Fig. 4. Each NUFT domain includes 4 rock cells along the drift and another 4 cells in the edge regime, all fully connected regarding heat and moisture flows. The number of nodes in each three-dimensional (3D) NUFT domain is 15x75x8, providing adequate discretization and acceptable grid independence. The grid in the x and z direction is identical to the two-dimensional discretization that was applied and verified in the AMR Rev01D work conducted by DOE [6].

The entire drift is surrounded by 4 sections in the first, and 4 sections in the second NUFT rock domain, giving 8 3D mountain-scale cells (i=1...8). The plane of symmetry is an approximation that is included in the rock model but not in the model of the airway. It results in only a small model error while reducing the computer memory requirements by half.

The numerical model assumes a porous, wet, but unsaturated rock formation in which both heat and moisture transport are present and affect the thermal and psychrometric waste container environment. The rock properties with dual-porosity elements in NUFT 3.0s were used identical to those applied by BSC [6] for a representative stratigraphic block at YM.

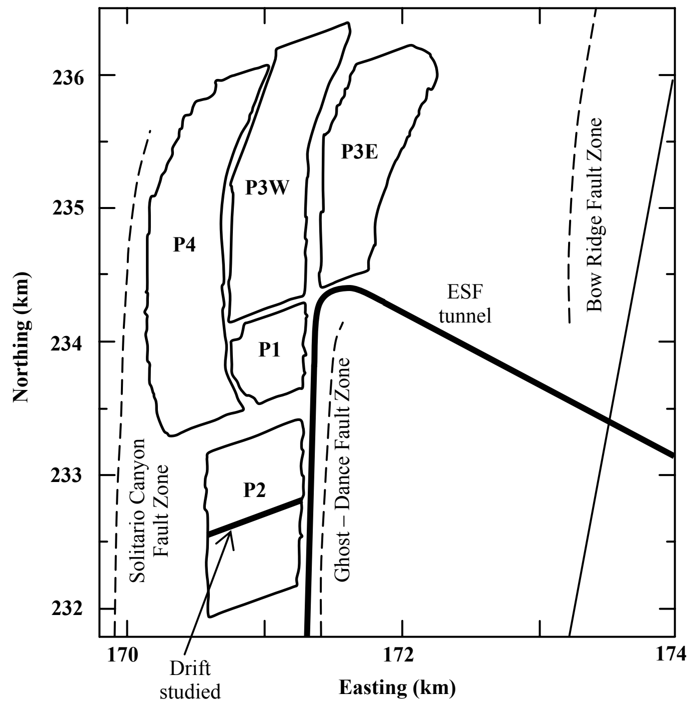

Figure 1. Plan of conceptual emplacement panels at Yucca Mountain (After Harrington [3]).

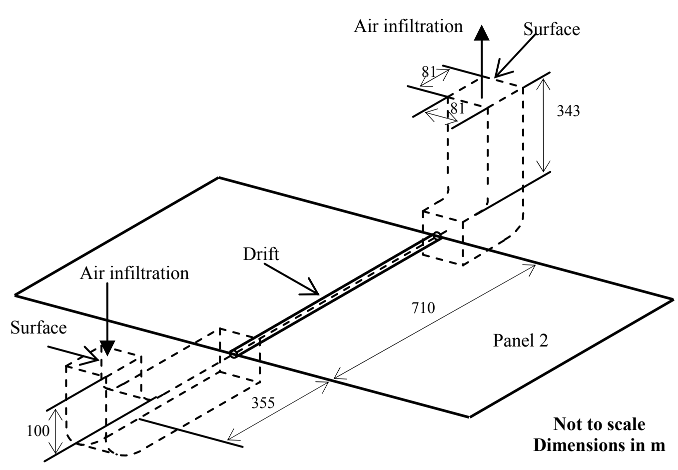

Figure 2. Conceptual model domain for natural air infiltration

Initial and boundary conditions

The atmospheric climate boundary conditions on the surface were varied according to the modern-time, monsoon, and glacial-transition cycles with time. The known, constant virgin rock temperature and 100% saturation were applied at the bottom of the rock domain, representing the water table. On the other outside vertical planes, the rock domain is assumed to be adiabatic. Boundary conditions on the drift surface are defined and discussed later in the paper when describing the NTCF rock model.

The temperature and moisture saturation initial conditions in the rockmass at the time of waste emplacement were initialized by simulating 10 complete climate cycles of 74,000 years each as the likely pre-history for the current conditions at YM.

The NTCF model of the rock domain

A modeling method called NTCF is used in all versions of MF, to re-process the time-dependent heat and moisture responses from the thermohydrologic NUFT model into matrix equations [7,8]. A linear NTCF processor is applied in the present study, using first-order matrix polynomial equations for modeling heat and moisture fluxes on the drift surface boundaries with constant-coefficient matrices. During the NUFT runs, the input boundary conditions on the drift surface are temperature and partial vapor pressure functions, varying with time and location. In addition, the total barometric pressure is also prescribed as boundary condition for the NUFT runs. The output variables from NUFT are spatial and temporal heat and moisture flux variations on the drift wall. The NTCF procedure determines dynamic admittance matrices from the NUFT input and output functions. The NTCF model matrices represent connections between inputs and outputs. Within the useful application regime of the NTCF model, the dependence of the matrices is negligible upon the input boundary conditions used in the NUFT calculations. The mountain-scale NTCF model for the i^{th} rock cell (i=1…8, see Fig. 3) along the drift length expresses the time-dependent, wall heat (qh) and moisture (qm) fluxes as follows:

$$qh_i = hh_i \cdot \left[T_i - Tinit_i\right] + hm_i \cdot [P_i - Pc_i] \tag{1}$$

$$qm_i = mh_i \cdot \left[T_i - Tinit_i\right] + mm_i \cdot [P_i - Pc_i], \tag{2}$$

where qh_i and qm_i are vectors composed of heat and moisture flux elements at time divisions $t_1,..,t_N$; T_i and P_i are wall temperature and partial vapor pressure vectors; $Tinit_i$ is the initial, constant wall temperature; while Pc_i is the partial vapor pressure variation vector for the predicted, central condition around which the NTCF model is determined. In Eq. (1), the hh_i is a dynamic admittance matrix of heat flux, generated by the wall temperature driving force, and hm_i is another, cross-effect component matrix of heat flux, generated by the wall partial vapor pressure driving force. Similarly, mh_i and mm_i are dynamic admittance matrices for the moisture flux expression in Eq. (2). The hh_i, hm_i, mh_i, and mm_i are all NxN matrices, determined using the NTCF modeling method [7,8].

Within each 3D mountain-scale rock cell (i=1…8), further divisions are made to capture the drift-scale temperature and humidity variations along the drift. The numerical discretization points on the drift wall are bundled into 420 averaged, independent surface nodes along the drift with respect to temperature and partial vapor pressure variations in the refined NTCF model. Each mountain-scale rock cell for i=1…8 is rescaled into j sub-divisions according to Table 2. The re-scaling of the hh_i, hm_i, mh_i, and mm_i mountain-scale 3D cell matrices into drift-scale hh_{ij}, hm_{ij}, mh_{ij}, and mm_{ij} matrices are accomplished by proportioning them by the ratio between the i^{th} cell and the ij^{th} drift segment surfaces, A_i and A_{ij}:

$$hh_{ij} = hh_i \cdot \frac{A_{ij}}{A_i} \tag{3}$$

$$hm_{ij} = hm_i \cdot \frac{A_{ij}}{A_i} \tag{4}$$

$$mh_{ij} = mh_i \cdot \frac{A_{ij}}{A_i} \tag{5}$$

$$mm_{ij} = mm_i \cdot \frac{A_{ij}}{A_i} \tag{6}$$

The re-scaling procedure generates 420 individual drift-scale hh_{ij}, hm_{ij}, mh_{ij}, and mm_{ij} "daughter" matrices without any additional NUFT runs, all inheriting the mountain-scale heat and moisture transport connections from the original, mountain-scale, "parent" matrices hh_i, hm_i, mh_i, and mm_i. The average size of the spatial rock domain in the axial drift direction is 1.7 m that is sufficient to generate temperature variations even along individual waste packages. The multi-scale NTCF rock model defines heat and moisture flux vectors as a function of the 420 time-dependent input vectors of surface temperature and partial vapor pressure boundary conditions. It is important to emphasize that both the heat and moisture fluxes as well as the temperature and partial vapor pressure vectors are all considered unknown at this point and subject to coupling calculations with the in-drift CFD models for the drift. The 420 nodes represent the interface boundary at selected points between a rock cell and the airway that include the waste packages. The NTCF rock model includes both drift-scale and mountain-scale heat and moisture flow components without using any sub-models and/or any superpositions.

Table 2. Drift-scale NTCF subdivisions in each mountain-scale rock cell.

i	1	2	3	4	5	6	7	8
j	21	42	63	84	84	63	42	21

The linear NTCF model requires a few update iterations [1,2,4]. The second iteration of NTCF module is currently in progress, following the first-step calculation reported in [4]. While the heat transport sub-model of the first NTCF iteration is quite acceptable, the moisture sub-model is not, due to strong nonlinearities. It was decided to use a robust, approximate model for the moisture flow across the drift wall assuming that 100% of the ground surface percolation reaches into the drift. Therefore, the NTCF sub-model for moisture is replaced by a time-dependent, but temperature-independent and simplified model. It will be discussed later that this assumption is reasonable while it underestimates the moisture flow predicted by NUFT. The amount of moisture flux is time dependent and summarized in Table 3.

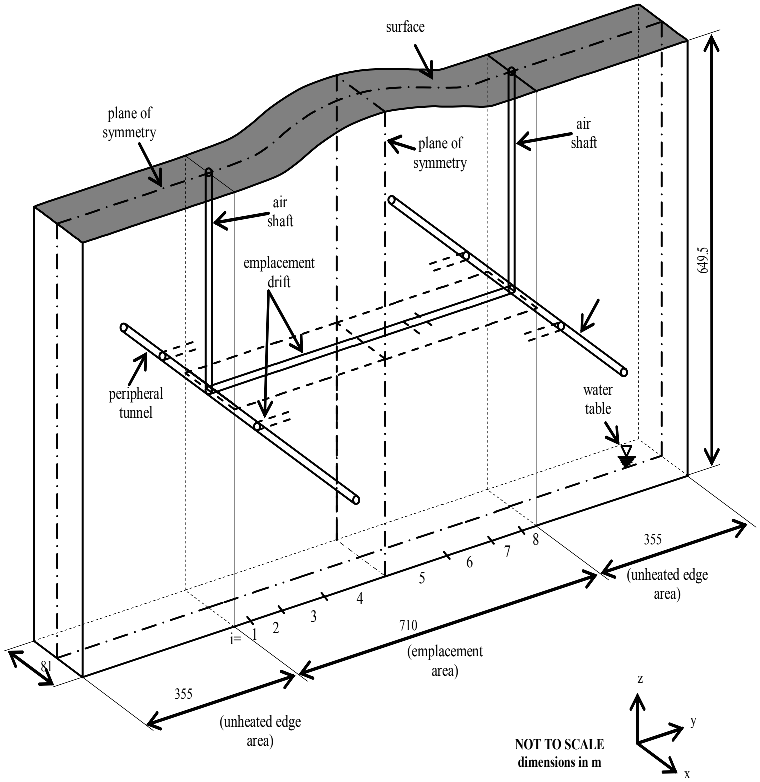

Figure 3. The rockmass domain around an emplacement drift in Panel 2.

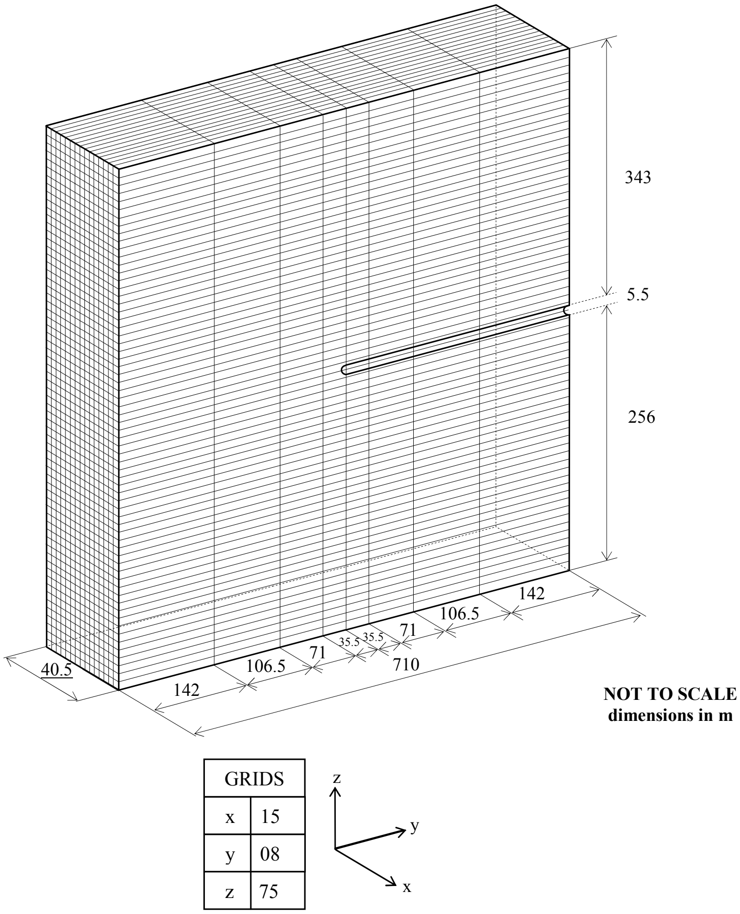

Figure 4. NUFT domain discretization grid

Table 3. Rock model moisture flux across drift wall.

Time period [year]	Percolation [mm/yr]	Moisture flux per linear m drift [kg/(m.s) x 10^{+6}]
0 - 600	12	2.1127
600 - 2000	20	3.5211
2000 - 5000	37	6.4789

THE MODEL OF THE AIRWAY WITH THE WASTE CONTAINERS

The CFD models in MF

The energy balance equation in the CFD model of MF is used in a simplified form, as follows, for an x-directional flow with v_i velocity in a flow channel of cross section dy times dz:

$$\rho c\frac{\partial T}{\partial t}+\rho c v_i\frac{\partial T}{\partial x}=\rho c a\frac{\partial^2 T}{\partial x^2}+\rho c a\frac{\partial^2 T}{\partial y^2}+\rho c a\frac{\partial^2 T}{\partial z^2}+\dot{q}_h \tag{7}$$

In Eq. (7), ρ and c are density and specific heat of moist air, a is the molecular or eddy thermal diffusivity for laminar or turbulent flow, respectively, and $\dot{q}_h$ is the latent heat source or sink for condensation or evaporation, respectively. Equation (7) is discretized and solved numerically and simultaneously along all parallel flow channels for the temperature field T in MF. The parallel flow channels represent the natural coordinate system of the flow field that must be known for the calculations. A few, typical flow velocity profiles are built-in functions in MF. Various boundary conditions, such as temperature, flux, or convective, may be applied for the solution of the energy equation.

An example of the solution was published and compared with FLUENT, as well as experimental, published results for turbulent flow [9]. A Yucca Mountain drift section of 150m long was discretized into 50 segments along the airflow. In the annulus between the waste packages and the drift wall, 60 unequally spaced segments were used along the radius. The flow was assumed to be fully developed hydraulically when entering the drift section. The eddy diffusivity and the velocity profiles were obtained from the dimensionless equations published by Kays and Leung [10], and were built into MF. The results showed excellent agreement between MF, FLUENT, and the experimental results.

The simplified moisture transport convection-diffusion equation in the CFD model of MF is similar to Eq. (7) as follows:

$$\rho\frac{\partial \rho_v}{\partial t}+\rho v_i\frac{\partial \rho_v}{\partial x}=\rho D\frac{\partial^2 \rho_v}{\partial x^2}+\rho D\frac{\partial^2 \rho_v}{\partial y^2}+\rho D\frac{\partial^2 \rho_v}{\partial z^2}+\dot{q}_{cm}+\dot{q}_{sm} \tag{8}$$

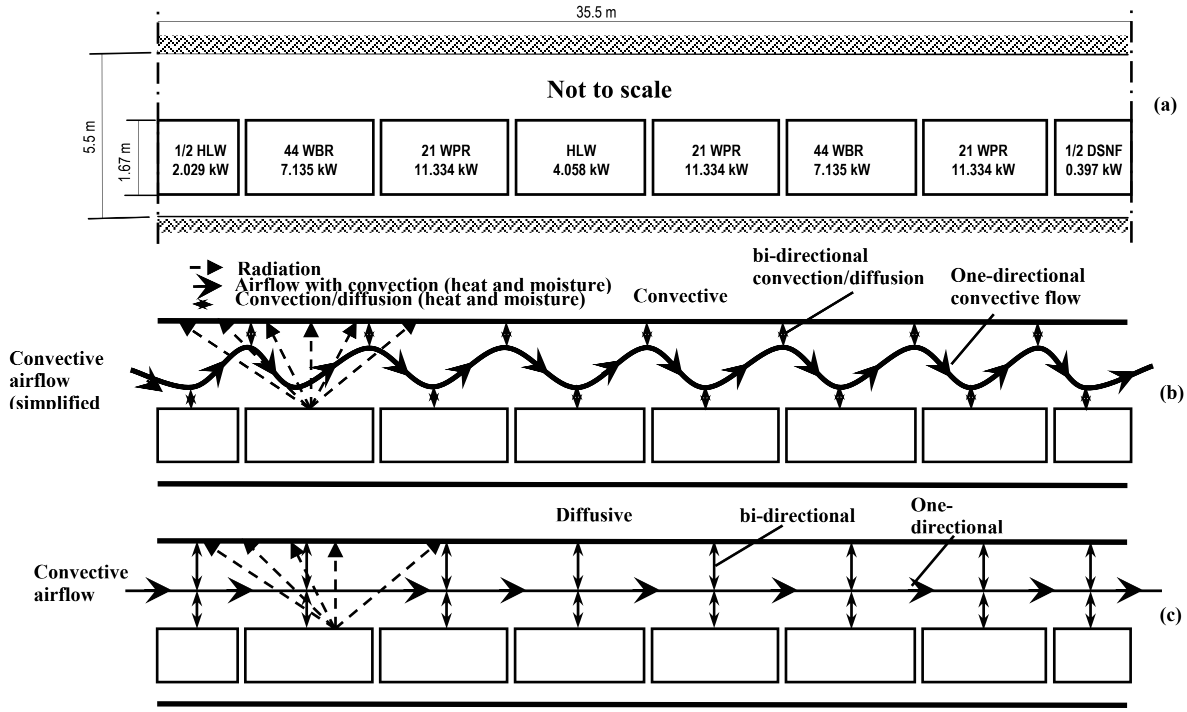

Figure 5. Airway configuration, (a) A repeated sequence of eight waste packages in an emplacement drift; (b) convective model configuration; (c) diffusive model configuration

In Eq. (8), ρ_v is the partial density of water vapor, D is the molecular or eddy diffusivity for vapor for laminar or turbulent flow, respectively, $\dot{q}_{cm}$ is the moisture source or sink due to condensation or evaporation, respectively, and $\dot{q}_{sm}$ is the vapor flux in superheated steam form.

It is possible to reduce the number of discretization elements in the computational domain by lumping nodes. MF allows for defining connections between lumped volumes, applying direct heat and moisture transport relations between them. A large selection of transport coefficient-based models is available for the user for laminar and turbulent flows as well as for natural convection. When only a few flow channels are used in the model configuration, such as in the present paper, a lumped-parameter CFD model is realized.

The current lumped-parameter CFD model for heat transport in the airway applies 2100 nodes for the entire drift. The same number of nodes is used in the CFD model for moisture. In the CFD domain, a sequence of 8 different (two halves and six full) waste packages, shown in Fig. 5a, is first mirrored to form a 16-package sequence, and second, repeated 10 times in the emplacement drift. The entire emplacement drift is 710 m in length, housing a total of 140 waste packages. Drip shields are not included in the present analysis. The CFD models of the emplacement drift are integral, continuous 3D models.

Heat and moisture transport by laminar or turbulent convection are modeled on the drift and the waste container wall. The heat and moisture transport coefficients in the annulus between the waste containers and the drift wall are calculated in MF using transport coefficients in the lumped-parameter CFD during pre-closure. Thermal radiation between the waste packages and the drift wall, between waste packages, as well as between drift wall segments are incorporated in the CFD models. Natural, secondary flow due to the local temperature differences in the drift generates natural convection during post-closure. This effect is superimposed on the general, one-directional air infiltration caused by the large, mountain-scale buoyancy effect. The dominantly natural heat transport coefficient on the drift and waste package walls during post-closure are all set to a constant value of 1.85 W/(m^{2}K), a value consistent with the results of more detailed numerical modeling [11]. Differential-parameter CFD models [9] can also be used in MF if refinement of the transport coefficients is necessary, however, this option is not applied in the present study.

Two different CFD model configurations were used in the calculations for the post-closure time period. Figure 5b shows the first, convective model, assuming that the air moves in a helical flow path transporting heat and moisture between the drift wall and waste package surfaces. The flow path in this model assumes a cork-screw-type flow upward from container to airspace, airspace to drift wall, and downward from the drift wall to the airspace and to the container, while all these superimposed on a slow forward progression along the drift. This airflow path separates the drift wall nodes from the waste package surface nodes, as depicted in Fig. 5b. Therefore, the convective heat and moisture transport between the drift wall and the waste packages are oriented by the moving air. The second, diffusive model is based on a simplified straight path of the air moving along the drift length, shown in Fig. 5c. In this model configuration, the heat and moisture transport between the drift wall and the waste package surfaces are diffusive, bi-directional. Consequently, the lumped-parameter CFD models with diffusive model configuration may predict an instantaneous flux exchange in radial direction within each cross section. Such an exchange, however, is not plausible physically under variable surface temperature and humidity conditions in the airflow direction. Therefore, the convective

CFD model configuration is considered to be superior to the diffusive configuration regarding the description of the physical transport processes.

TOTAL SYSTEM MODEL

The NTCF and CFD models are coupled on the rock-air interface by MF until the heat and moisture flows are balanced at the common surface temperature and partial vapor pressure at each surface node and time instant. In the post-closure time period, the natural infiltration airflow rate varies with time, as it depends on the time-variable temperature and relative humidity.

The solution of the coupled thermohydrologic-ventilation model in this study includes only two iteration loops:

1. Heat balance iteration between the NTCF and airway CFD models for each time division.
2. Moisture balance iteration between the NTCF and airway CFD models for each time division.

The other iteration loops (NTCF re-functionalization, air infiltration flow balancing) are not needed here since the results of a previous study [4] is applied.

INPUT DATA

The input data used in the calculation essentially agree with those used in the AMR Rev01 study [6]. The main input parameters are as follows:

Rock input data:	NUFT3.0 input deck specified in the AMR Rev01 study. The spatial rock domain is shown in Figs. 3 and 4.
Drift dimensions:	710 m long, 5.5 m in diameter.
Airflow rate:	15 m3/s at 25^{o}C intake temperature and 30% relative humidity until year 50; balanced infiltration variations afterwards, shown in Fig. 6, after [4].
Waste packages:	140 waste packages in the emplacement drift. A mirrored repeated sequence of eight waste packages with variable heat load, (two halves and six full) in a repeating drift segment of 35.5 m, shown in Fig. 5.
Waste mass load:	56 MTU/acre.
Drip Shield:	No drip shield is assumed in the model configuration.

Other input data used in MF and NUFT are documented in a report submitted to BSC [12]. The mountain-scale infiltration airflow was determined in a previous study [4] and used here without modification.

A main pressure balance iteration cycle was used in [4] to determine the exact airflow rate at which the buoyancy pressure and the pressure loss components agreed within an error limit. Figure 6a shows the balanced pressure, while the balanced infiltration airflow rate with time is given in Fig. 6b.

RESULTS AND DISCUSSIONS

Temperature and Relative Humidity Distributions

Spatial and temporal temperature and relative humidity variations from the MF calculations are given for the central, representative drift in Fig. 7. Sub-figures a, c, and e depict temperatures of the drift wall, air, and the waste packages as a function of time and drift length. Sub-figures b, d, and f show the relative humidities on the surface of the drift wall, in the air, and on the waste packages as a function of time and drift length.

Figure 7 shows the temperature and relative humidity results for both the pre- and the post-closure time periods, assuming a constant airflow rate of 15 m3/s during pre-closure, and the variable infiltration air mass flow rate of Fig. 6a during post-closure. The evolution of two thermal peaks are shown in the temperature variations for the drift wall, shown in Fig. 7a, one around year 5 during pre-closure, and one between years 75 and 100 during post-closure, depending on the drift location. The second peak is reached relatively rapidly, due to the young age of the waste, when compared to the previous study [1] in which the time for peak temperature evolution during post-closure was about 1000 years, following a 300-year pre-closure ventilation. The second peak is much higher in amplitude, underlying the criticality of the post-closure analysis, for both the maximum temperature evolution as well as the threshold limitation for localized corrosion. Waste package temperatures exceed 140^{o}C, the limit for likely localized corrosion for Alloy 22 waste package material [13]. This condition is predicted for an extended period of time and for a large section of emplacement drift with over 100 waste packages. If drip shields were included in the calculation, the predicted temperatures of the waste package surface would rise even higher. The longitudinal, saw-tooth-like fluctuations in both temperatures and relative humidities are caused by the variation of the heat dissipation of the individual waste packages.

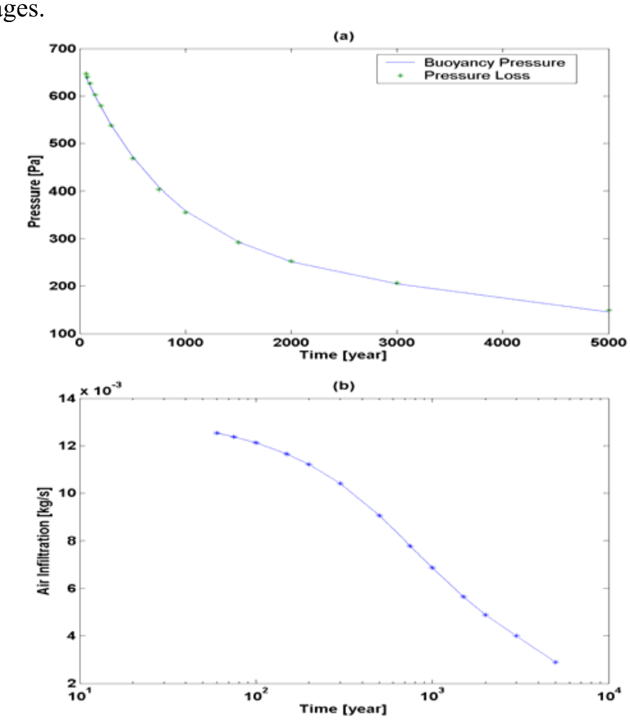

Figure 6. (a) Balanced total pressure loss and buoyancy pressure difference as a function of time; (b) Natural, mountain-scale air infiltration mass flow rates through an emplacement drift (After [4]).

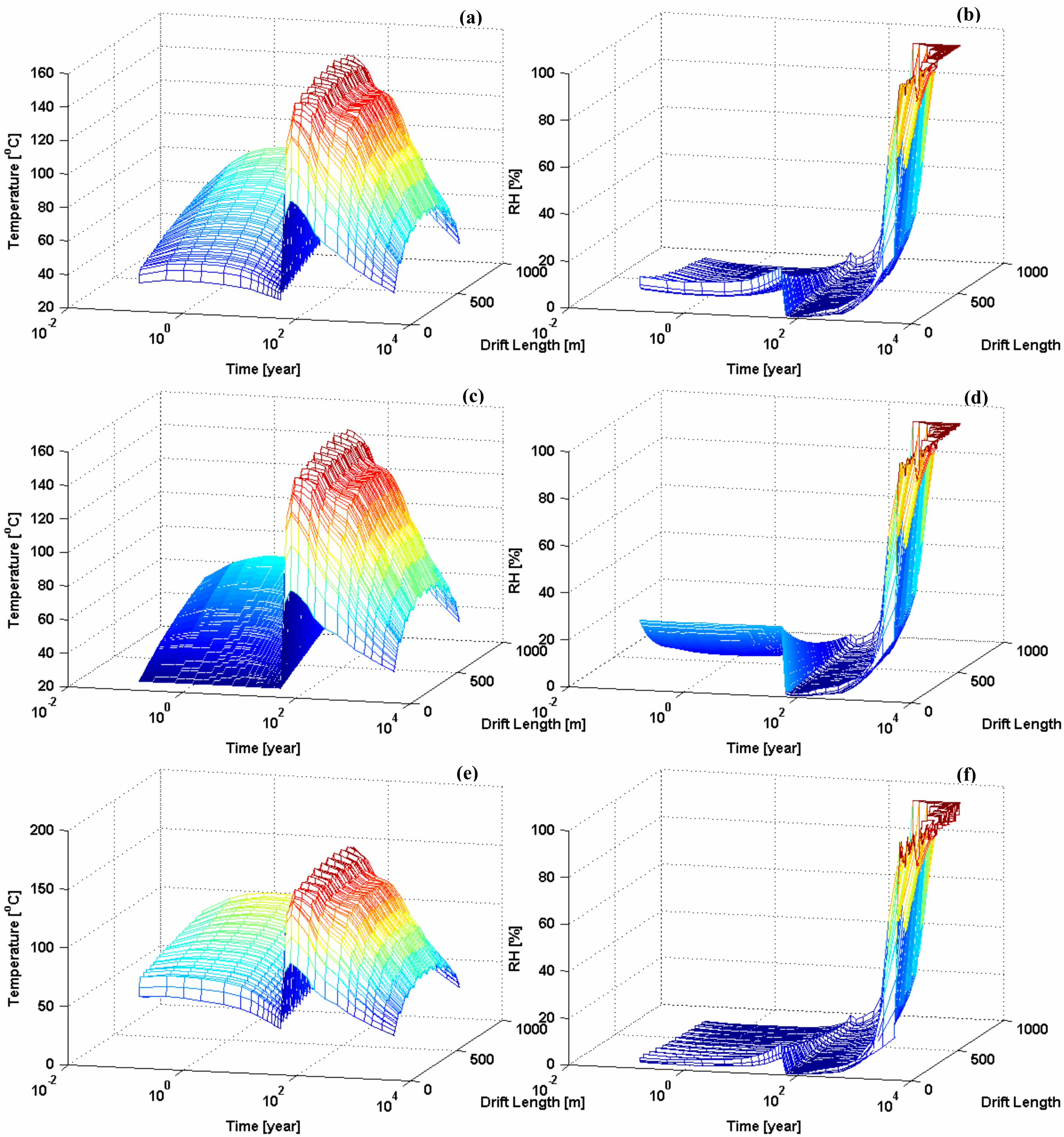

Figure 7. (a) Wall temperature; (b) wall relative humidity; (c) air temperature; (d) air relative humidity (RH); (e) waste package temperature; and (f) waste package relative humidity (RH) distributions in time and space.

The maximum differences between the drift wall and air, as well as between waste packages and air, are only about 10°C at the time of the peak temperatures and lower afterward. Under this condition, the buoyancy driving force for local, natural air convection in each drift cross section is moderate, with a Rayleigh number in the order of 10^9 and with a natural heat transport coefficient around 1.85 W/(m^{2}K) between the waste package and the air, as well as between the air and the drift wall. The convective heat transport in this case is lower than the heat transport due to radiation that is a parallel, by-pass mechanism to convection, modeled in the lumped-parameter CFD model. Therefore, the sensitivity to the convective heat transport coefficient in this regime is moderate, and the lumped-parameter CFD model based on heat transport coefficients was not seen to be in need of replacement with more elaborate heat and moisture convection elements.

The temperature variation along the drift axis is very significant, still over 60°C at year 2000. The edge-cooling effect is increasing with time between years 50 and 2000, during which period the waste decay heat is still strong enough to heat the middle section of the drift, but the time is already long enough to cool down the edge area. The current results support the initial assumption that evaporation in the middle and hot drift section and cold-trap condensation in the relatively cold edge drift section will take place in the central drift of Panel 2. Other drifts in the same panel will likely follow the same trend, as well as drifts in other panels under certain airflow conditions during post-closure. This suggests that an engineered natural draft ventilation system, as has been suggested by Nye County, has the potential to improve system performance by eliminating condensate formation.

Due to the very low air infiltration, the temperature variation along the drift axis closely copies that of an un-ventilated repository during post-closure. This recognition may allow studying of the cold-trap process with a simplified, psychrometric moist airflow model. However, the heat-driven moisture flow will still need to be calculated using a coupled, mountain-scale heat and moisture model along the drift. Currently, only the MF model can solve the complex task, using the multi-scale NTCF technique. No other published models, as reviewed in [4], include the 3D, mountain-scale heat and moisture flow components in the thermohydrologic model coupled to in-drift CFD models.

Cold-Trap Condensate Drippage

In a previous work [4], condensation was detected near the edge of the drift due to moisture transport in the air from the middle, hot and humid, section to the colder drift edge.

Condensate formation is currently modeled based on partial vapor pressure trimming in the moisture transport CFD sub-model solution in MF. An example is given in Fig. 8, showing the saturated vapor pressure, the un-trimmed and trimmed partial vapor pressures as well as the barometric (total) pressure on the drift wall along length. The results in Fig. 8 were obtained by stopping the MF run at the end of the balancing iterations at Year 1000, and accessing the internal variables for illustration purposes. The un-trimmed partial vapor pressure curve section above the barometric pressure limit is hypothetical, since the moisture CFD model in MF enforces the partial vapor pressure, P_v, to say between physical limits. The enforcement is accomplished by iteratively, numerically adjusting the $\dot{q}_{sm}(i)$ and $\dot{q}_{cm}(i)$ terms in Eq. (8) for each grid in the CFD model domain until the following conditions are met:

a. Condition for superheated steam removal

$$increase\ \ (-)\dot{q}_{sm}(i):\quad if\ P_v(i) > P_b(i)\ and\ P_s(i) > P_b(i) \tag{9}$$

b. Condition for condensate removal

$$increase\ \ (-)\dot{q}_{cm}(i):\quad if\ P_v(i) > P_s(i)\ and\ P_s(i) \le P_b(i) \tag{10}$$

where P_v is the partial vapor pressure,
P_s is the saturated vapor pressure, and
P_b is the total, barometric pressure.

Initially, all flux terms $\dot{q}_{sm}$ and $\dot{q}_{cm}$ are set to zero for all nodes. Condensate or superheated steam fluxes are identified implicitly and numerically from the correct mass balance equations represented by the CFD model. The identification is simultaneously performed during the balancing iterations between the CFD and NTCF models. Condensate may be detected at surface nodes or at nodes assigned to air; in the later case, the condensate is assumed to be mist. The fate of the condensate by drainage, or condensate imbibing into the rock wall is currently not modeled, but this effect is likely to be important and subject of future studies with MF. The current model assumes that the condensates gracefully drain through the rock. The $\dot{q}_h$ and $\dot{q}_{cm}$ terms in Eqs. (7) and (8) are linked through the latent heat of water evaporation in MF.

Comparison between the two in-drift air models revealed a major impact on the cold-trap condensate amount and distribution. It can be seen from Fig. 9 that the diffusive CFD model predicts condensate only on the drift wall surface as it is colder than the waste package surface. However, the convective CFD model predicts condensate at surfaces as well as air nodes.

The temperature fields of the new calculation agree almost exactly with those in the previous study [4] for the drift wall and waste package. Since new air nodes are introduced in the CFD model, the air temperatures and humidities were averaged for comparison.

The relative humidity distributions are also similar and show a good, general agreement with the previous results [4]. A major difference is seen in the water condensation distribution with time and location, when applying convective coupling between the points on a flow path that spirals from air near waste package to air near drift wall and repeats with near waste package in the next drift cell and so forth. This convective flow path allows condensate formation on a waste package surface that is in a drift cell with a wall temperature lower than that of the waste package. In contrast, the model configuration in the previous paper [4] applied convective connections between air nodes in subsequent drift cells, but diffusive connections between the waste package and the air, as well as between the air and the drift wall within each drift cell. It is interesting to observe that a diffusive connection prevents the formation of water condensate on the waste package if a colder surface, that is, the drift wall, is present in the same cell.

This observation has far-reaching consequences. The equivalent-conductivity models used for studying air temperature and relative humidity in the emplacement drift are all incapable of correctly capturing the physical transport processes that govern condensate formation in an emplacement drift with air movement. Thus, while the equivalent properties of the conduction-diffusion blocks in a basically porous-media model can be adjusted to predict more-or-less correctly heat flows, the delicate balance of the moisture, and especially, the condensate formation will be distorted.

Examination of the vapor inflow into a 710 m-long drift from the NUFT results indeed supports the shell-balance concept. The vapor accumulation in the form of condensates from the balanced results of MF is compared with the vapor mass flow calculated directly using NUFT for the same drift wall temperature distribution. Comparison between the simplified robust moisture transport model results and the direct NUFT vapor inflow rates is shown in Fig. 10. Results are shown for the rock cells i=5 to 8, between 355 m and 710 m locations. As shown, the robust model under-predicts the total vapor inflow to the drift. After the 2nd NTCF iteration and the re-calculation, there will likely be significantly more condensate due to much higher vapor inflow rate in the hot drift segments for the same time period.

Computational Performance

The NTCF modeling technique reduced the number of necessary NUFT runs, making it feasible to complete the complex calculations in approximately five weeks in spite of the average number of 600 and 240 iterations, for convective and diffusive models respectively, with the thermohydrologic model for the 5,000 year time period. For comparison, a single NUFT run with one set of boundary condition variations for 5,000 years for the complete rock domain (with entrance and exit segments) took approximately 150 hours on a small workstation. Comparing run times between MF with the NTCF method and a hypothetical case without the NTCF method indicates that without using the NTCF method, but replacing it with direct NUFT runs and assuming the same number of balancing iterations, the modeling task being presented would take a minimum of 240 times 150 hours, an 4.1 years of non-stop computation. The reason for the convective model taking about 2.5 times longer is first, the size of the CFD model which is about 33% more than the diffusive CFD model and second, the formation of condensate on a larger number of nodes.

CONCLUSIONS AND RECOMMENDATIONS

- An integrated, pre- and post-closure thermohydrologic-ventilation study was successfully completed using both mountain-scale and drift-scale rockmass model-elements using MF. The model applied a multi-scale rockmass model-element without the need for solving sub-tasks and using subsequent superposition. The model integrated open-loop ventilation during pre-closure and mountain-scale air infiltration during post-closure within one continuous task.
- Heat conductivity reduction in the rockmass due to desaturation during pre-closure was automatically included in the post-closure calculations.
- The forced ventilation was found to be efficient in keeping temperatures well below boiling during the pre-closure time period.
- Two different in-drift air model configurations were used for post-closure simulation. Both models predicted condensate on the drift wall.
- Condensate on the waste package surface is predicted during post-closure if a convective model is used in the drift.
- The waste package surface temperature reached a peak value between years 75 and years 200, exceeding the temperature limit of 140^{o}C known to be the safe threshold limit for localized corrosion for the likely waste container material of Alloy 22. This will likely gets worse if drip shields are used.
- A longer period of pre-closure ventilation may favorably reduce the maximum waste package surface temperature. Previous, comparable studies [1,2] showed that a 300 years pre-closure ventilation period results in a maximum post-closure waste package temperature lower than 120^{o}C. Therefore, a longer pre-closure time period may be advantageous.
- The relative humidity increased up to 100% during post-closure in the cold exit section of the emplacement drift, and liquid water formations were predicted. This result provides far less favorable storage conditions than those expected when an engineered, post-closure ventilation was provided [1,2].

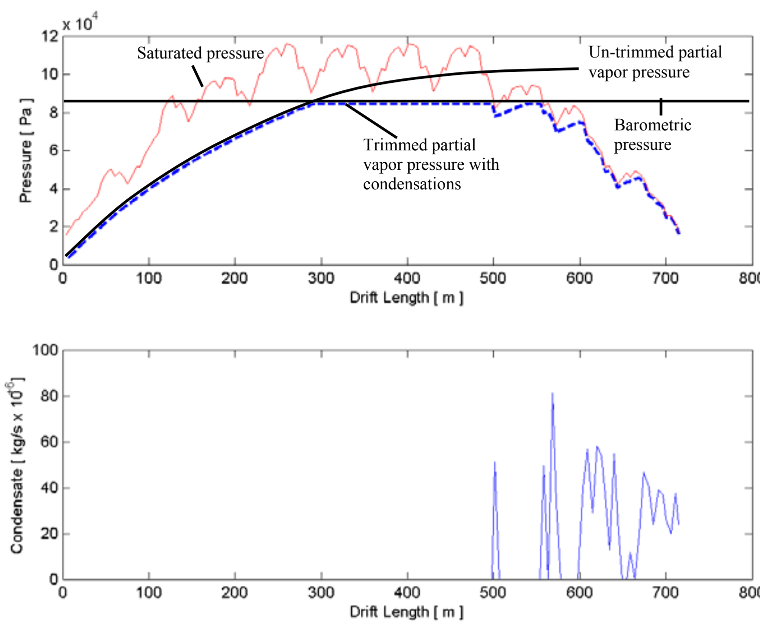

Figure 8. Condensate formation based on partial vapor pressure trimming

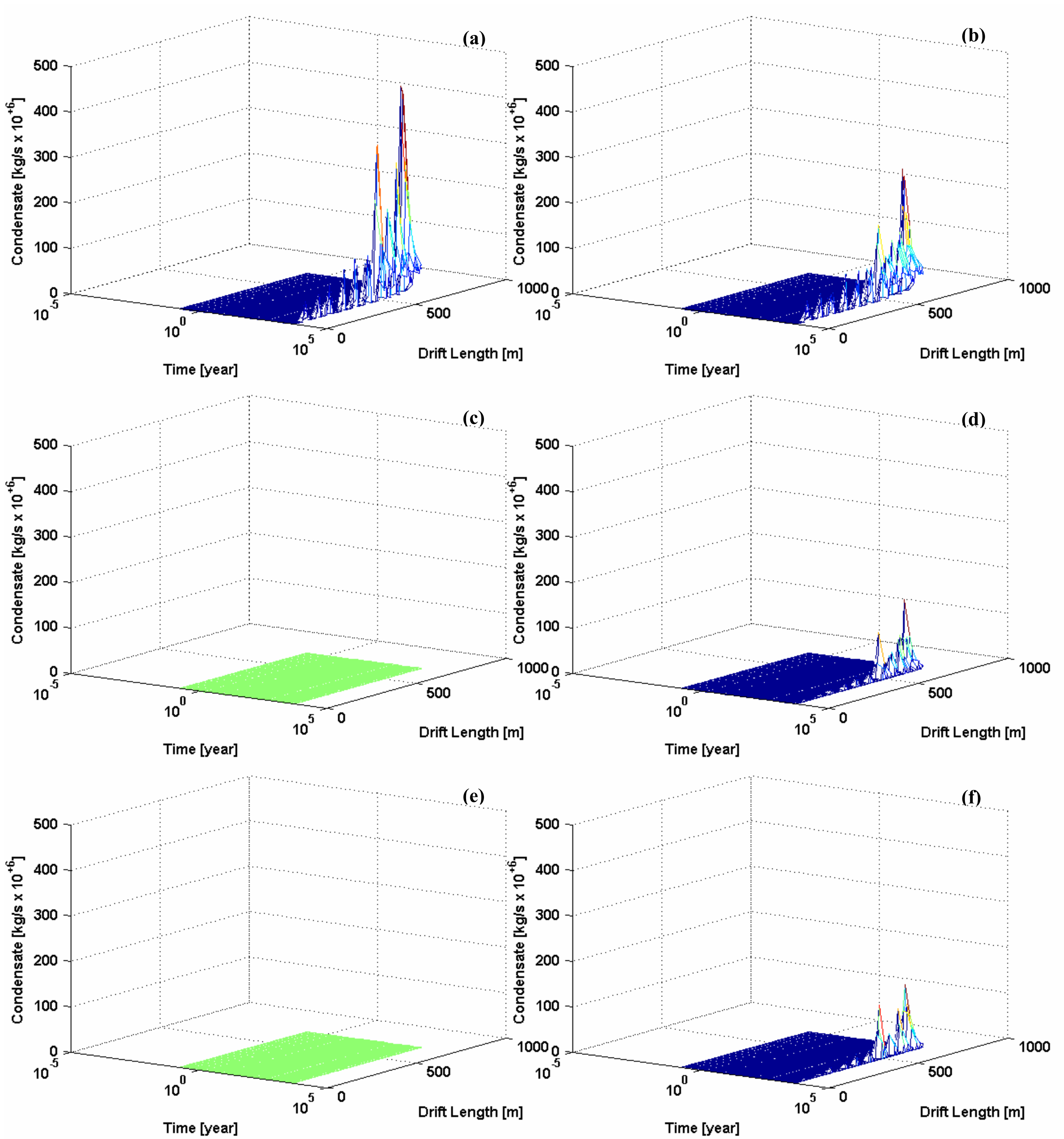

Figure 9. (a) wall condensate, diffusive CFD model; (b) wall condensate, convective CFD model; (c) mist in the air, diffusive CFD model; (d) mist in the air, convective CFD model; (e) waste package condensate, diffusive CFD model; (f) waste package condensate convective CFD model.

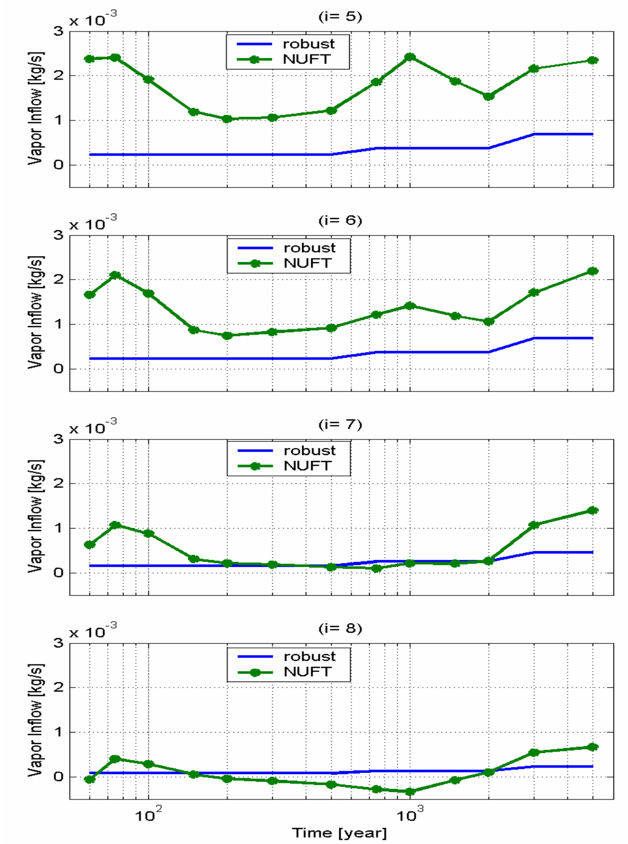

Figure 10. Comparison between the simplified robust moisture transport model results and the direct vapor inflow rates calculated by NUFT.

- A fully-coupled, thermohydrologic-ventilation model and software, MF is proven efficient in solving the multiphase, non-equilibrium transport problem of heat, moisture, and ventilating airflows involving the large and geometrically complex geologic region at YM. It is recommended to apply the NTCF modeling methodology and software MF for multi-scale, coupled heat and moisture flow studies with or without ventilating air movements at YM.
- The second NTCF iteration for the reported task is in progress. Based on the comparison in Fig. 10, the switch back to NTCF moisture model from the robust model of this paper will likely cause more condensate and higher relative humidities.

ACKNOWLEDGMENTS

The review and editorial comments of Dr. Dale Hammermeister, Nye County On-Site representative, Dr. John Walton, Professor at the University of Texas at El Paso, and Dr. Pierre Mousset-Jones, Professor, Mackay School of Mines, UNR, are highly appreciated. The support of the Nye County Department of Natural Resources under Grant No. DE FC28 02RW12163 is gratefully acknowledged.

REFERENCES

[1] Danko, G., and Bahrami, D.. 2003. “Powered, and Natural, Passive Ventilation at Yucca Mountain.” Proceedings, 10th Int. High-Level Radioactive Waste Management Conference, pp.683-689.

[2] Danko, G., 2003. “Coupled Hydrothermal-Ventilation Studies for Yucca Mountain.” Annual Report for 2003. NWRPO-2003-05, Pahrump, Nevada: Nye County Department of Natural Resources.

[3] Harrington, P., 2004. “Repository Design Status.” Presentation to the Nuclear Waste Technical Review Board Panel on the Engineered System, January 20, Las Vegas, NV.

[4] Danko, G., Bahrami, D., 2004. “Coupled, Multi-Scale Thermohydrologic-Ventilation Modeling with MULTIFLUX” 2004 SME Annual Meeting, February 23-25, Denver, CO.

[5] BSC (Bechtel SAIC Company). 2002. “Ventilation Model.” ANL-EBS-MD-000030 REV 01D draft. Las Vegas, Nevada: Bechtel SAIC Company.

[6] Nitao, J., 2000. “NUFT, Flow and Transport code V3.0s.” Software Configuration Management, Yucca Mountain Project – STN: 10088-3.0S-00. Prepared at the Lawrence Livermore National Laboratory.

[7] Danko, G., 2000. “MULTIFLUX Software Documentation.” University of Nevada, Reno.

[8] Danko, G., 2004. “Numerical Transport Code Functionalization Procedure and Software Functions.” Proceedings of ASME, Heat Transfer/Fluid Engineering, July 11-15, 2004, Charlotte, North Carolina, USA

[9] Danko, G., and Bahrami, D. 2002. “The Application of CFD to Ventilation Calculations at Yucca Mountain.” 28th Waste Management ’02 Conference, Tucson, AZ, pp1-8.

[10] Kays, W. M. and Leung, E. Y., Heat Transfer in Annular Passages: Hydrodynamically Developed Turbulent Flow with Arbitrarily Prescribed Heat Flux, Int. J. Heat Mass Transfer, Vol. 6 pp. 248-249, 1963.

[11] Webb, S.W., Francis, N.D., Dalvit-Dunn, S., and Itamura, M.T., 2003. “Pre- and Post-Closure Natural Convection Effects in Yucca Mountain Drifts.” Proceedings, 10th Int. High-Level Radioactive Waste Management Conference, pp. 667-674.

[12] Danko, G., Bahrami, D., and Lanka, S., 2003. “Technical Support Services for the MULTIFLUX Software.” MOL.20031208.0025, Final Report, submitted to BSC, Nevada.

[13] Farmer, J., 2003. “Chemical Environment Evolution on Alloy 22.” Presentation to the Nuclear Waste Technical Review Board, January 28, Las Vegas, NV.

Proceedings of ASME
Heat Transfer/Fluid Engineering
July 11-15, 2004, Charlotte, North Carolina, USA

HT-FED2004-56049

NUMERICAL TRANSPORT CODE FUNCTIONALIZATION PROCEDURE AND SOFTWARE FUNCTIONS

G. Danko
University of Nevada, Reno
Email: Danko@unr.edu
(775) 784-4284

ABSTRACT

A numerical – computational procedure is described to determine a multi-dimensional functional or an operator for the representation of the computational results of a numerical transport code. The procedure is called Numerical Transport Code Functionalization (NTCF). Numerical transport codes represent a family of engineering software to solve, for example, heat conduction problems in solids using ANSYS[1]; heat and moisture transport problems in porous media using NUFT[2]; or laminar or turbulent flow and transport problems using FLUENT[3], a computational fluid dynamic (CFD) model. The NTCF procedure is developed to determine a model for the representation of the code for a variety of input functions.

Coupled solution of multiphysics problems often require repeated, iterative calculations for the same model domain and with the same code, but with different boundary condition values. The NTCF technique allows for reducing the number of runs with the original numerical code to the number of runs necessary for NTCF model identification.

The NTCF procedure is applied for the solution of coupled heat and moisture transport problems at Yucca Mountain, Nevada. The NTCF method and the supporting software is a key element of MULTIFLUX[4], a coupled thermohydrologic-ventilation model and software. Numerical tests as well as applications for Yucca Mountain, Nevada are presented using both linear and nonlinear NTCF models. The performance of the NTCF method is demonstrated both in accuracy and modeling acceleration.

INTRODUCTION

A general, numerical method is described for phenomenological model identification of boundary-value transport problems. The method is built on the processing of time-dependent boundary value relationships between input and output variables of known, analytical or numerical solutions of transport problems. Software codes, available for modeling physical transport problems, can be used to generate numerical outputs for model-building. In transport problems, there exists a causal relationship between input and response variables. Typical examples include the flow of mass, momentum, or energy, generated by boundary-value driving forces.

The purpose of building a phenomenological model between input and response functions is to predict the result of the transport problem in a simple, closed-form, analytical-type expression that is fast to evaluate. The desired form of the model is a linear or nonlinear, multi-variable operator equation or set of equations. Such a model represents a relationship between general, time-variable inputs and outputs, some known and some unknown, considered as boundary values.

A vast literature describes the theory of dynamic system identification and there is no attempt made in this paper to provide a review. Reference to the basic work is in order to recognize the contribution of deFigueiredo, Dwyer, Eykhoff, Kalman, Volterra, Weiner and Zadek, among many others, in non-linear system identification [1, 2]. Although the tools may be the same, the aim of the work is very different: the sole purpose of seeking an NTCF model is to increase computational efficiency for an already given numerical transport model.

The method of identifying the phenomenological model involves a modeling processor that (1) generates a systematic data set, from a numerical transport code (NTC), and (2) identifies a matrix operator equation (or set of equations) from the results. The NTCF model allows working directly with matrix equation(s), instead of running the original numerical code, when a boundary variable is changed. Therefore, the NTCF technique may simplify the way a numerical model or software is used, and accelerate the calculations especially in boundary coupling applications where a large number of iterations is necessary.

The NTCF model is determined numerically, based on a system of solutions of an NTC, by evaluating outputs for a

[1] ANSYS, a multiphysics software package by ANSYS,Inc.
[2] NUFT (Non-equilibrium, Unsaturated-saturated Flows and Transport), porous-media transport code, developed by John Nitao at the Lawrence Livermore National Laboratory.
[3] FLUENT, a software package by Fluent, Inc.
[4] MULTIFLUX, by University of Nevada, Reno.

given set of inputs. Figure 1 shows the conceptual logic and data flow charts of the NTCF model identification. The NTCF model is given in an implicit operator equation in Fig. 1, defining a closed-form relationship between general input and output functions. The goal is to find an NTCF model that is faster to evaluate than the original NTC model. The paper describes the theoretical foundations of the NTCF method, the applicable software functions, analytical and numerical tests, and practical applications.

NTCF MODEL FORMULATION

The Basic NTCF Model with Stepwise Boundary Function

The time-variable relationship between the input (driving force) and output (resulting flux) of a transport model can be expressed in the form of a matrix-vector equation. A single-variable, non-steady-state heat transport problem is used as an example to derive the basic matrix-vector equation. According to Duhamel's theorem [3], if $q=A(t)$ is the heat flux density at time t on the surface of a solid in which the initial heat flux is zero while the surface is kept at unit temperature from time zero, then the solution of the problem when the surface is kept at variable temperature $T(t)$ is given by the following equation:

$$q(t) = \int_{\tau=0}^{t} T(\tau)\frac{\partial}{\partial t} A(t-\tau)\, d\tau + T(t)\, A(0) \qquad (1)$$

The $A(t)$ function in Eq. (1) is called the indicinal admittance. In order to introduce a boundary variable vector, time divisions $t_1, t_2, \ldots, t_n, \ldots, t_N$ are introduced that eliminate the continuous time-variable. The temporal discretization of t defines an N-dimensional space in which q and T vectors of the same dimension can be used and related. In the basic NTCF model, it is assumed that the continuous input variable $T(t)$ is approximated with a stepwise function with T_i constant in each $[t_{i-1}\ t_i]$ interval. Using Eq. (1) for $t=t_i$, the $q_i=q(t_i)$ output component of q can be written for $i=1\ldots N$ as follows:

$$q(t_1) = T_1 \int_{\tau=0}^{t_1} \frac{\partial}{\partial t_1} A(t_1-\tau)\, d\tau + T(t_1)\, A(0)$$

$$\vdots$$

$$\begin{aligned} q(t_N) = T_1 &\int_{\tau=0}^{t_1} \frac{\partial}{\partial t_N} A(t_N-\tau)\, d\tau + \ldots + \\ T_N &\int_{\tau=t_{N-1}}^{t_N} \frac{\partial}{\partial t_N} A(t_N-\tau)\, d\tau + T(t_N)\, A(0) \end{aligned} \qquad (2)$$

The definite integrals in Eqs. (2) can be evaluated, first, by substituting a new variable $\lambda=t_i-\tau$, $i=1\ldots N$, and second, by canceling the integration and differentiation in each integral. The results can be written as follows:

$$\begin{aligned} q(t_1) &= A(t_1)\, T_1 \\ q(t_2) &= [A(t_2) - A(t_2-t_1)]T_1 + A(t_2-t_1)T_2 \\ &\vdots \\ q(t_N) &= [A(t_N) - A(t_N-t_1)]T_1 + \\ &\quad [A(t_N-t_1) - A(t_N-t_2)]T_2 + \cdots + A(t_N-t_{N-1})T_N \end{aligned} \qquad (3)$$

Applying vector-matrix notation in Eqs. (3) gives:

$$q = \lfloor h_{ij} \rfloor \cdot T = h \cdot T \qquad (4)$$

where

$$h = \begin{bmatrix} A(t_1) & 0 & & 0 \\ A(t_2)-A(t_2-t_1) & A(t_2-t_1) & & 0 \\ \vdots & & & \vdots \\ A(t_N)-A(t_N-t_1) & A(t_N-t_1)-A(t_N-t_2) & \cdots & A(t_N-t_{N-1}) \end{bmatrix} \qquad (5)$$

The essence of the NTCF technique is that the h matrix of the operator is determined from the numerical transport code being functionalized. Instead of using the $A(t)$ function as a response from the NTC to a single step-change input, an alternative method is applied for the basic model, which does not require the explicit determination of $A(t)$. The method uses a direct fit to the output data of the NTC, therefore, results in a quasi-linear fit if A is allowed to vary due to non-linearities. In the simple, one-variable example, N runs are needed with the NTC, each with a different T temperature vector, in order to provide input data for identification of h with a unique solution.

In the NTCF process, first, a central temperature vector with elements T_i, $i=1\ldots N$ is selected, and second, N linearly independent column vectors are formed from T for N runs. This can be accomplished by arranging T_i into a T matrix according to the schematic as follows:

$$T = \begin{bmatrix} T_1 & T_1 & T_1 & \cdots & T_1 \\ T_1 & T_2 & T_2 & \cdots & T_2 \\ T_1 & T_2 & T_3 & \cdots & T_3 \\ \vdots & \vdots & \vdots & \ddots & \vdots \\ T_1 & T_2 & T_3 & \cdots & T_N \end{bmatrix} \qquad (6)$$

The set of organized, numerical runs with the NTC is comprised of using the N boundary condition histories represented by the N column vectors in the T matrix. The results of the N runs are N response histories $[q_{ij}]$ that can be arranged into a q matrix. Since $q=h * T$ is expected according to Eq. (4), h can be expressed as follows:

$$h = q\ T^{-1} \qquad (7)$$

Since the input T matrix is specially constructed, the inverse, T^{-1} matrix will be a triple-diagonal matrix, in which the sum of the elements in the first column or in the first row are both 1, whereas the sum in any other row or column is zero. It can be shown by direct calculation that the h matrix in Eq. (7) is identical to the h matrix in Eq. (5) in a linear case. The h matrix will be a lower-triangle matrix, satisfying the expectation that only past and present boundary condition values may affect a present response. Note that each of the q_{ij} heat flux element is calculated at the end of the corresponding $[t_{i-1} \;\; t_i]$ time interval.

An intuitive variation option was made to the NTCF procedure to use the average of the q_{ij} response over the $[t_{i-1} \;\; t_i]$ time period, instead of the value at the end-point time. Good results with the averaging in practical calculations have led to the following question: can stepwise boundary condition variation be used in the NTC in order to represent piecewise-linear or higher-order interpolation in the NTCF model? This question initiated the application of a built-in, piecewise-linear boundary variation in the NTCF model. It will be shown that the h obtained from Eq. (7) based on the averaged $M_i[q_{ij}]$ responses is identical to the solution for a linear system with a piecewise-linear input variation on the boundary, provided that the time division is equidistant. However, if the time division varies, the simple averaging becomes inadequate and a different, variable-interval averaging must be used as it is discussed later in the paper.

The A(t) indicinal admittance function can be determined numerically in a linear case by inverse convolution, decomposing the $q(t_1), q(t_2), \ldots, q(t_n), \ldots, q(t_N)$ responses obtained for a stepwise boundary function. The inverse convolution may be obtained from Eq. (3) for an equidistant time division as follows:

$$\begin{aligned} &A(t_1) = q(t_1)\,/\,T_1 \\ &A(t_2) = [q(t_2) - A(t_1)(T_2 - T_1)]\,/\,T_1 \\ &\vdots \end{aligned} \tag{8}$$

Based on Eq. (8), an inverse convolution procedure *iconv* can be realized. The procedure can be applied to a stepwise input function $T(\tau)$ and NTC output result function $q(\tau)$ sampled at $\tau \in (0,t]$ time instants. The result is the indicinal admittance $A(t)$ as follows:

$$A_1(t) = iconv[{}^{\mathrm{N}}q_1(t) - {}^{\mathrm{N}}q_0(t),\; T_1(t) - T_0(t)] \tag{9}$$

The Basic NTCF Model with Piecewise-Linear Boundary Function

A complementary form of the convolution integral in Eq. (1) is used to derive the basic equations for the algorithm for a piecewise-linear boundary function. Linear connection between the base points of a boundary function is often desirable over a stepwise approximation. The evaluation of the NTCF matrices for piecewise and higher order boundary-value variations in the time domain is based on the second form of the Duhamel's integral as follows:

$$q(t_n) = \int_0^{t_n} A(t_n - \tau)\, T'(\tau)\, d\tau \quad + A(t_n)T(0) \tag{10}$$

Equation (10) may be obtained by partial integration of Eq. (1). Since T' is the slope, the integral can be directly evaluated in each time interval. After summation and assuming a stationary initial condition $T_0 = T(0) = 0$, the result is as follows:

$$q(t_n) = m_1 \int_0^{t_1} A(t_n - \tau)\, d\tau + m_2 \int_{t_1}^{t_2} A(t_n - \tau)\, d\tau + \ldots + m_n \int_{t_{n-1}}^{t_n} A(t_n - \tau)\, d\tau \tag{11}$$

Each integral in Eq. (11) can be expressed with an integral mean value, $M[A]$. For the general term, after substituting $\lambda = t_n - \tau$, is given:

$$M[A]_{t_n - t_{i+1}}^{t_n - t_i} = \frac{1}{(t_{i+1} - t_i)} \int_{t_n - t_{i+1}}^{t_n - t_i} A(\lambda)\, d\lambda \tag{12}$$

According to Eq. (12), the averaging time intervals in the $M[A]$ integral mean values generally do not coincide with the time division intervals, unless the division is equidistant. In a matrix-vector form, a new, modified interval-averaged h matrix is obtained:

$$h = \begin{bmatrix} M[A]_0^{t_1} & 0 & 0 \\ M[A]_{t_2 - t_1}^{t_2} - M[A]_0^{t_2 - t_1} & M[A]_0^{t_2 - t_1} & 0 \\ \vdots & & \vdots \\ M[A]_{t_N - t_1}^{t_N} - M[A]_{t_N - t_2}^{t_N - t_1} & M[A]_{t_N - t_2}^{t_N - t_1} - M[A]_{t_N - t_3}^{t_N - t_2} & \cdots M[A]_0^{t_N - t_{N-1}} \end{bmatrix} \tag{13}$$

The h matrix in Eq. (13) is fundamentally different from that in Eq. (5) in that it represents piecewise-linear connections, instead of steps. The first advantage of the result is that the piecewise connection between the $T_1 \ldots T_N$ boundary values is generally a better approximation than the stepwise variation for a smooth boundary function. This means that a coarser time division and smaller matrix dimension can be used for the same model accuracy. The second advantage is that the NTC input boundary function variation is still stepwise, namely, a discretized input for generating the required output for the application. The convolution integral is often used to generalize a stepwise solution; this technique is built in the NTCF model.

In order to evaluate the integral mean values in Eq. (12), the $A(t)$ function has to be numerically determined at fine time sub-divisions in each time interval from the NTC run. Since the constant $A(t)$ function is applicable only to a strictly linear case, generalization is needed for non-linear models. This is accomplished in the basic model using a series of $A_i(t)$ functions and a generalized input variation matrix according to Eqs. (15) and (16), described later in the paper.

Higher-order polynomial connection between base points in the time domain may also be considered. The algorithms may be derived based on quadratic and higher-order boundary function interpolation polynomials as follows:

$$T(t) = L_0(T_i, T_{i+1}, \ldots) + L_1(T_i, T_{i+1}, \ldots) \cdot t + L_2(T_i, T_{i+1}, \ldots) \cdot t^2 + \ldots \tag{14}$$

where L_0, L_1, L_2, …are linear functions of T_i, $i = 1 \ldots N$. Substituting Eq. (14) into Eq. (10) and performing partial integration, the non-liner terms will yield interval-dependent constants, and the final result will still be a linear matrix operator in T.

In summary, the NTCF method applies a stepwise boundary variation in the NTC runs, and an averaged output evaluation of the responses to represent piecewise-linear, or higher-order polynomial boundary variations in the time domain. The averaging schematics are derived analytically. Numerical integrals are used to approximate the analytical expressions in the NTCF procedure. The results are implemented both in the NTCF runtime organizer to collect responses at fine time subdivisions, and in the post-processor to evaluate the NTCF matrices.

An example is given for comparing stepwise and piecewise approximation results for a simple heat conduction used in the MULTIFLUX and the NTCF tests [4,5]. The input variations and the responses are shown in Fig. 2.a and b, respectively. The test example uses an analytical solution, emulating an NTC with a fast-running and precise analytical-based numerical solution for algorithm testing. The model results are shown in Fig. 2.b using three different NTCF post-processing methods. The modified interval average process according to Eq. (13) is shown to be superior to other representations involving simple averaging and end-point responses.

Quasi-Linear NTCF Model

A quasi-linear NTCF model may be determined for non-linear cases using a generalization of $A_i(t)$ with the application of an $A_1(t), A_2(t),...$ series. First, the stepwise input variation along the columns in Eq. (6) is modified, by generalization, in order to narrow the range of variation in T around the $T^c=[T_1,...,T_N]^T$ central values. With an appropriate selection of the $f_1,...,f_{N-1}$ functions, the stepwise variations in the columns can be made close to the central values, while keeping the determinant of T non-zero. Narrowing the regime of T will provide a linearized h operator defined around T^C. The generalized input matrix is as follows:

$$T=\begin{bmatrix} T_1 & T_1 & T_1 & \cdots & T_1 \\ f_1(T_2) & T_2 & T_2 & \cdots & T_2 \\ f_1(T_3) & f_2(T_3) & T_3 & \cdots & T_3 \\ \vdots & \vdots & \vdots & & \vdots \\ f_1(T_N) & f_2(T_N) & f_3(T_N) & \cdots & T_N \end{bmatrix} \tag{15}$$

Second, a set of $q(\tau_i)$ matrices is obtained as result from the NTC for the T boundary conditions according to the columns in Eq. (15). The τ_i parameters are varied in the (0, 1] interval (excluding zero), where $\tau_t =1$ defines q responses at time-division end-points, while $\tau_i <1$ defines response at time sub-division i, a point in each time interval. Third, the $h(\tau_i)$ matrix (an intermediate result) is evaluated for each i time sub-division from Eq. (7), that is, $h(\tau_i)=q(\tau_i)*T^{-1}$. Fourth, the $A_1(\tau_i)$ is determined based on the definition of the indicial admittance, being a response to a unit boundary value change. Multiplying the $h(\tau_i)$ matrix with a unit step vector at t_1, the result will be a vector $[A_1(t_1-\tau_i*t_1), A_1(t_2-\tau_i*(t_2-t_1)),..., A_1(t_N-\tau_i*(t_N-t_{N-1}))]^T$, constituting $A_1(\tau_i)$. Fifth, the union of $A_1(\tau_i)$ for $i=1...M$ is taken to form a representation of $A_1(t)$ for the entire time regime given at fine time divisions. Finally, the process is repeated with unit step vectors at $t_2,...,t_N$, for obtaining $A_2(t),..., A_N(t)$, the functions needed for the averaging schematic in order to obtain piecewise linear (or higher-order) connection in the time domain. Instead of using Eq. (13), the final h matrix is evaluated as follows for the non-linear model, processed around the T^C central vector in this generalized case:

$$h=\begin{bmatrix} M\,[A_1]_0^{t_1} & 0 & 0 \\ M\,[A_1]_{t_2-t_1}^{t_2}-M\,[A_1]_0^{t_2-t_1} & M\,[A_2]_0^{t_2-t_1} & 0 \\ \vdots & & \vdots \\ M\,[A_1]_{t_N-t_1}^{t_N}-M\,[A_1]_{t_N-t_2}^{t_N-t_1} & M\,[A_2]_{t_N-t_2}^{t_N-t_1}-M\,[A_2]_{t_N-t_3}^{t_N-t_2}\cdots M\,[A_N]_0^{t_N-t_{N-1}} \end{bmatrix}$$

16)

In summary, the quasi-linear model identification applies the NTC results reported at fine time divisions for the determination of $A_1(t),..., A_N(t)$ generator functions, based on a series of $h(\tau_i)$ matrices, identified in a user-defined domain, e.g., a narrow vicinity of a T^C central boundary variation with time. The $A_i(t)$ generator functions, different in each column in Eq. (16), are used to generate the final h operator for this case.

Non-linear NTCF Functional Model Using Volterra Series Solution

It may be advantageous to pursue an expanded NTCF model fit over a wide range of boundary value variation, applying a Volterra series expression [1], a generalization of the single integral in Eq. (1):

$$q(t)=\int_{\tau=0}^{t} T(\tau)\frac{\partial}{\partial t}A_1(t-\tau)\,d\tau+$$
$$\int_{\tau=0}^{t}\int_{\tau=0}^{t} T(\tau_1)T(\tau_2)\frac{\partial^2}{\partial t^2}A_2(t-\tau_1,t-\tau_2)\,d\tau_1 d\tau_2+\int_{\tau=0}^{t}\int_{\tau=0}^{t}\int_{\tau=0}^{t}\cdots \tag{17}$$

Modification of Eq. (17) is introduced for NTCF model formulation, namely (a) factorization, (b) diagonalization, and (c) scaling. The fundamental difference between the NTC model-building and the conventional, non-linear system model identification is that a comprehensive NTCF model is desired to be built on sparse data, that is, a minimum number of NTC runs. Consequently, a successively improving Volterra series with modified, approximate kernels is seen as an advantageous strategy in NTC non-linear model identification.

(a) Factorization. The first modification to Eq. (17) is to approximate the derivative of the second, two-variable A_2 kernel with a product of two, one-variable functions, followed by similar simplification in the consecutive terms. For the second kernel as an example, it reads:

$$\frac{\partial^2}{\partial t^2}A_2(t-\tau_1,t-\tau_2)=\frac{\partial}{\partial t}A_{2,1}(t-\tau_1)\cdot\frac{\partial}{\partial t}A_{2,2}(t-\tau_2) \tag{18}$$

With this modification, Eq. (17) will not be same. However, the new functions, $A_{2,1}$, an $A_{2,2}$ will be adjusted to accommodate the change during model fitting.

(b) Diagonalization. The second simplification is introduced by equating $A_{2,1}$ with A_1. This simplification is considered to be of a weighting choice: for any $A_{2,1}$, an $A_{2,2}$ can be determined. Therefore, the unknown in the second kernel reduces to a one-variable function. Similar simplifications can be made in the consecutive kernels in the higher-order terms, reusing the previous kernels and adding always a new one-variable function.

After re-naming $A_{2,2}$ for A_2, the first two terms of the modified Volterra equation reads:

$$q(t) = \int_{\tau=0}^{t} T(\tau)\frac{\partial}{\partial t} A_1(t-\tau)\, d\tau + \int_{\tau=0}^{t} T(\tau)\frac{\partial}{\partial t} A_1(t-\tau)\, d\tau \int_{\tau=0}^{t} T(\tau)\frac{\partial}{\partial t} A_2(t-\tau)\, d\tau + \cdots \tag{19}$$

The justification for the simplification of the kernel, shown for the second term, is that it is not possible to identify a two-variable $A_2(t, \tau_1, \tau_2) \in R^2$ function from the result of a single $q \in R^1$ output variation. However, a "diagonal" approximation can be used as shown, based on a simplifying restriction regarding the function form.

The $A_1(t, \tau)$ function in the first factor of the second Volterra term is a mere weighting choice. Flexibility in the selection of the function form for the derivative of A_1 allows for other choices than the one described. Modification, e.g., with an additive constant, may be needed for avoiding zero values of the first integral that would result in singularity for the determination of the A_2 function from the second integral. For brevity, it is assumed in the further discussions that the integrals do not vanish in the *(0, t]* interval.

c. Scaling. Yet a third modification is needed to make the modified Volterra series successive, that allows for improving the model fit with additional terms, while keeping the previous terms unchanged. For this condition, the T boundary function is measured as a difference from the corresponding input boundary variation that is associated with a particular term. It is assumed that $T_0(t)$, $T_1(t)$, $T_2(t)$,… are used for generating the ${}^{N}q_0(t)$, ${}^{N}q_1(t)$, ${}^{N}q_2(t)$,… NTC outputs at fine τ_l time divisions. The following scaling is used in the integrals with the first, second, third, etc kernels:

$$I(T - T_0, A_1^{'}, t) = \int_{\tau=0}^{t} [T(\tau) - T_0(\tau)] A_1^{'}(t-\tau)\, d\tau \tag{20}$$

$$I(T - T_1, A_2^{'}, t) = \int_{\tau=0}^{t} [T(\tau) - T_1(\tau)] A_2^{'}(t-\tau)\, d\tau \tag{21}$$

$$I(T - T_0, A_3^{'}, t) = \int_{\tau=0}^{t} [T(\tau) - T_3(\tau)] A_3^{'}(t-\tau)\, d\tau \tag{22}$$

⋮

With the notations used in Eqs. (20)-(22), the modified Volterra series is as follows:

$$\begin{aligned} q(t) = {} & q_0(t) + \\ & I(T - T_0, A_1^{'}, t) + \\ & I(T - T_0, A_1^{'}, t) \cdot I(T - T_1, A_2^{'}, t) + \\ & I(T - T_0, A_1^{'}, t \cdot I(T - T_1, A_2^{'}, t) \cdot I(T - T_2, A_3^{'}, t) + \cdots \end{aligned} \tag{23}$$

In Eq. (23), the initial T_0 may be zero, constant, or a "virgin value" variation, caused by another process. For $T=T_0$, $q= q_0$, that may be non-zero, if the NTC model defines a non-homogeneous initial and boundary condition problem. As seen in Eq. (23), T_1 affects only second term, T_2 only the second and third terms, etc. This property allows for the explicit determination of the A_1, A_2,... successively from a forward progression.

The first term in Eq. (23) is identical to the NTC result for the T_0 input, therefore, $q_0(t)= {}^{N}q_0(t)$. The $A_1(t)$ in the second term of Eq. (23) is identified using the T_1 input and the ${}^{N}q_1(t)$ output. Eqs. (20) and (23) give:

$${}^{N}q_1(t) - {}^{N}q_0(t) = \int_{\tau=0}^{t} [T_1(\tau) - T_0(\tau)] A_1^{'}(t-\tau)\, d\tau \tag{24}$$

The $A_1(t)$ generator function in Eq. (24) can be determined using inverse convolution. Since the $T_1(t)$-$T_0(t)$ function is stepwise, changing only at $t_1, t_2, \ldots, t_N$ time instants, the integral can be decomposed, and $A_1(\tau)$ be determined at fine τ sub-divisions from the NTC results. Using the notation of Eq. (9):

$$A_1(t) = iconv[{}^{N}q_1(t) - {}^{N}q_0(t),\ T_1(t) - T_0(t)] \tag{25}$$

The $A_2(t)$ function in the third term of Eq. (23) is identified using the T_2 input and the ${}^{N}q_2(t)$ output. Using Eqs. (21) and (23), the convolution integral with the unknown $A_2(t)$ function can be expressed:

$$\frac{{}^{N}q_2(t) - {}^{N}q_0(t)}{I(T_2 - T_0, A_1^{'}, t)} - 1 = \int_{\tau=0}^{t} [T_2(\tau) - T_1(\tau)] A_2^{'}(t-\tau)\, d\tau \tag{26}$$

From Eq. (26), $A_2(\tau)$ is determined by inverse convolution:

$$A_2(t) = iconv[\frac{{}^{N}q_2(t) - {}^{N}q_0(t)}{I(T_2 - T_0, A_1^{'}, t)} - 1,\ T_2(t) - T_1(t)] \tag{27}$$

The procedure for the third and higher Volterra series terms can be repeated. Each time, a new NTC run is needed for input. The general equation for the third term is:

$$\frac{{}^{N}q_3(t) - {}^{N}q_0(t)}{I(T_3 - T_0, A_1^{'}, t)\, I(T_3 - T_1, A_2^{'}, t)} - \frac{1}{I(T_3 - T_1, A_2^{'}, t)} - 1 = \int_{\tau=0}^{t} [T_3(\tau) - T_2(\tau)] A_3^{'}(t-\tau) d\tau \tag{28}$$

$A_3(\tau)$ is determined by inverse convolution from the left hand side of Eq. (28):

$$A_3(t) = iconv\left[\frac{{}^{N}q_3(t) - {}^{N}q_0(t) - I(T_3 - T_0, A_1^{'}, t)}{I(T_3 - T_0, A_1^{'}, t)\, I(T_3 - T_1, A_2^{'}, t)} - 1, T_3(t) - T_2(t)\right] \tag{29}$$

In summary, the first four elements of the third-order, modified, approximate Volterra series functional model are completed. The successive procedure may continue by adding new terms.

A few examples are given with first-, second-, and third-order Volterra series NTCF models. Other, basic NTCF models are tested elsewhere [4, 5]. In addition, the first-order Volterra series solution provides a test for the simplest NTCF model. The NTCF model tests use NUFT as an NTC, calculating temperature-driven, time-dependent heat and moisture fluxes on the surface of a conceptual emplacement tunnel at Yucca Mountain, Nevada. The set-up of the NTC model is identical to the test cases used in [5] for Yucca Mountain. Based on previous experiences with the problem, nearly linear and slightly non-linear models are expected, respectively, for the heat and the moisture fluxes. Figure 3 shows the stepwise input temperature variations, T_0, T_1, T_2, and T_3, used for the various NTCF models identification. Figure 4 depicts two different input temperature variations, T_a, and T_b, both still stepwise, for NTCF functional model fitness tests. Both T_a, and T_b are significantly different in shape from the T_0, T_1, T_2, and T_3 inputs to provide for NTCF model validation.

Comparison between the predictions of the three NTCF models and the NTC (NUFT) results for heat is shown in Fig. 5. Figure 5 a proves that all the NTCF models achieve perfect fit for the NTC heat fluxes, used as input data for model identification. The agreements prove that the identification procedure is correct and the models reproduce the values used for their identification as inputs. Figures 5 b and c show the results of three different NTCF models against the direct NTC results for the two different model fitness tests; the results yield nearly perfect agreement for all models.

The three NTCF models and the NTC (NUFT) results for moisture flux are shown in Fig. 6 a-c. Figure 5 a proves that all the NTCF models achieve perfect fit to the NTC results, verifying the algorithms. Figures 6 b and c show the fitness test results of three different NTCF models against the direct NTC results for the two different model fitness tests; the results show that the NTCF models improve with increasing order; however, the 2nd-order model is nearly as good as the 3rd-order model.

Non-linear NTCF Matrix Model Using Volterra Series Solution

The method described using piecewise-linear or higher-order polynomial connections between base points of the boundary values can be used to transform the continuous-time functional model into a discrete-time matrix model. For piecewise approximation, Eq. (13) can directly be applied to form h_1, h_2, h_3,… matrices from the A_1, A_2, A_3, … generator functions. With this, the NTCF matrix model from the Volterra functional is as follows:

$$\begin{aligned} q = q_0 + {} & \\ & h_1(T - T_0) + \\ & [h_1(T - T_0)] * [h_2(T - T_1)] + \\ & [h_1(T - T_0)] * [h_2(T - T_1)] * [h_3(T - T_2)] + \cdots \end{aligned} \tag{30}$$

The star sign in Eq. (30) denotes an element-by-element multiplication between vectors.

Two examples are given using NTCF matrix operator models based on the previous examples. The input temperature variations are shown in Figure 7, piecewise-linear for both T_a, and T_b. The NTCF model results versus the NTC (NUFT) piecewise-linear input boundary function results are shown in Fig. 8 for heat and Fig. 9 for moisture fluxes. The results show excellent agreement between the NTCF models and the NTC results for heat for all models. For moisture flux, a 2nd, or 3rd-order model is seen to be in need for efficient modeling with a good predicting power. However, all models provide perfect fit for the input variations used in the model identification, and the trade-off between more frequent re-functionalization vs. increase in the nonlinear NTCF order must be carefully weighted.

NTCF Model for Multivariate, Multi-dimensional problems

Similar treatment can be used for more than one variable and for domains of more than one layer in the NTC model. A typical example for a two-variable, one-layer quasi-linear model is the transport of heat and moisture in a two-dimensional domain:

$$qh = hh(T - T_0) + hm(P - P_0) \tag{31}$$

$$qm = mh(T - T_0) + mm(P - P_0) \tag{32}$$

The heat and the moisture fluxes as time-dependent vectors, qh and qm, are functions of both temperature and partial vapor pressure vectors, T and P. Four coefficient matrices can be determined using the NTCF procedure, using built-in functions in MULTIFLUX [6]. The model in this simplest, quasi-linear form captures both temperature-driven main effects, and vapor pressure-driven cross effects. Other forms with user-defined equations may also be used.

An example of a multi-dimensional problem is heat and moisture transport in a three-dimensional domain. Figure 10 shows a four-layer model for which flow interactions between the layers are to be included. The T and P, time and layer-dependent variables are super-vectors, and the matrix coefficients are super-matrixes. A two-variable, eight-layer NTCF model is used in [6].

APPLICATIONS

Linearized NTCF Applications

An independent industry group, Bechtel-SAIC Corp. (BSC), Yucca Mountain Project, Nevada, has compared the NTCF-based MULTIFLUX results with the results using a conventional ANSYS solution for a ventilation test problem [7]. The comparison of temperatures is shown in Fig. 11. This study proved that the transport processes in the rock were correctly modeled through the application of the NTCF methodology and that correct balancing was achieved between the NTCF and CFD modules, responsible for modeling the heat and moisture transport in the airway. Three repetitions of the functionalization, as outside iterations with updated T^C and P^C central boundary values, were needed due to NTC (NUFT) model non-linearities. Very significant increase in the computational efficiency was achieved using MULTIFLUX, due to the repeated application of the NTCF model, without actually re-running the NTC (NUFT) model in each iteration step.

Validation tests of the MULTIFLUX code with the NTCF method were made recently [4,5]. One set of tests [4] were made using a quasi-three-dimensional convection-conduction ventilation problem for comparison. The method was to compare solutions to the test problem with the use of MULTIFLUX to the reference, analytical solution. The reference calculation was generated by John Walton, Professor, University of Texas, El Paso, using a Carslaw and Jaeger analytical solution [4]. The other solution was made with MULTIFLUX. First, a linearized NTCF model was identified for an arbitrary, small T^C temperature variation within the expected regime using NUFT. Second, a simple CFD model for the air convection was configured within MULTIFLUX, using 500 longitudinal divisions, as cells, along the air flow. Third, the NTCF wall model and the airflow model were coupled, by equating the temperature and heat flux at each division point and time interval. Figure 12 shows the air temperature history comparisons at 1m, 250m and 500 m distances along the airway between the MF and other reference solutions [4]. The test demonstrated that the linearized NTCF model in MF was capable of accurately modeling the time dependent heat flow. It was proven that re-functionalization was not needed in this low-temperature, nearly linear case. Since only one functionalization was necessary, the MF code produced results faster than the analytical solution, re-using the same matrix model in each cell, although numerical coupling and iterations were needed between the convection in the air channel and the conduction in the wall.

In thermohydrologic-ventilation simulations, the NTCF method may reduce the complete simulation time from several years to a few days or weeks assuming the same computer simulation platform [6].

CONCLUDING REMARKS

As a sub-set of system identification, a new modeling approach is presented to model an existing NTC model.

Simple, linear, or linearized models are described based on known techniques, with a new approach to represent higher-order interpolation in the boundary-value variations in the NTC model, based on stepwise variation as boundary condition in the NTC model. The NTCF model is presented in a matrix-vector form, the most efficient in computation.

A simplified, successive Volterra series NTCF model is described for non-linear applications, both in time-continuous functional, as well as in discretized, matrix operator forms. The diagonal approximation and the weighting choice used in the formulation are seen to have considerable advantages in increasing modeling efficiency. Adding new terms in the Volterra series based on generating new NTC results can compensate for the approximation in the previous, imperfect terms in the series. The accuracy of the NTCF model can be increased by increasing the number of NTC runs used for NTCF model identification.

Numerical examples are presented using heat and moisture fluxes of NTCF model outputs as responses to inputs of first-kind temperature and partial vapor pressure boundary conditions. This input-output selection is used as an example. It is also possible to identify an inverse NTCF model in which second-kind input boundary conditions are applied. For example, boundary heat flux may be an NTCF model input for which surface temperature will become an output. It is interesting to observe that an inverse NTCF model may be derived by directly inverting the NTCF matrix equation. For example, $T=h^{-1}*q$ may directly be obtained from Eq. (4). Such a technique has been used in NTCF model applications in MULTIFLUX [7].

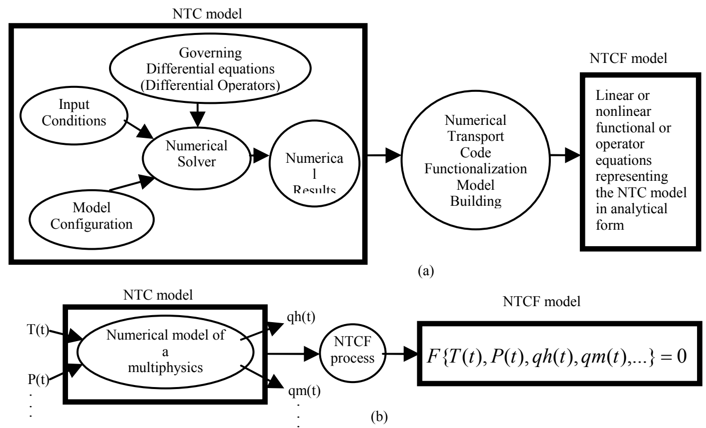

Figure 1. (a) Logical and (b) data flow charts of the NTCF model identification.

ACKNOWLEDGMENTS

The most able assistance of Mr. D. Bahrami is gratefully acknowledged in preparing the figures and performing the NUFT calculations for the tests.

REFERENCES

[1] Eykhoff, P., 1974. “System Identification, Parameter and State Estimation.”, John Wiley & Sons, (2e)

[2] DeFigueiredo, R. J. P., Dwyer, T. A. W, III, 1980. “A Best Approximation Framework and Implementation for Simulation of Large-Scale Nonlinear Systems.” IEEE Transactions on Circuits and Systems, vol. CAS-27, No. 11, November 1980.

[3] Carslaw, H. S., Jaeger, J. C.(1986), Conduction of Heat in Solids (2e), p. 30.

[4] Danko, G., 2003. “Coupled Hydrothermal-Ventilation Studies for Yucca Mountain.” Annual Report for 2003. NWRPO-2003-05, Pahrump, Nevada: Nye County Department of Natural Resources.

[5] Danko, G., Bahrami, D., and Lanka, S., 2003. "Technical Support Services for the MULTIFLUX Software." MOL.20031208.0025, Final Report, submitted to BSC, Nevada: Bechtel SAIC Company.

[6] Danko, G., 2004. "Heat and Moisture Flow Simulation with MULTIFLUX." Proceedings of ASME, Heat Transfer/Fluid Engineering, July 11-15, 2004, Charlotte, North Carolina, USA.

[7] BSC (Bechtel SAIC Company). 2002. "Ventilation Model." ANL-EBS-MD-000030 REV. 01D. Las Vegas, Nevada: Bechtel SAIC Company.

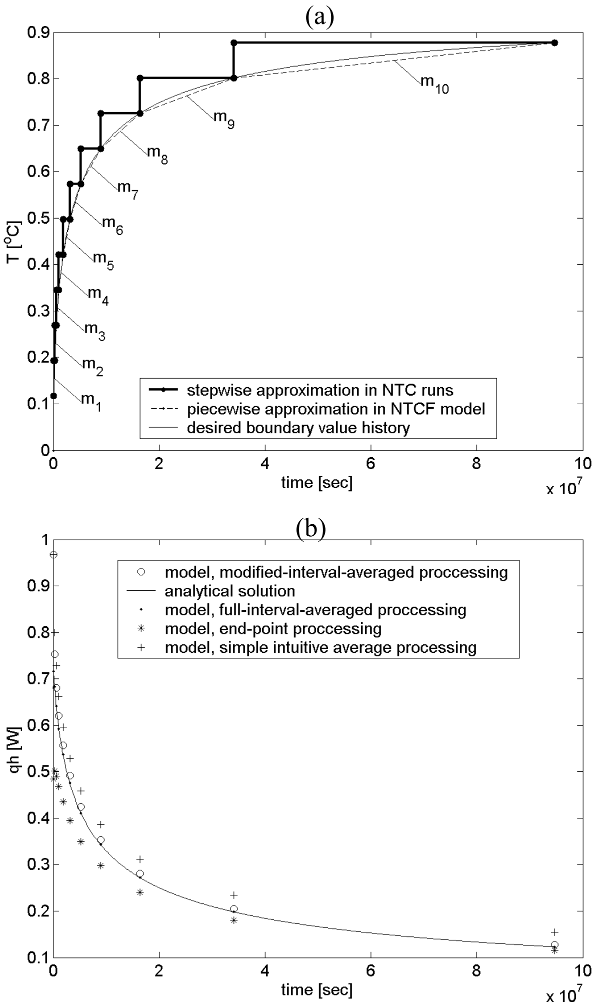

Figure 2. (a) Stepwise and piecewise input approximations for NTCF algorithm tests (b) Results of three different NTCF post-processing methods.

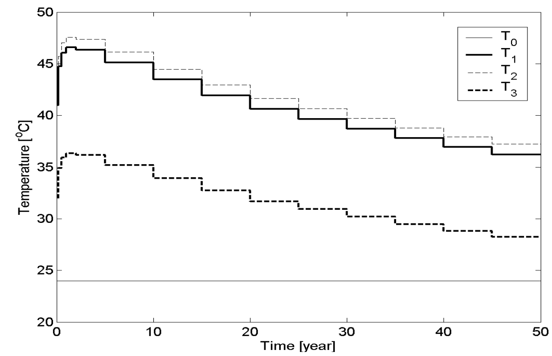

Figure 3. Stepwise input temperature variations used for NTCF models identification.

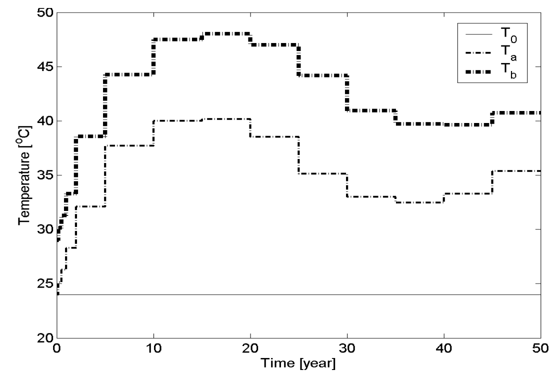

Figure 4. Stepwise input temperature variations used for NTCF functional model fitness tests.

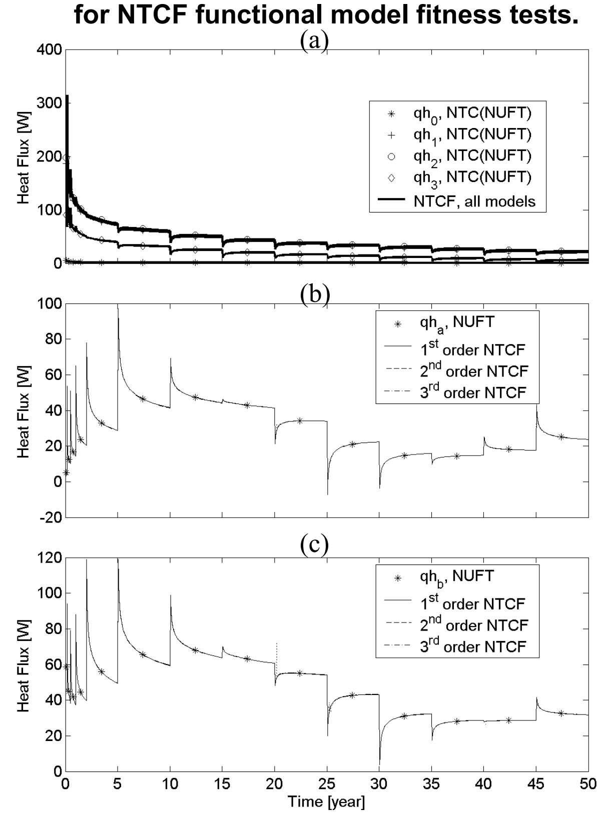

Figure 5. Comparison between the 1st, 2nd, and 3rd – order NTCF model results and the NTC (NUFT) results for heat flux; (a) back-calculated results used for model identification, (b) and (c) two NTCF model fitness test results against direct NTC (NUFT) results.

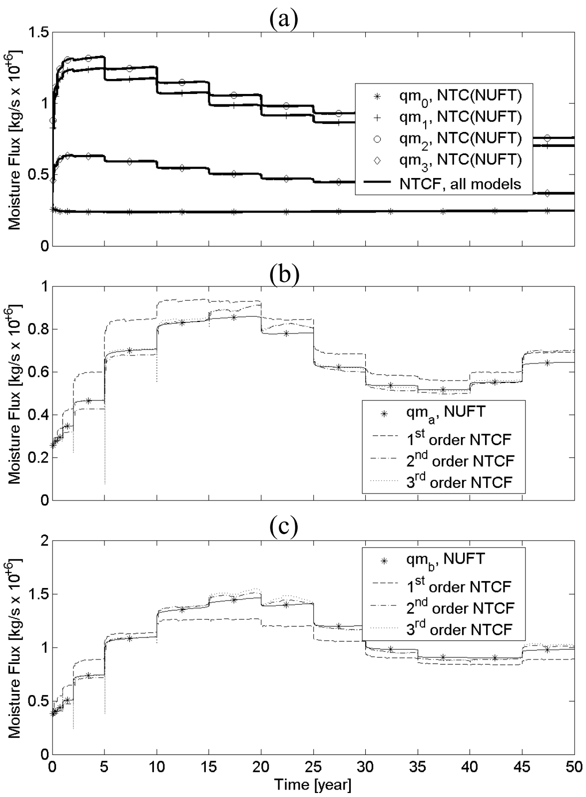

Figure 6. Comparison between the 1st, 2nd, and 3rd –order NTCF model results and the NTC (NUFT) results for moisture flux; (a) back-calculated results used for model identification, (b) and (c) two NTCF model fitness test results against direct NTC (NUFT) results.

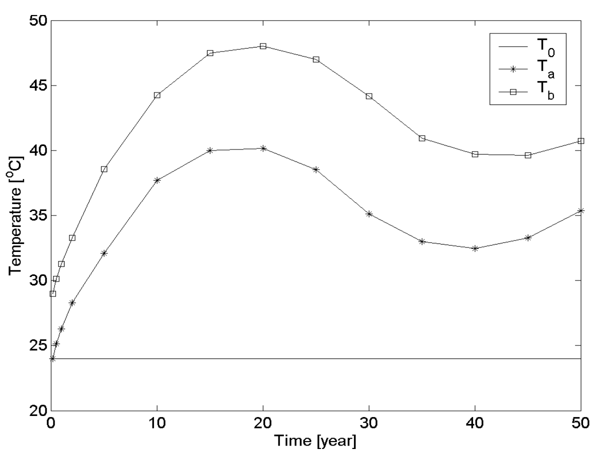

Figure 7. Piecewise-linear input temperature variations for T_a, and T_b.

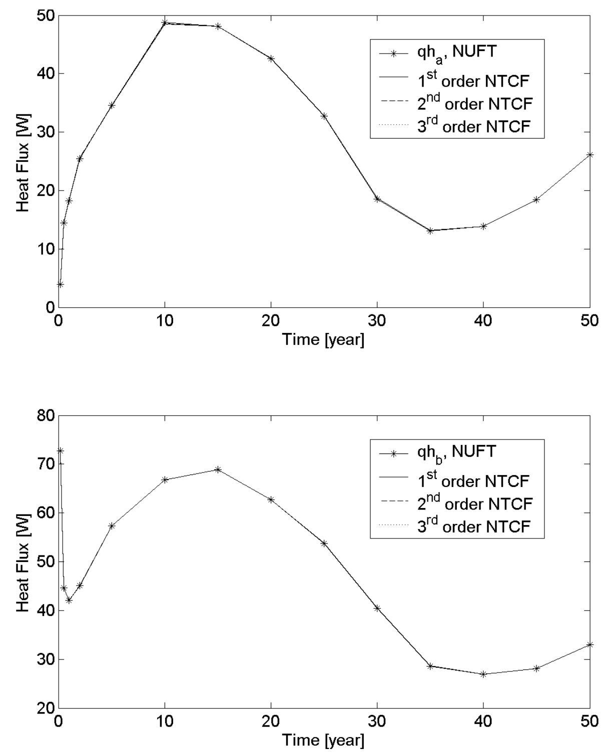

Figure 8. All NTCF model results versus the NTC (NUFT) piecewise-linear input boundary function results for heat flux.

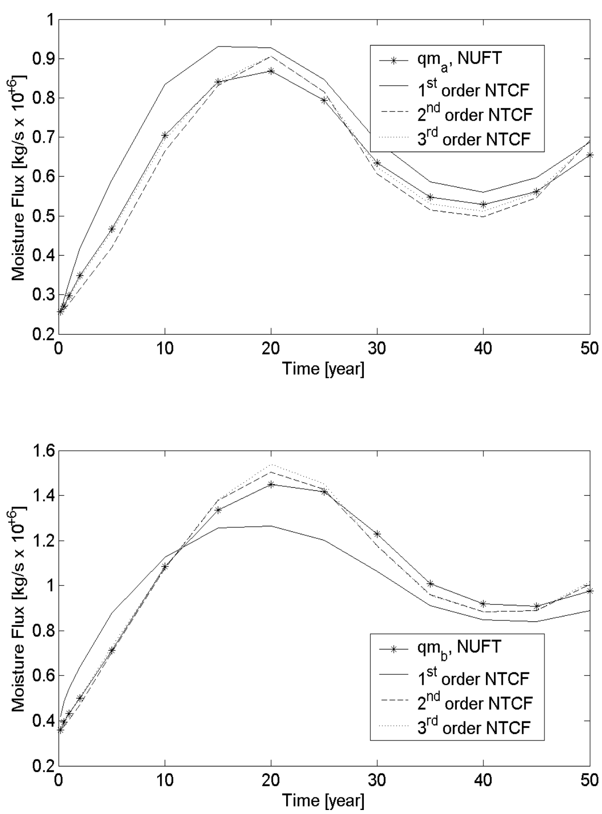

Figure 9. All NTCF model results versus the NTC (NUFT) piecewise-linear input boundary function results for moisture flux.

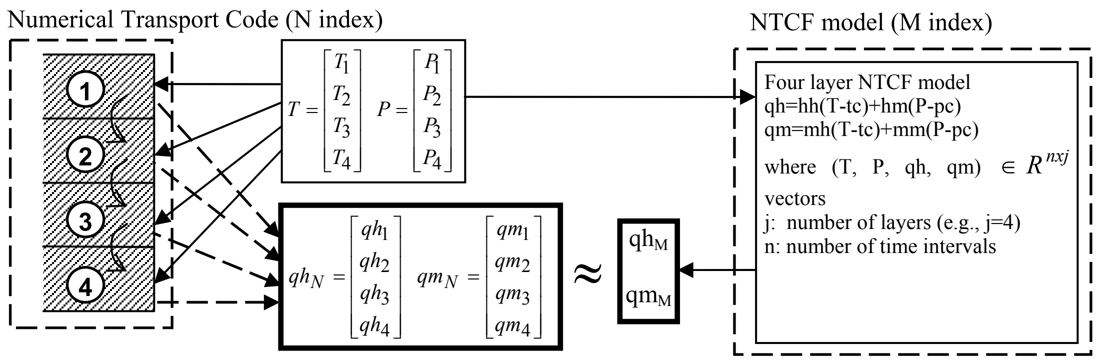

Figure 10: Application example of an NTC model (N index) and corresponding NTCF model (M index) for a four-layer model.

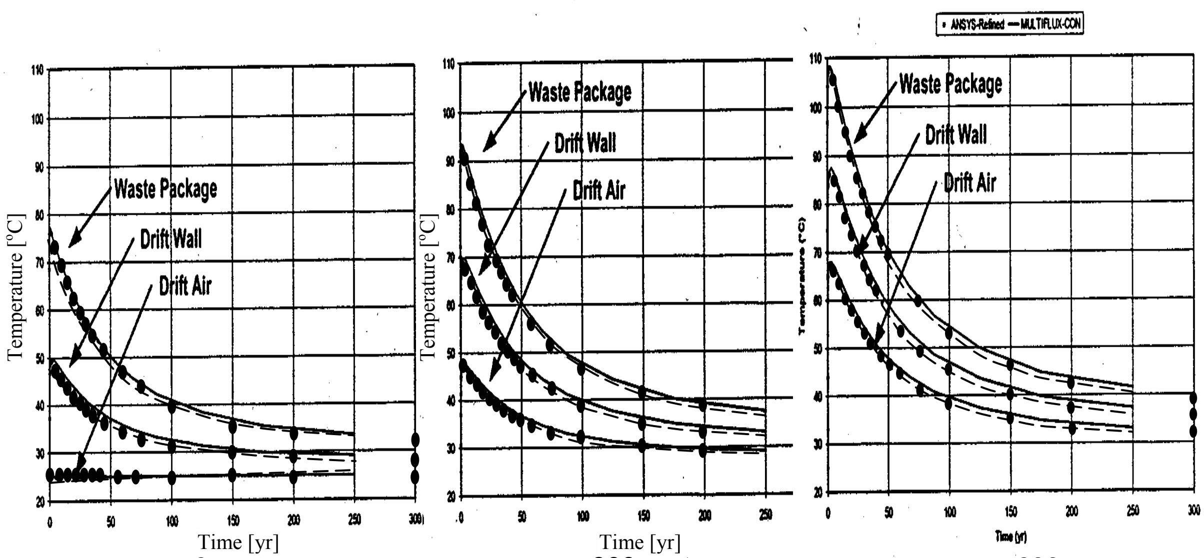

Figure 11. Ventilation calculation results of the NTCF-based MULTIFLUX (solid lines) and ANSYS (dots) [7].

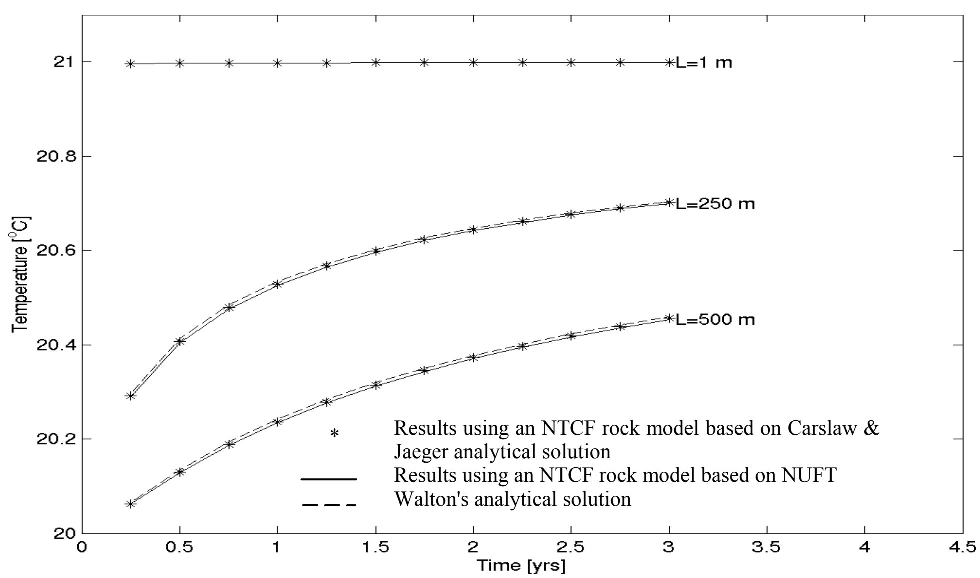

Figure 12. Air temperature history comparisons at 1m, 250m and 500 m distance along the airway between a reference analytical solution according to Walton, and MULTIFLUX with NUFT as well as Carslaw & Jaeger rock models. [4].

Preprint 04-144

COUPLED, MULTI-SCALE THERMOHYDROLOGIC-VENTILATION MODELING WITH MULTIFLUX

G. Danko
D. Bahrami
Univ. of Nevada
Reno, NV

ABSTRACT

Spatial and temporal temperature and humidity variations for 5000 years are simulated in an emplacement airway within the conceptual, high-level nuclear waste repository proposed to be built at Yucca Mountain, Nevada. A multi-scale model is configured using MULTIFLUX, a thermohydrologic-ventilation code. The predicted surface temperature of most waste packages during post-closure exceed 140ºC, the threshold limit known for likely localized corrosion for Alloy 22 waste package material. Small amounts of infiltration air flow through the mountain in Panel 5 are found to transport liquid water condensate to some of the waste packages emplaced along the peripheral section of the drift due to edge cooling.

INTRODUCTION

Ventilation calculations are part of the thermal and hydrologic studies necessary for supporting the design of a high-level nuclear waste repository. In general, there are three main purposes for ventilation calculations: (1) to predict temperature variation with time in the emplacement airways, called drifts, during the pre-closure time period of construction and waste emplacement; (2) to determine the initial conditions, both in rockmass temperature and humidity distributions, for the thermohydrologic analysis for the post-closure time period; and (3) to analyze the evolution of the temperature and humidity distributions with the effect of air infiltration through the repository system during the most critical, first few thousands of years of the post-closure time period. A complete ventilation analysis, directed at the three main purposes, was successfully completed using the coupled theromohydrologic-ventilation model and software MF3.0, for a conceptual repository design at YM (Danko and Bahrami, 2003, Danko, 2003).

Pre-Closure Ventilation Analysis

The temperature peak evolution during the pre-closure time period has been studied using simple and approximate ventilation model configurations, described in the AMR Rev01D report (BSC, 2002). The calculations used the ANSYS-based BSC ventilation software and a previous MULTIFLUX version, MF2.3, and were in close agreement. Both software products can be configured to realize an approximate model for the prediction of the overall temperature evolution during pre-closure. A recent, follow-up study confirmed the agreement between MF3.0 and the ANSYS-based BSC ventilation model (Danko et al., 2003). The MF3.0 ventilation model produced a complete temperature and relative humidity simulation of a 600 m drift section for a 300 year operation in 20 minutes, an unparalleled performance when compared to the BSC ventilation calculation requiring several days of computation. In addition, the MF3.0 model is NUFT-based which includes the theromohydrologic processes in the rockmass (Nitao, 2000), unlike the BSC ventilation model that is ANSYS-based, incorporating only heat conduction in the rock surrounding the ventilated drift. The pre-closure ventilation simulation with a theromohydrologic model configured using MF3.0 was found not only to be more efficient than the conduction-only model, but it also provided important theromohydrologic initial conditions for post-closure simulations.

Linkage between Pre-Closure and Post-Closure Thermal Analyses

Pre-closure ventilation affects the initial conditions for post-closure, and likewise the thermal performance of the repository for an extended period of time. It is important to simulate pre-closure thermal performance for establishing accurate post-closure initial conditions. The predicted thermohydrologic parameters for post-closure may be affected by many uncertainty factors. Calculation error components may include the effects of (a) uncertainties in the input parameters and/or rock thermal properties, such as lithophysal thermal conductivity (Danko et. al, 2003); (b) modeling approximations; and (c) numerical inaccuracies. Some design errors, due to modeling uncertainties, may be compensated for during pre-closure. Based on monitoring the temperature evolution of the repository, the operation parameters may be adjusted as a compensatory measure. For example, the ventilation air quantity, or the duration of the open-loop ventilation may be manipulated in order to adjust the temperature fields to the desired level during pre-closure.

The nature of post-closure thermohydrologic issues is very different from that of pre-closure, since it is extremely difficult to contemplate any remedial course that may be necessary for design error correction after permanent closure of the repository. The thermal effects are slow in evolution, making the reliance on pre-closure monitoring and extrapolation operatively ineffective: once built, the repository cannot be easily modified for temperature corrections. The thermal analysis of the post-closure time period must be of the highest accuracy and it must be based on accurate initial conditions affected by the pre-closure operation that includes ventilation. An integrated model is needed that links the pre- and the post-closure periods with thermohydrologic coupling. Such a model may be configured using MF3.0, of which the pre- and the post-closure simulations are performed within one integrated task (Danko and Bahrami, 2003).

Post-Closure Analysis with Air Infiltration

The thermal and hydrologic issues for the post-closure time period are often related to performance, involving the effects upon the release of radionuclides. However, the first few hundred or thousand years, which are the most critical time periods regarding the thermal surge, are also of paramount importance to the safety of the elements of the repository system. Underlying the criticality of the temperature surge during post-closure is that overheating may result in uncorrectable consequences in the long-term containment performance of the repository. For example, the temperature of the fuel rods within the waste packages must stay below the limit for the cladding, in order to avoid compromising the integrity of the internal structure of the waste packages. Another problem with high operating temperature may be that of waste package corrosion. If the waste package is constructed of Alloy 22, the threshold of crevice corrosion is about 140ºC, which should not be exceeded in order to avoid the onset of localized corrosion of the waste packages (Farmer, 2003).

Passive, long-term, mountain-scale air infiltration will likely develop through the natural fracture system at Yucca Mountain (Stuckless and Toomey, 2003, Danko and Bahrami, 2003). Air flow will permeate through the mountain and the emplacement drifts generated by the density difference between the incoming cold and dry and exiting hot and humid air. The effects of theromohydrologic-driven air infiltration were studied for a previous conceptual design with a long pre-closure ventilation period of 300 years (Danko and Bahrami, 2003, Danko, 2003). During pre-closure, fan-driven ventilation was assumed for 30 years. Natural, buoyancy-driven ventilation through open shafts and tunnels was assumed until year 300 at which time the intake and exit airways were assumed to be backfilled with broken rock. The combined effect of waste decay heat and moisture evaporation was shown to move an infiltration mass flow rate approximately equivalent to a ventilation air flow rate of 0.1 kg/s in each emplacement drift for thousands of years. The variable rate of air infiltration with time through the rubble-backfilled ventilation shafts was iteratively evaluated by balancing the pressure loss of the air flow with the buoyancy pressure gain across the mountain.

Thermohydrologic or Thermal Modeling in an Emplacement Drift with Ventilation

A ventilation model describing only dry, two-dimensional (2D) heat transport in the rock with distributed line heat load in the drift represents the simplest modeling approach (BSC, 2002). Recent investigations (Buscheck et al., 2003, Manepally and Fedors, 2003) describe more advanced models with edge-cooling phenomena using multi-scale thermohydrologic models (MSTHM).

Buscheck et al. (2003) applied the superposition of four sub-models: (a) a three-dimensional (3D), smeared-source, mountain-scale heat conduction-only model, (b) a line-averaged, 2D, drift-scale thermohydrologic model, (c) a smeared-heat-source, one-dimensional, drift-scale heat conduction model, and (d) a drift-scale, discrete-source, 3D, heat conduction and radiation model, based on effective thermal conductivities. The effect of ventilation was simulated separately using an ANSIS-based ventilation model, de-coupled form the MSTHM analysis. Re-coupling ventilation to the thermohydrologic model was accomplished by reducing the waste heat load output by the amount of heat removed by the air in the MSTHM. However, the rock drying caused by pre-closure ventilation was not included in the MSTHM.

Manepally and Fedors (2003) applied only two sub-models, (a) a 3D mountain-scale heat conduction model, and (b) a 2D drift-scale thermohydrologic model, based on Multiflo v1.5 (Lichtner et al., 2000). The coupling of the two sub-models was made by determining a time- and location-dependent edge-cooling reduction factor from the temperature field results of the mountain-scale model simulation, and applying it as a heat-load reduction factor in the drift-scale thermohydrologic model. The effect of ventilation was modeled by reducing the waste decay heat by the amount of heat removed by the air in the drift-scale model. The heat convection and radiation in the drift was modeled using a constant, effective thermal conductivity of the air.

Considering the effect of ventilation during the simulation, neither multi-scale thermohydrologic models incorporated the effect of moving air in the emplacement drift with variable temperature and humidity along the flow path. Recent, natural heat convection studies by Itamura et al. (2003) described axial air recirculation flows in a short section of an emplacement drift, using a CFD model with FLUENT. However, the CFD model included only heat flow, and was not coupled to the model of the rockmass.

Danko and Bahrami (2003) applied an integrated drift- and mountain-scale rockmass model, coupled to the in-drift ventilation model with air movement. However, the mountain-scale model-element used a preliminary configuration, incorporating only heat conduction, unlike the model-element used in the present analysis.

A summary of various models reviewed is given in Table 1 for comparison.

Table 1. Comparison of Models Studying Thermohydrologic Conditions in an Emplacement Drift with Ventilation

Publication reference	Mountain-scale heat flows included	The multi-scale solution is based on superposition	Ventilation is coupled to mountain-scale flows	Ventilation model is part of the porous-media rock model	Ventilation is modeled using a CFD code	Waste package-scale relative humidity variations are predicted
BSC (2002)	no	N/A	no	no	no	no
Buscheck et al. (2003)	yes	yes	no	yes	no	no
Danko and Bahrami (2003)	yes	no	yes	no	yes	yes
Manepally and Fedors (2003)	yes	no	no	yes	no	no
Webb et al. (2003)	no	N/A	no	no	yes	no

Study Goals

A modified, updated conceptual design arrangement is analyzed in the present study. Following the most recent DOE design (MacKinnon, 2003), the pre-closure ventilation time period is only 50 years, after which the access shafts and tunnels are assumed to be backfilled and tightly sealed. The goal of the study is to evaluate the spatial and temporal variations of temperature and relative humidity in an entire emplacement drift for the most critical, first 5000 years.

DESCRIPTION OF THE THEROMOHYDROLOGIC-VENTILATION MODEL

The Integrated Pre- and Post-Closure Task

Temperature and relative humidity variations are analyzed from the beginning of waste emplacement for a 5,000-year period that includes two distinct thermal cycles, one during the pre-closure, and one during the post-closure time periods. The following ventilation conditions are specified:

- The drift is mechanically ventilated with a forced, constant air flow rate of 15 m^3/s for 50 years, using fan(s),
- With the access shafts and connecting tunnels backfilled and sealed, the emplacement drifts are exposed to natural air infiltration during post-closure through the fracture system of YM until the end of the study time period. It is assumed that the emplacement drifts are not backfilled, and that the gradual collapse of the drifts over time will not prevent the slow flow of air through the drifts in axial direction.

The Conceptual Repository Arrangement and Model

The arrangement follows the conceptual design developed by DOE (MacKinnon, 2003) using five emplacement panels at YM, shown in Figure 1. One emplacement drift at the center location of Panel 5 is selected for the present analysis. Panel 5 is surrounded by unheated edges and, therefore, will likely develop a temperature field colder around the edges than in the center. An air flow across such a temperature distribution in any direction may give rise to moisture condensation along the relatively cold exit edge sections. This edge-cooling effect phenomenon will affect all the panels shown in Figure 1, but Panel 5 is selected for modeling simplicity.

A post-closure airflow in the drift in any direction may develop since both ends of each drift are connected to the atmosphere through the natural fracture system at YM. A small airflow may not affect the temperature field significantly; however, it may carry heat-driven moisture from the relatively hot, middle section of the emplacement drift toward the cooler exit section. Under certain conditions, condensation may occur, generating liquid-phase water in the emplacement area. The thermohydrologic model configured in MF3.0 includes model-elements that describe the large-scale air movement and related psychrometric processes in the in the emplacement drift.

Stuckless and Toomey (2003) argue, on the basis of natural analogues, that such large-scale air flows will develop at YM. Buoyancy-driven, large-scale air infiltration flow across the emplacement area with engineered shaft backfill was shown in a previous study using MF3.0 simulation (Danko and Bahrami, 2003). The subject of the present analysis is to include only natural air infiltration through YM.

A conceptual model domain for natural airflow is shown in Figure 2. It is reasonable to assume that a flow area square in cross-section will be available to channel air infiltration to each drift, with sides of the square equal to the center-to-center drift spacing as a minimum dimension. The intake and exit columns are close to the Solitario and Ghost Dance fault zones at YM, making them likely to connect to the atmosphere through natural fractures and connected lithophysal cavities in the rock. High air permeabilities in the order of

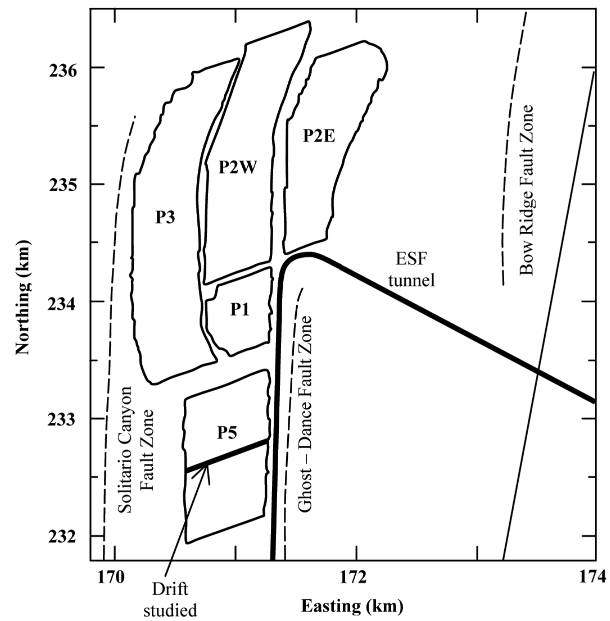

Figure 1. Plan of conceptual emplacement panels at Yucca Mountain (After MacKinnon, 2003).

$3*10^{-11}$ to $9*10^{-11}$ m^2 were reported around the fault zones at YM in U.S. Geological Survey investigations. (LeCain, 1997, Rousseau et al., 1999, LeCain et al., 2000). A mean permeability value of $6*10^{-11}$ m^2 is used for the intake and exit rockmass in the natural air infiltration model domain of the present study.

In a previous study (Danko and Bahrami, 2003), a nearly constant air mass flow rate of 0.1 kg/s with time was obtained from the balancing iterations equating the buoyancy pressure driving force with the air flow pressure loss in each emplacement drift. The same modeling approach is followed in the present study.

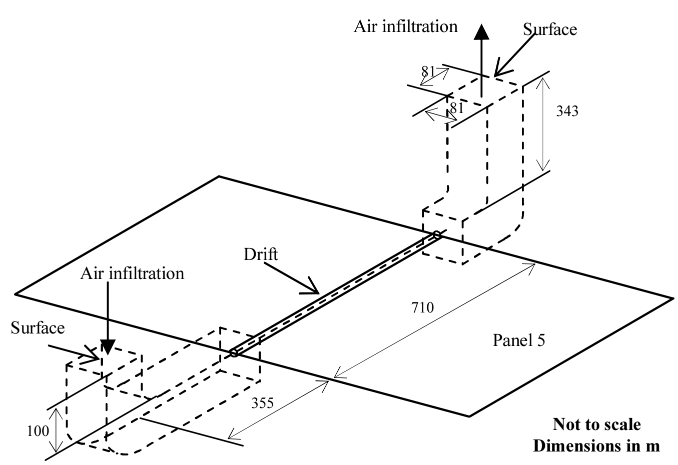

Figure 2. Conceptual model domain for natural air infiltration

The thermohydrologic-ventilation model is used to determine a balanced, likely infiltration air flow rate as a function of time for the assumed geometry and permeability. Since the resistance to the air flow through natural fractures at YM may be considered uncertain, the balanced infiltration air flow rate from the MF3.0 calculation results is perturbed, taking two higher, and one lower air flow rate variations. The two increased air flow rates are multiples of 20 and 2 of the balanced air flow rate variation, while the decreased air flow rate is ½ of the balanced flow rate variation. The four infiltration air flow variations are referred to as high, medium, balanced, and low.

The geometry of the rockmass surrounding the center drift in Panel 5 is shown in Figure 3. Two peripheral drifts located perpendicular to emplacement drifts act as manifolds to distribute and collect air flows for the emplacement drifts in Panel 5, of which only 3 are indicated in Figure 3. The two vertical shafts, an intake and an exhaust, are used to connect the peripheral drifts to the atmosphere for pre-closure ventilation, also shown in Figure 3. The peripheral drifts and the shafts, however, are assumed to be backfilled and completely sealed during the assumed repository closure at year 50.

The Model of the Rock Domain

The rock domain, shown in Figure 3, is divided into 8 three-dimensional (3D) mountain-scale rock cells (i=1...8) surrounding the entire drift. The unheated rock area at each edge is further divided into 4 connected rock cells. Symmetry is assumed between i=4 and i=5, bounded with an adiabatic surface, dividing the entire rock domain into two mirrored halves, an entrance and an exit drift section area. Each section includes 4 rock cells along the drift and another 4 cells in the edge regime, all fully connected regarding heat and moisture flows. With the other symmetry line along the drift axis, the total rockmass can be represented by one quarter of the domain, providing a significant reduction in the number of nodes to 15x75x8 in the 3D numerical model. The plane of symmetry is an approximation that is included in the rock model but not in the model of the airway. It

Figure 3. The rock-mass domain around an emplacement drift in Panel 5.

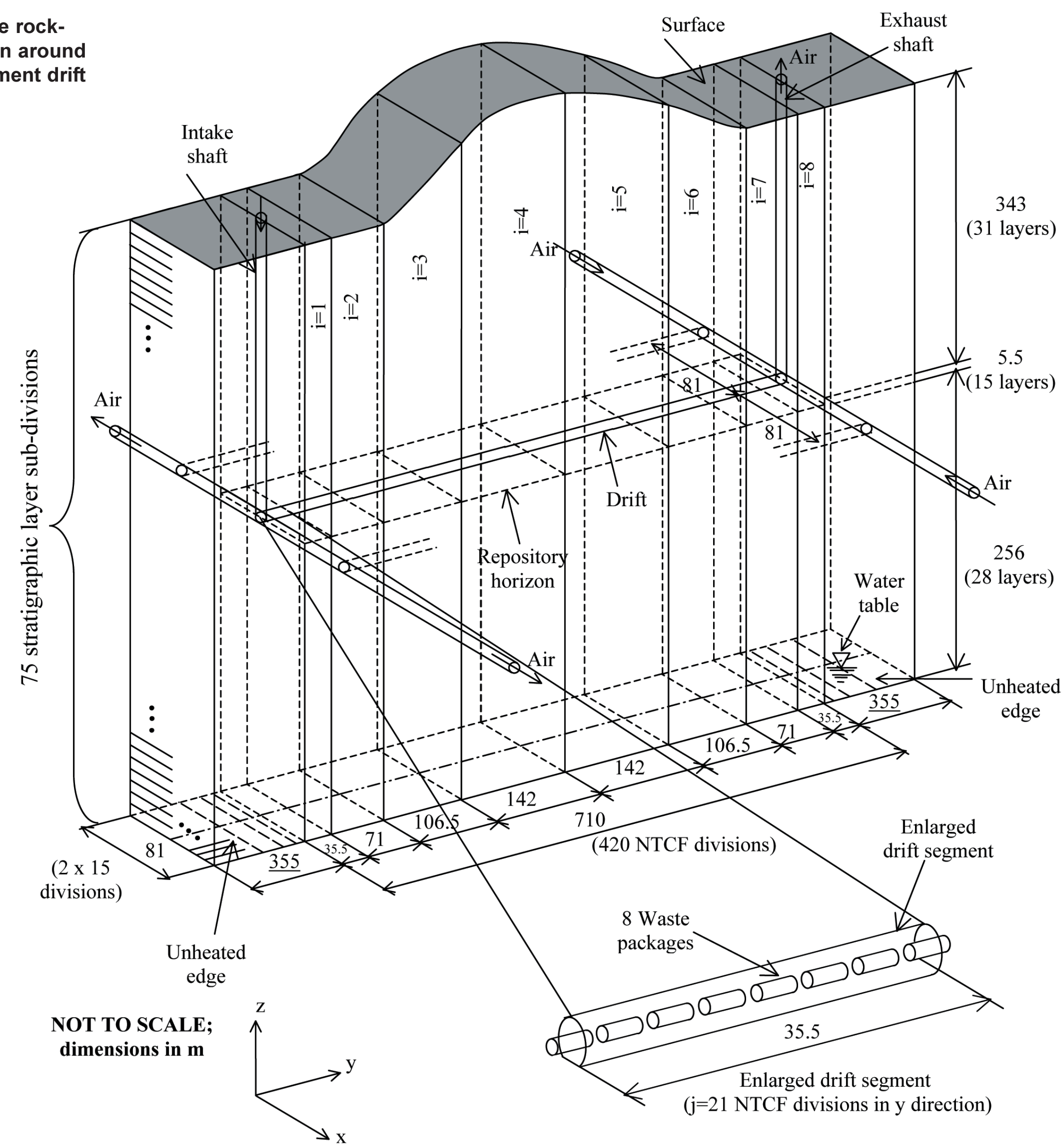

results in only a small model error while reducing the computer memory requirements by half. On the other outside vertical planes, the rock domain is assumed to be adiabatic.

The numerical model assumes a porous, wet, but unsaturated rock formation in which both heat and moisture transport are present and affect the thermal and psychrometric waste container environment. The rock properties used by BSC (2002) for a representative stratigraphic block at YM were applied. The atmospheric climate boundary conditions on the surface were varied according to the modern-time, monsoon, and glacial-transition cycles with time. The temperature and moisture saturation initial conditions in the rock-mass at the time of waste emplacement were initialized by simulating 10 complete climate cycles of 74,000 years each as the likely pre-history for the current conditions at YM.

MF3.0 is configured to model the cells using NUFT (Nitao, 2000) as a module for simulating heat and moisture flows in the rock domain. A modeling method called NTCF (Numerical Transport Code Functionalization) is used in all versions of MF, to compress and process the time-dependent heat and moisture responses from the thermohydrologic process model into matrix equations (Danko, 2000). A linear NTCF processor is applied in the present study, using first-order matrix polynomial equations for modeling heat and moisture fluxes on the drift surface boundaries with constant-coefficient matrices. The mountain-scale NTCF model for the *ith* rock cell (*i=1…8,* see Fig. 1) along the drift length expresses the time-dependent, wall heat (qh) and moisture (qm) fluxes as follows:

$$qh_i = hh_i \cdot [T_i - Tinit_i] + hm_i \cdot [P_i - Pc_i] \qquad (1)$$

$$qm_i = mh_i \cdot [T_i - Tinit_i] + mm_i \cdot [P_i - Pc_i], \qquad (2)$$

where qh_i and qm_i are vectors composed of heat and moisture flow elements at time divisions $t_1,..,t_N$; T_i and P_i are wall temperature and partial vapor pressure vectors; $Tinit_i$ is the initial, constant wall temperature; while Pc_i is the partial vapor pressure variation vector for the predicted, central condition around which the NTCF model is determined. In Eq. (1), the hh_i is a dynamic admittance matrix of heat flow, generated by the wall temperature driving force, and hm_i is another, cross-effect component matrix of heat flow, generated by the wall partial vapor pressure driving force. Similarly, mh_i and mm_i are dynamic admittance matrices for the moisture flux expression in Eq. (2). The hh_i, hm_i, mh_i, and mm_i are all *NxN* matrices, determined using the NTCF modeling method (Danko, 2000)

Within each 3D mountain-scale rock cell (*i=1…8*), further divisions are made to capture the drift-scale temperature and humidity variations along the drift. The numerical discretization points on the drift wall are bundled into 420 averaged, independent surface nodes along the drift with respect to temperature and partial vapor pressure variations in the refined NTCF model. Each mountain-scale rock cell for *i=1…8* is re-scaled into *j* sub-divisions according to Table 2. The re-scaling of the hh_i, hm_i, mh_i, and mm_i mountain-scale 3D cell matrices into drift-scale hh_{ij}, hm_{ij}, mh_{ij}, and mm_{ij} matrices are accomplished by proportioning them by the ratio between the i^{th} cell and the ij^{th} drift segment surfaces, A_i and A_{ij}:

$$hh_{ij} = hh_i \cdot \frac{A_{ij}}{A_i} \qquad (3)$$

$$hm_{ij} = hm_i \cdot \frac{A_{ij}}{A_i} \qquad (4)$$

$$mh_{ij} = mh_i \cdot \frac{A_{ij}}{A_i} \qquad (5)$$

$$mm_{ij} = mm_i \cdot \frac{A_{ij}}{A_i} \qquad (6)$$

The re-scaling procedure generates 420 individual drift-scale hh_{ij}, hm_{ij}, mh_{ij}, and mm_{ij} "daughter" matrices without any additional NUFT runs, all inheriting the mountain-scale heat and moisture transport connections from the original, mountain-scale, "parent" matrices hh_i, hm_i, mh_i, and mm_i. The average size of the spatial rock domain in the axial drift direction is 1.7 m that is sufficient to generate temperature variations even along individual waste packages. The multi-scale NTCF rock model defines heat and moisture flux vectors as a function of the 420 time-dependent input vectors of surface temperature and partial vapor pressure boundary conditions, all considered unknown and subject to coupling calculations with the in-drift CFD model. The 420 nodes represent the interface boundary at the representative points between a rock cell and the airway that include the waste packages. The NTCF rock model includes both drift-scale and mountain-scale heat and moisture flow components without using any sub-models and subsequent superposition.

Table 2. Drift-scale NTCF subdivisions in each mountain-scale rock cell.

i	1	2	3	4	5	6	7	8
J	21	42	63	84	84	63	42	21

The Model of the Airway with the Waste Containers

A lumped-parameter CFD (Computational Fluid Dynamics) model is used in MF to describe the air flow, heat, and moisture transport in the airway. A sequence of 8 different (two halves and six full) waste packages, shown in Figure 4, is first mirrored to form a 16-package sequence, and second, repeated 10 times in the emplacement drift. The entire emplacement drift is 710 m in length, housing a total of 140 waste packages. Drip shields are not included in the present analysis. The CFD model of the emplacement drift is an integral, continuous 3D model.

Heat and moisture transport by laminar or turbulent convection are modeled on the drift and the waste container wall. The heat and moisture transport coefficients in the annulus between the waste containers and the drift wall are calculated in MF3.0 using transport coefficients in the lumped-parameter CFD during pre-closure. Thermal radiation between the waste packages and the drift wall, between waste packages, as well as between drift wall segments are incorporated in the CFD model. Natural, secondary flow may be due to the local temperature differences and related local, superimposed natural convection. The dominantly natural heat transport coefficient on the drift and waste package walls during post-closure are all set to a constant value of 1.85 W/(m^{2}K), a value consistent with the results of more detailed numerical modeling (Webbs et al., 2002). A differential-parameter CFD model (Danko and Bahrami, 2002) can also be used in MF3.0 if refinement of the transport coefficients is necessary, however, this option is not applied in the present study.

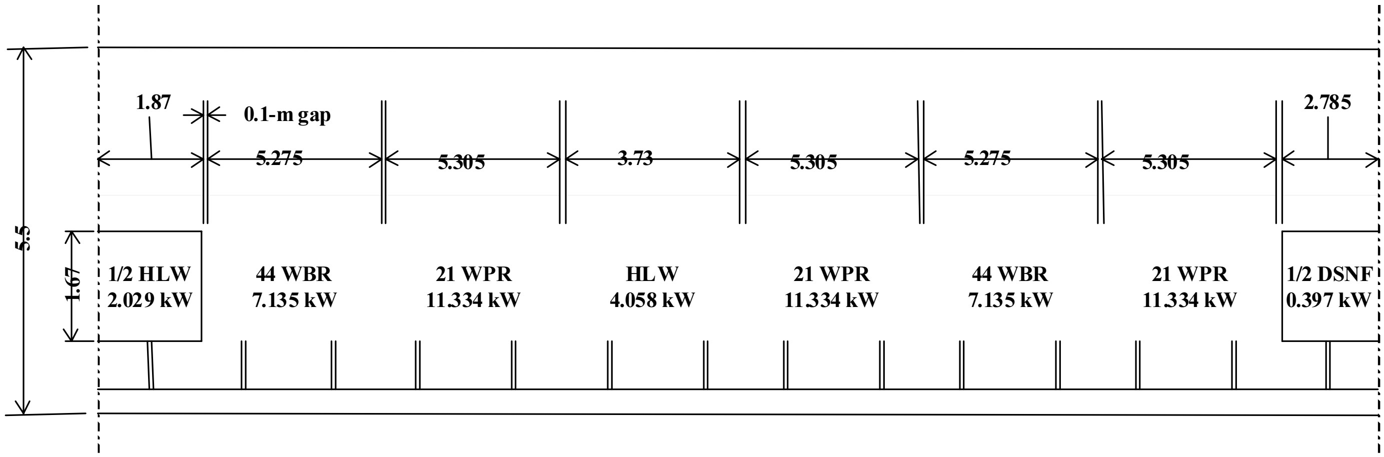

Figure 4. A repeated sequence of eight waste packages in an emplacement drift.

Total System Model

The NTCF and CFD modules are coupled on the rock-air interface by MF3.0 until the heat and moisture flows are balanced at the common surface temperature and partial vapor pressure at each surface node and time instant. In the post-closure time period, the natural infiltration air flow rate varies with time, as it depends on the time-variable temperature and relative humidity. The air flow rate is iteratively calculated from the pressure balance, equating the pressure loss through the system with the buoyancy driving pressure difference caused by differences between the intake and exhaust air densities.

The buoyancy pressure difference for the given configuration is modeled as a chimney effect between the intake and exit air columns. The intake column assumes 243 m of atmospheric air at 18.7°C temperature and 30% relative humidity, and a 100 m intake air column, already in the fractured rock at elevated temperature and modified relative humidity. The temperature and relative humidity in this 100 m intake section is linearly interpolated along the vertical direction between the values at the drift intake segment, taken from model calculations during iteration, and the atmosphere. The exit air column assumes variable, elevated temperature as well as relative humidity, varying along the vertical section of the rockmass over the edge of the panel at the end of the drift. The vertical variation is linearly interpolated between the values at the drift discharge segment and the atmosphere. Since the intake air column is colder and dryer than the exit column, an infiltration air flow is driven from intake to exit.

The pressure loss for an air flow rate is modeled for the geometry given in Figure 2, and using a mean permeability value of $6*10^{-11}$ m^2 in Darcy's formula. A generous, 50% increase in the pressure loss is included for taking into consideration any potential air flow resistance increase due to drift degradation and/or partial collapse. The pressure loss model is dynamic, including the variation of infiltration air flow rate that is iteratively calculated.

The modeling concept is that first, a balanced infiltration air flow rate variation with time is determined, and second, the balanced rate is perturbed, in order to check the sensitivity to infiltration air flow rate, as well as in acknowledgement of the fact that the mountain-scale air flow permeability is a highly uncertain parameter. As described earlier, four infiltration air flow rate variations are applied, high, medium, balanced, and low.

The solution of the coupled thermohydrologic-ventilation model includes four nested iteration loops as follows:

- NTCF model re-functionalization with NUFT
- Buoyancy pressure and air flow pressure loss iteration for a given temperature and humidity variation in the entire model domain
- Heat balance iteration between the NTCF and airway CFD models for each time division
- Moisture balance iteration between the NTCF and airway CFD models for each time division

Being in the outside loop, one set of NUFT runs and NTCF model preparation serves three internal, nested iteration loops, incorporating approximately 1500 total iteration cycles during balancing. The NTCF modeling technique is an efficient way to reduce the necessary number of NUFT runs during the iterative numerical calculations. With this balancing structure, the number of time-intensive NUFT runs is minimized. Two-three NTCF model re-functionalizations have been used (BSC, 2002, Danko and Bahrami, 2003), however, only one step was applied in the present study.

Input Data

The input data used in the calculation essentially agree with those used in the AMR Rev01 study (BSC, 2002). The main input parameters are as follows:

Rock input data:	NUFT3.0 input deck specified in the AMR Rev01 study. The spatial rock domain is shown in Figure 3.
Drift dimensions:	710 m long, 5.5 m in diameter.
Air flow rate:	15 m3/s at 25oC intake temperature and 30% relative humidity until year 50; variable, balanced, as well as perturbed infiltration variations afterwards, shown in Figure 5.
Waste packages:	140 Waste Packages (WP) in the emplacement drift. A mirrored-repeated sequence of eight WPs with variable heat load, (two halves and six full) in a repeating drift segment of 35.5 m, shown in Figure 4, composes the total of 140 WPs.
Waste mass load:	56 MTU/acre.

Drip Shield: No drip shield is assumed in the model configuration.

The MF and NUFT input decks necessary for the simulation are documented in a report submitted to BSC (Danko et al., 2003).

RESULTS AND DISCUSSIONS

Infiltration Air Mass Flow Rates

The simulated air temperature and humidity results with a trial air flow rate allow for the calculation of (1) the buoyancy pressure as the driving force for the air infiltration in the model domain shown in Figure 2; and (2) the total pressure loss of the infiltration air flow across the system. The main pressure iteration cycle determined the exact air flow rate at which the two pressure component agreed within the pressure error limit. The balanced infiltration air flow rate variation with time is given in Figure 5. The three other flow rates, as perturbed functions, are also shown in Figure 5. Ten total iteration steps were needed to achieve balancing within a 10 Pa average pressure error. During the balancing calculations with the four nested iteration loops previously described, MF3.0 used each NTCF model approximately 3 times for moisture and 50 times for heat balance iterations in each time division.

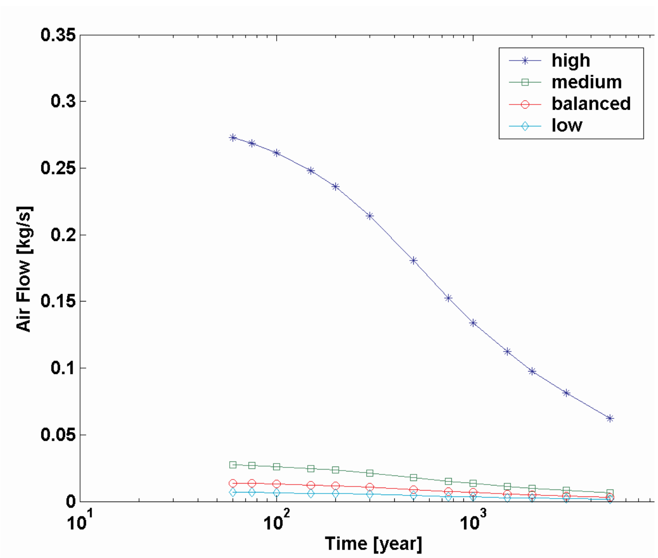

Figure 5. Natural air infiltration mass flow rates through an emplacement drift. The high, medium and low infiltration air flow rates are multiples of the balanced mass flow rate function by factors of 20, 2, and 0.5, respectively.

Temperature and Relative Humidity Distributions

Spatial and temporal temperature and relative humidity variations from the MF3.0 calculations are given for the central, representative drift for four different infiltration air mass flow rates in Figures 6, 7, 8, and 9. Sub-figures a, c, and e in all figures depict temperatures of the waste packages, air, and the drift wall as a function of time and drift length. Sub-figures b, d, and f in all figures show the relative humidities on the surface of the waste packages, in the air, and on the drift wall as a function of time and drift length.

Figures 6.a-f show the temperature and relative humidity results for both the pre- and the post-closure time periods, assuming constant air flow rate of 15 m^3/s during pre-closure, and a perturbed, high infiltration air mass flow rate variation during post-closure. The evolution of two thermal peaks are shown in the temperature variations for the drift wall, shown in Figure 6.a, one around year 5 during pre-closure, and one between years 75 and 100 during post-closure, depending on the drift location. The second peak is reached relatively rapidly, due to the young age of the waste, when compared to the previous study (Danko and Bahrami, 2003) in which the time for peak temperature evolution during post-closure was about 1000 years, following a 300-year pre-closure ventilation. The second peak is much higher in amplitude, underlying the criticality of the post-closure analysis, for both the maximum temperature evolution as well as the threshold limitation for localized corrosion. Waste package temperatures exceed 140ºC, the limit for the onset of localized corrosion for Alloy 22 waste package material, for an extended period of time and for a large section of emplacement drift with over 100 waste packages. If drip shields were included in the calculation, the predicted temperatures of the waste package surface would rise even higher. For better readability, temperature differences relative to the wall temperature are depicted in Figs. 6.c and 6.e for the waste package and the air nodes. The longitudinal, saw-tooth-like fluctuations in both temperatures and relative humidities are caused by the variation of the heat dissipation of the waste packages.

It is interesting to see in Figures 6.b, d, and f that the relative humidities do not increase above 30% at any time during the study period for the high infiltration air mass flow rate. This result favorably agrees with the previous studies (Danko and Bahrami, 2002), in which the relative humidity was consistently below 50%, although with a higher air infiltration mass flow rate, due to an engineered, natural buoyancy-driven, post-closure air flow supply.

The maximum differences between the drift wall and air, as well as between waste packages and air, are only about 10ºC at the time of the peak temperatures and lower afterward. Under this condition, the buoyancy driving force for local, natural air convection in each drift cross section is moderate, with a Rayleigh number in the order of 10^9 and with a natural heat transport coefficient around 1.85 W/(m^2K) between the waste package and the air, as well as between the air and the drift wall. The convective heat transport in this case is lower than the heat transport due to radiation that is a parallel, bypass mechanism to convection, modeled in the lump-parameter CFD model. Therefore, the sensitivity to the convective heat transport coefficient in this regime is moderate, and the lumped-parameter CFD model based on heat transport coefficients need not be replaced with more elaborate heat and moisture convection elements.

Figures 7, 8, and 9 with sub-figures a-f show the temperature and relative humidity results for only the post-closure time periods for the medium, balanced, and low infiltration air mass flow rate variations. The pre-closure temperature and relative humidity variations are the same for these cases as given in Figures 6.a-f, since the pre-closure ventilation is the same for all post-closure conditions. As compared to the results in Figure 6, the low air flow rates increase the relative humidities along the cold, exit drift section up to 100%, and liquid water condensate forms on some of the cold nodes of the drift wall. The detailed spatial variations of temperature, relative humidity, and liquid water condensate mass flux are given in Figure 10 for the three different air mass flow rates at selected time periods during post-closure.

The temperature variation along the drift axis is very significant, still over 60ºC at year 2000. The edge-cooling effect is increasing with time between years 50 and 2000, during which period the waste decay heat is still strong enough to heat the middle section of the drift, but the time is already long enough to cool down the edge area. The current results support the initial assumption that evaporation in the middle and hot drift section and cold-trap condensation in the relatively cold edge drift section will likely take place in the central drift of Panel 5. This scenario is seen with the medium, balanced, and low infiltration air mass flow rates. The trend in Figures 7-9 shows that the lower the air flow rate, the more problem emerges with cold-trap condensation, both in magnitude as well as the duration of the appearance of liquid condensate in the drift. Other drifts in the same panel will likely follow the same trend, as well as drifts in other panels under certain air flow conditions during post-closure. This suggests that an engineered natural draft ventilation system as has been suggested by Nye County has the potential to improve system performance.

Due to the very low air infiltration, the temperature variation along the drift axis closely copies that of an un-ventilated repository during post-closure. This recognition allows the studying of the cold-trap process with a simplified, psychrometric moist airflow model. However, the heat-driven moisture flow will still need to be calculated using a mountain-scale heat and moisture model along the drift length and with time. Currently, no other published models, as summarized in Table 1, include the mountain-scale moisture flow component in the thermohydrologic model-element, other that MF3.0 reported in this paper, using the multi-scale NTCF technique.

Cold-Trap Condensate Drippage

The total amount of condensates collected in the drift sections with 100% relative humidity as a function of time for three infiltration air mass flow rates are given in Table 3. In the current theromohydrologic-ventilation model configured in MF3.0, the condensate is assumed to be partially re-evaporated on the waste packages, while a portion of the condensate is assumed to be removed from the system by drainage. The total condensate that appears on the drift wall is given in the wall columns in kg/s unit, while the total minus re-evaporated condensate in the drift is given in the net columns of Table 3. The spatial variations of liquid water condensate mass flux along the drift length are given in Figure 10 for the three different air mass flow rates at the end of year 2000.

Condensate dripping on the waste packages and re-evaporating afterward is currently modeled based on partial vapor pressure trimming in the moisture transport CFD sub-model solution in MF3.0. Total condensate removal by drainage, or condensate imbibing into the rock wall is currently not modeled, but this effect is likely to be important and subject of future studies with MF3.0. The effect of drip shield is another subject of further investigation.

The appearance of condensates at low-temperature drift sections and waste packages is the result of a complex moisture transport mechanism at YM. This mechanism appears to pump vapor, due to heat from a large rock mass and drift surface area, towards a small, cold drift section where it becomes a focused condensate. The amount of condensate appears to be higher than expected from the equilibrium water recharge rate due to percolation flux of 12 mm/yr in the current NUFT rockmass model during the first few 1000 years. Thus, the condensate collection in cold traps is likely to be part of an overall drying process of the rockmass. A definite disadvantage is seen in the drift emplacement design at the high thermal operating mode when considering that the otherwise advantageous drying process effectively delivers liquid water to some of the waste packages.

Time (year)	Infiltration Air Mass Flow							
	High		Medium		Balanced		Low	
	Wall.	Net	Wall.	Net	Wall.	Net	Wall.	Net
500	0	0	0	0	2.32E-03	1.20E-03	3.63E-03	1.54E-03
750	0	0	0	0	0	0	0	0
1000	0	0	1.14E-05	1.83E-09	8.48E-03	2.19E-03	2.45E-02	2.99E-03
1500	0	0	1.68E-03	8.67E-04	2.51E-03	7.21E-04	0	0
2000	0	0	5.75E-03	1.66E-03	1.09E-02	1.71E-03	3.81E-02	1.98E-03
3000	0	0	5.60E-03	1.19E-03	3.08E-03	8.26E-04	2.20E-03	2.39E-04
5000	0	0	7.27E-04	2.00E-04	9.77E-04	2.38E-04	2.68E-03	1.56E-04

Table 3. Rate of liquid water condensate accumulation due the cold-trap process in kg/s.

Pressure Balances at the Perturbed Infiltration Air Mass Flow Rates

The results of the buoyancy driving pressure and the pressure loss as a function of time for the four air mass flow rates are shown in Figure 11. The driving pressure and pressure loss agree within an average of 10 Pa for the balanced air flow rate, therefore, the curves are close and overlapped in Figure 11.

Comparison of the driving pressure differences with the pressure losses shows driving force deficits for the high and medium infiltration air flow rates. Therefore, these flow rates are indeed too high under the assumed conditions. The high air flow rate with its advantages in reducing relative humidity can only be achieved with an engineered design. The low infiltration air flow rate shows a slight excess in driving pressure.

The regime of the four different air flow assumptions seems to cover the likely infiltration air flow rate under the assumed conditions. However, it must be pointed out that the air permeability of the fractured rockmass is an uncertain parameter and a single, balanced infiltration air flow rate may still be only a hypothetical result. Rather than using a single, balanced result, an approach is presented with a systematic variation of flow rates that bound the likely scenario under assumed conditions at YM.

Computational Considerations

The NTCF modeling technique reduced the number of necessary NUFT runs, making it feasible to complete the complex calculations in approximately five weeks in spite of the average number of 1500 iterations with the theromohydrologic model for the 5,000 year time period. For comparison, a single NUFT run with one set of boundary condition variations for 5,000 years for the complete rock domain (with entrance and exit segments) took approximately 50 hours on a small workstation. Comparing run times between MF with the NTCF method and a hypothetical case without the NTCF method indicates that without using the NTCF method, but replacing it with direct NUFT runs and assuming the same number of balancing iterations, the modeling task being presented would take a minimum of 1500 times 50 hours, an 8.6 years of non-stop computation.

CONCLUSIONS AND RECOMMENDATIONS

- An integrated, pre- and post-closure theromohydrologic-ventilation study was successfully completed using both mountain-scale and drift-scale rockmass model-elements using MF3.0. The model applied a multi-scale rockmass model-element without the need for solving sub-tasks and using subsequent superposition. The model integrated open-loop ventilation during pre-closure and mountain-scale air infiltration during post-closure within one continuous task.
- The forced ventilation was found to be efficient in keeping temperatures well below boiling during the pre-closure time period.
- Subsequent to closure with backfill and seals in the access shafts and tunnels, four different, small air mass flow rates were assumed to develop through the natural fracture system of YM. A balanced air infiltration flow rate was determined based on iteratively equating the natural flow resistance and buoyancy driving pressure. Perturbed air flow rates around the balanced variation bounded the likely post-closure air infiltration scenario at YM under the assumed model conditions.
- Follow-up balancing calculations are recommended to refine the air flow rate assumptions, while maintaining the likely variations in air permeabilities of the rockmass.
- The WP surface temperature reached a peak value between years 75 and years 200, exceeding the temperature limit of 140ºC known to be the safe threshold limit for localized corrosion for the likely waste container material of Alloy 22.
- A longer period of pre-closure ventilation may favorably reduce the maximum WP surface temperature. Previous, comparable studies (Danko and Bahrami, 2003, Danko, 2003) showed that a 300 years pre-closure ventilation period results in a maximum post-closure WP temperature lower than 120ºC. Therefore, a longer pre-closure time period is recommended.
- The relative humidity increased up to 100% during post-closure in the cold exit section of the emplacement drift for three of the post-closure infiltration air mass flow rates, and liquid water formations were predicted. This result provides far less favorable storage conditions than those expected when an engineered, post-closure ventilation was provided in previous studies (Danko and Bahrami, 2003, Danko, 2003).
- The high infiltration air flow rate reduces the relative humidity below 30%, although this air flow rate is unlikely without an engineered solution. The relative humidity in previous studies (Danko and Bahrami, 2003, Danko, 2003) with a somewhat higher air flow rate was consistently lower than 50 % during the first 5,000 years. It is recommended to further study the feasibility of engineered, post-closure ventilation solutions in order to mitigate the negative effects of any low, spontaneous air infiltration that may develop through the mountain.
- A fully-coupled, theromohydrologic-ventilation model and software, MF3.0 is proven efficient in solving the multiphase, non-equilibrium transport problem of heat, moisture, and ventilating air flows involving the large and geometrically complex geologic region at YM. It is recommended to apply the NTCF modeling methology and software MF3.0 for multiscale, coupled heat and moisture flow studies with or without ventilating air movements at YM.

ACKNOWLEDGMENTS

The review and editorial comments of Dr. Dale Hammermeister, Nye County On-Site representative, Dr. John Walton, Professor at the University of Texas at El Paso, and Dr. Pierre Mousset-Jones, Professor, Mackay School of Mines, UNR, are highly appreciated. The support of the Nye County Department of Natural Resources under Grant No. DE-FC28-02RW12163 is gratefully acknowledged.

REFERENCES

BSC (Bechtel SAIC Company). 2002. “Ventilation Model.” ANL-EBS-MD-000030 REV 01D draft. Las Vegas, Nevada: Bechtel SAIC Company, ACC.

Danko, G, 2000. “MULTIFLUX Software Documentation.” University of Nevada, Reno.

Danko, G., and Bahrami, D. 2002. “The Application of CFD to Ventilation Calculations at Yucca Mountain.” 28th Waste Management ’02 Conference, Tucson, AZ, pp1-8.

Danko, G., and Bahrami, D.. 2003. “Powered, and Natural, Passive Ventilation at Yucca Mountain.” Proceedings, 10th Int. High-Level Radioactive Waste Management Conference, pp.683-689.

Danko, G., 2003. “Coupled Hydrothermal-Ventilation Studies for Yucca Mountain.” Annual Report for Period April 2002 through March 2003. Pahrump, Nevada: Nye County Department of Natural Resources.

Danko, G., Bahrami, D., and Lanka, S., 2003. “Technical Support Services for the MULTIFLUX Software.” Final Report, submitted to BSC, Nevada.

Farmer, J., 2003. “Chemical Environment Evolution on Alloy 22.” Presentation to the Nuclear Waste Technical Review Board, January 28, Las Vegas, NV.

Itamura, M.T., Francis, N.D., and Webb, S.W., 2003. “In-Drift Natural Convection Analysis of the Low Temperature Operating Mode (LTOM) Design.” Proceedings, 10th Int. High-Level Radioactive Waste Management Conference, pp. 675-682.

LeCain, G.D., 1997. “Air-Injection Testing in Vertical Boreholes in Welded and Nonwelded Tuff, Yucca Mountain, Nevada.” U.S. Geological Survey WRIR 96-4262 Report, p.16.

LeCain, G.D., Anna, L.O., and Fahy, M.F., 2000. “Results from Geothermal Logging, Air and Core-Water Chemistry Sampling, Air-Injectionb Testing, and Tracer Testing in the Northern Ghost Dance Fault, Yucca Mountain, Nevada, November 1996 to August 1998.” U.S. Geological Survey WRIR 99-4210 Report.

Lichtner, P.C., Seth, M.S., and Painter, S., 2000. “MULTIFLO User’s Manual MULTIFLO Version 1.5-Two-Phase Nonisothermal Coupled Thermal-Hydrologic-Chemical Flow Simulator.” San Antonio, TX: Center for Nuclear Waste Regulatory Analysis.

MacKinnon, R.J., 2003. “Update on Engineered Barrier System Performance: Performance Assessment Insights.” Presentation to the Nuclear Waste Technical Review Board, September 16, Armagosa Valley, NV.

Manepally, C., and Fedors, R., 2003. “Edge-Cooling Effect on the Potential Thermohydrologic Conditions at Yucca Mountain.” Proceedings, 10th Int. High-Level Radioactive Waste Management Conference, pp. 286-292.

Nitao, J., 2000. “NUFT, Flow and Transport code V3.0s.” Software Configuration Management, Yucca Mountain Project – STN: 10088-3.0S-00. Prepared at the Lawrence Livermore National Laboratory.

Rousseau, J.P., Kwicklis, E.M., and Gillies, D.C., (editors), 1999. “Hydrogeology of the Unsaturated Zone, North Ramp Area of the Exploratory Studies facility, Yucca Mountain, Nevada.” U.S. Geological Survey WRIR 98-4050 Report, p.107.

Webb, S.W., Francis, N.D., Dalvit-Dunn, S., and Itamura, M.T., 2003. “Pre- and Post-Closure Natural Convection Effects in Yucca

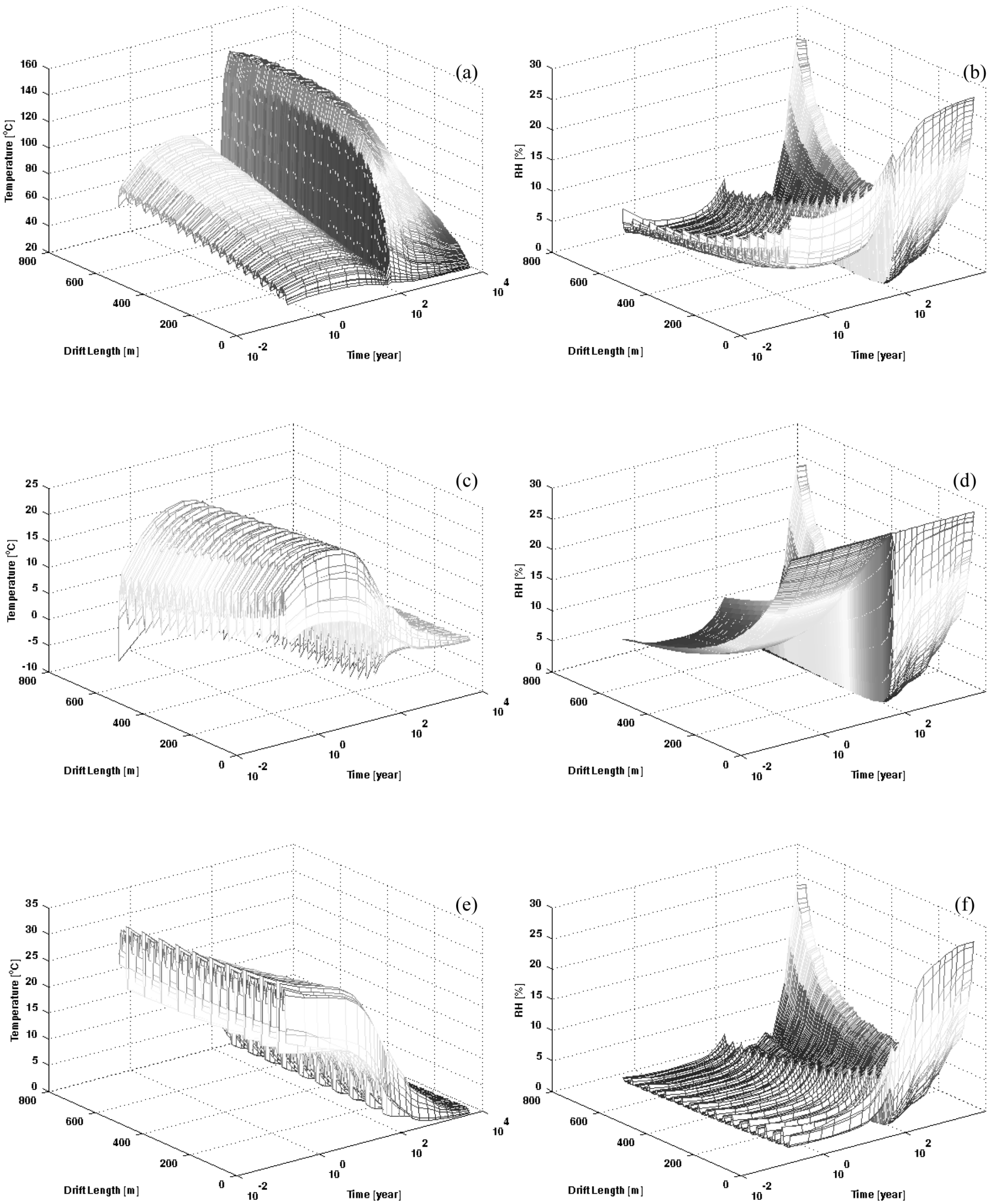

Figure 6. (a) Wall temperature; (b) Wall relative humidity; (c) Wall-air temperature difference; (d) Air relative humidity (RH); (e) WP-wall temperature difference; and (f) Wall relative humidity (RH) distributions in time and space; High infiltration air mass flow rate.

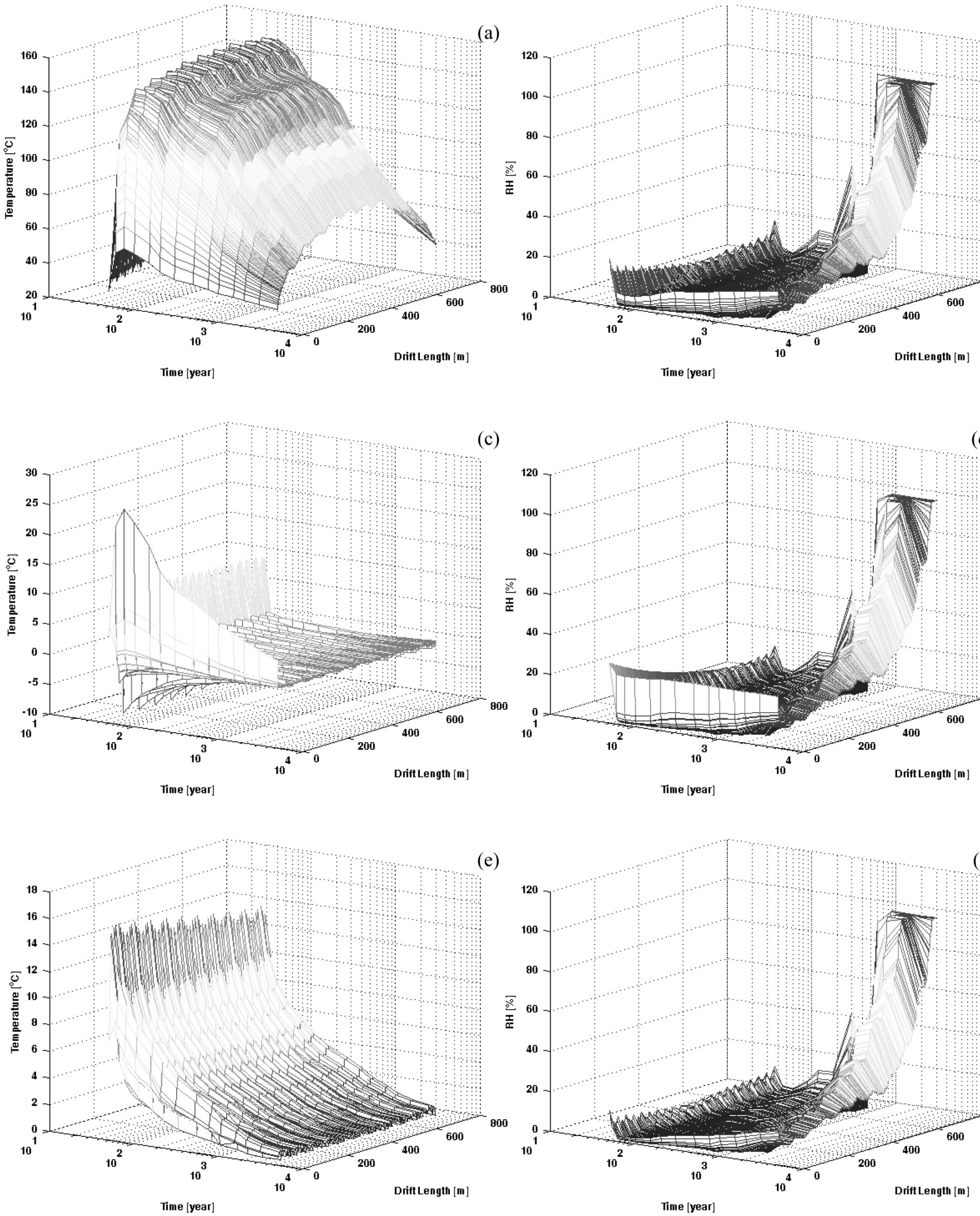

Figure 7. (a) Wall temperature; (b) Wall relative humidity; (c) Wall-air temperature difference; (d) Air relative humidity (RH); (e) WP-wall temperature difference; and (f) Wall relative humidity (RH) distributions in time and space; Medium infiltration air mass flow rate.

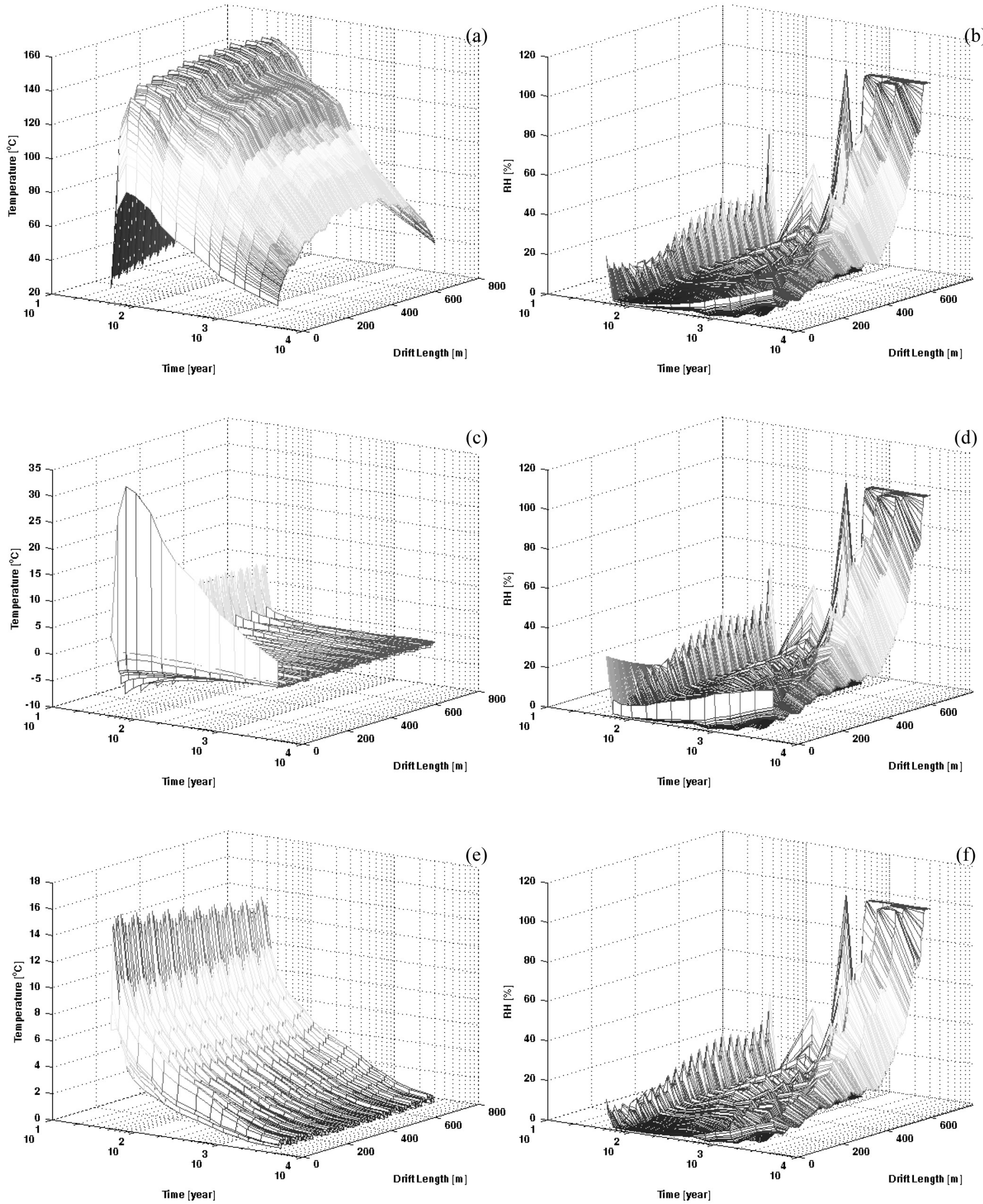

Figure 8. (a) Wall temperature; (b) Wall relative humidity; (c) Wall-air temperature difference; (d) Air relative humidity (RH); (e) WP-wall temperature difference; and (f) Wall relative humidity (RH) distributions in time and space; Balanced infiltration air mass flow rate.

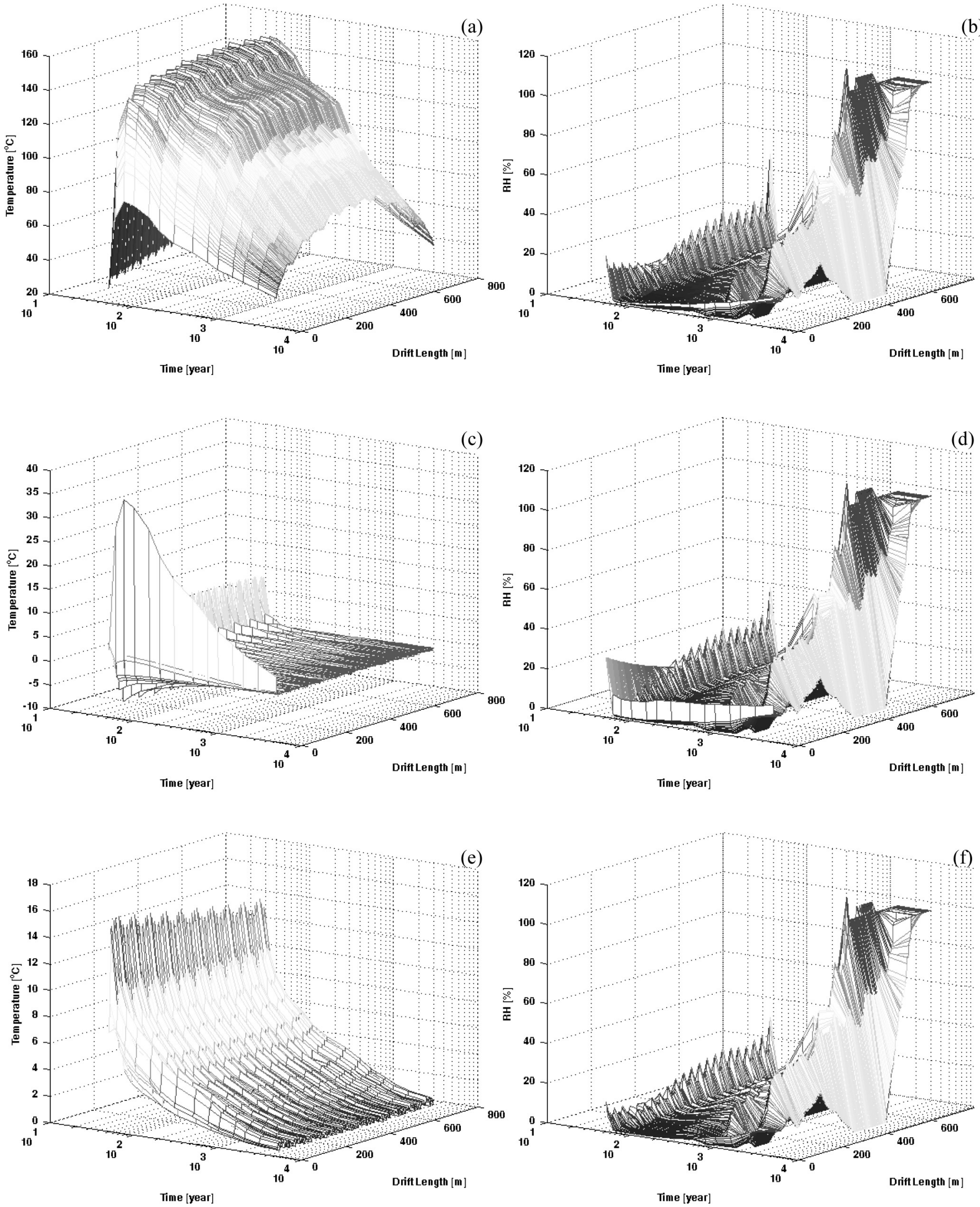

Figure 9. (a) Wall temperature; (b) Wall relative humidity; (c) Wall-air temperature difference; (d) Air relative humidity (RH); (e) WP-wall temperature difference; and (f) Wall relative humidity (RH) distributions in time and space; Low infiltration air mass flow rate.

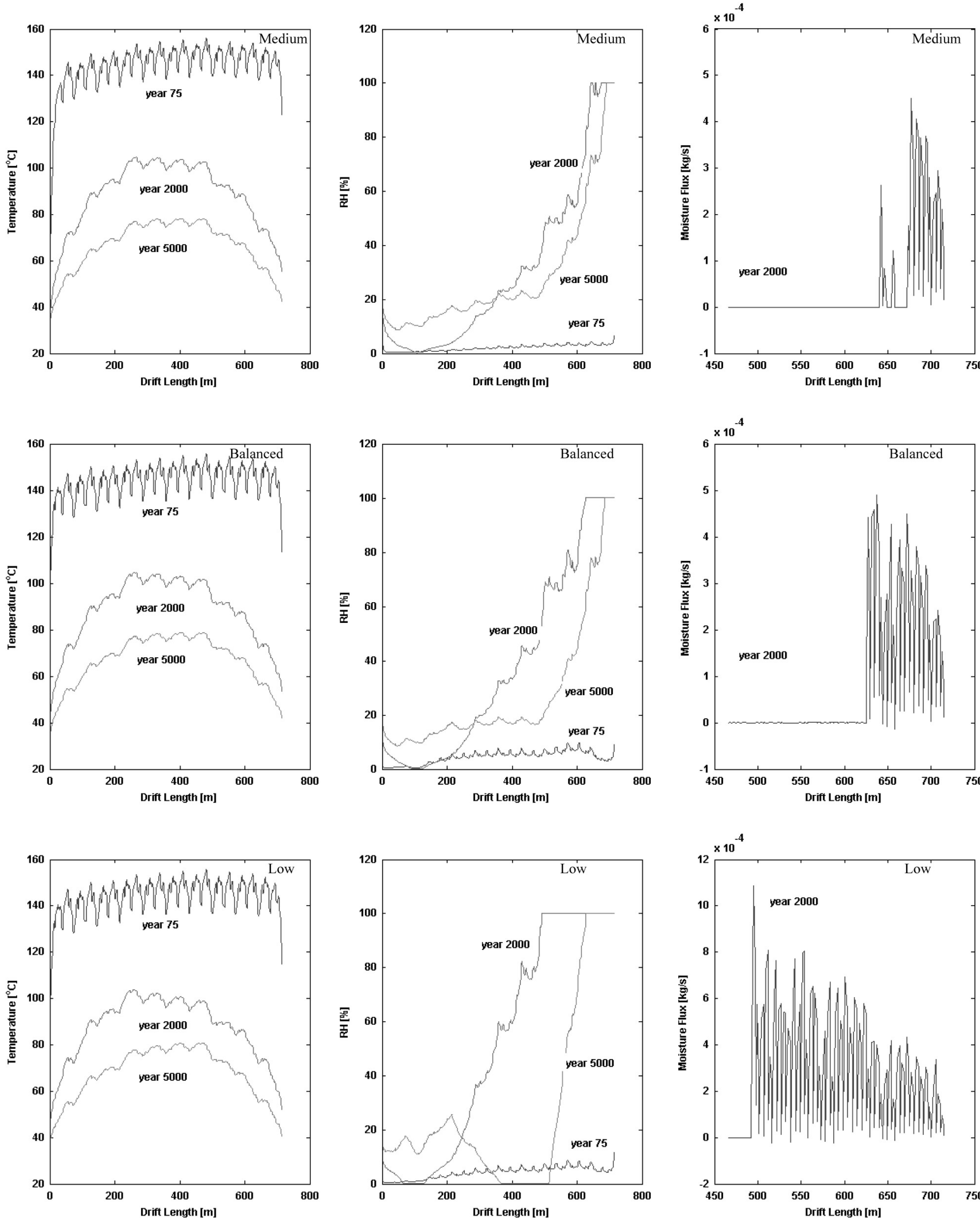

Figure 10. Drift wall temperature, relative humidity (RH), and water condensation distributions at selected time periods for the medium, balanced, and low infiltration air flow rates.

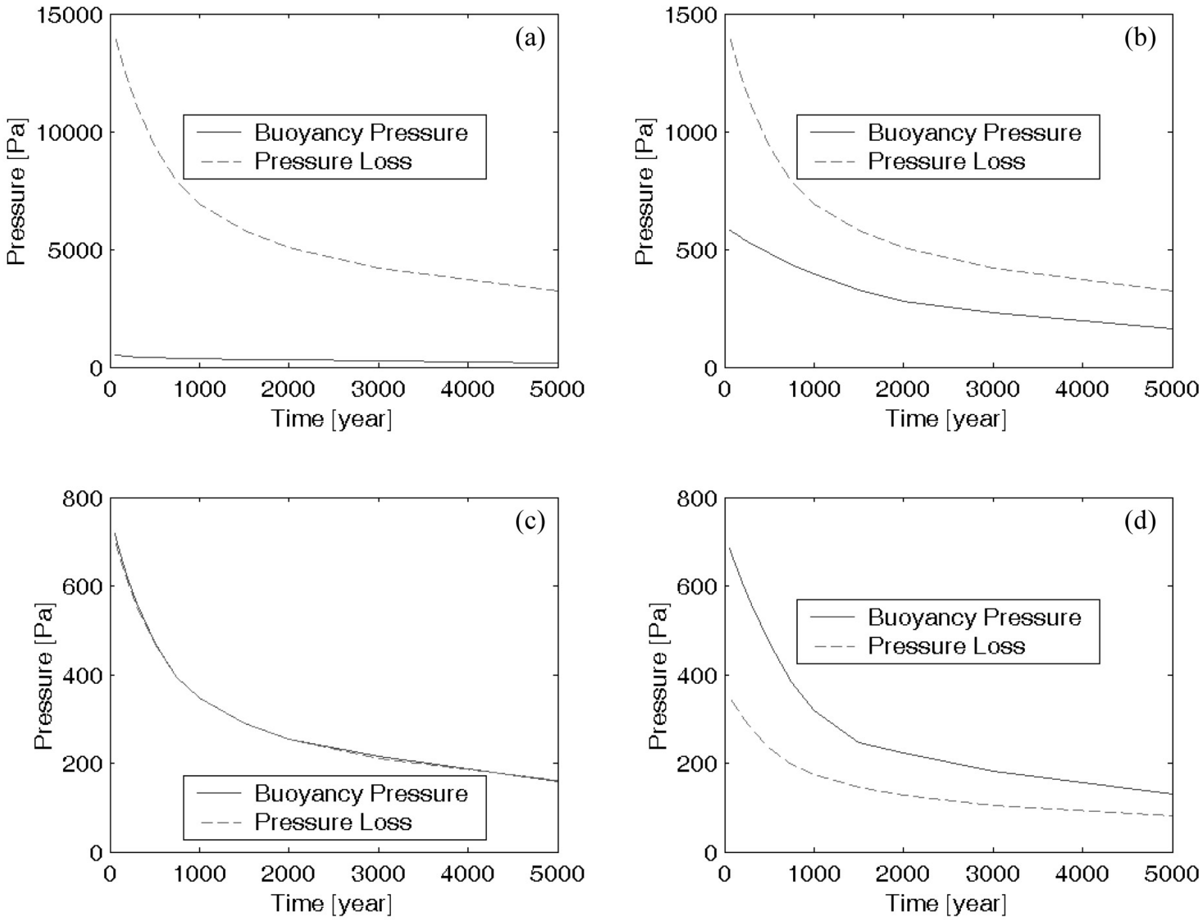

Figure 11. Buoyancy pressure and pressure loss for the four infiltration air mass flow rates: (a) high, (b) medium, (c) balanced, and (d) low.

Nye County Department
of Natural Resources and Federal Facilities

Status of Nye County Ventilation Studies

George Danko, Davood Bahrami, UNR,
danko@unr.edu

John Walton, UTEP, walton@utep.edu

Nuclear Waste Technical Review Board
January 2004

Outline

- Natural draft ventilation concept.
- MULTIFLUX code verification.
- Ventilation sensitivity study.
- Post-closure natural draft ventilation study.
  - An integrated thermo-hydraulic drift airflow model was prepared for 5000 years of pre- and post-closure.
  - Post closure natural ventilation will occur.
  - Cold-trap condensation is seen at the drift ends in the current design.
  - Design changes will be needed to eliminate condensation.

What do we mean by ventilation?

- Pre-closure ventilation and post-closure air infiltration.
- Concept:
  - Enhance natural breathing of mountain with rubble filled drifts or other means.
  - Permanent, flow driven by waste heat induced buoyancy.
  - Combine with more flexible pre-closure ventilation.
- Potential Advantages:
  - Smaller repository footprint.
  - Lower temperatures.
  - Dryer, less condensation.
  - Lower cost.
  - Lower corrosion.
  - Improved drift shadow.

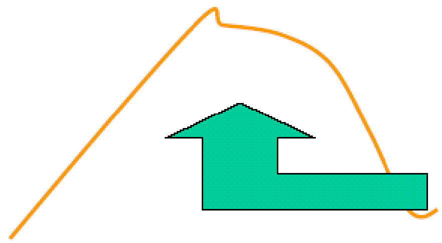

MULTIFLUX

- Lawrence Livermore National Laboratory porous/fractured-media flow and transport software model (NUFT) as a module for simulating heat and moisture flows in the rock domain.
- Computational fluid dynamics (CFD) module for the simulation of transport processes in the airway system, including the waste packages.
- Modules coupled on the rock-air interface:
  - Heat and moisture flows are balanced at interface.
  - Temperature and vapor pressure equalized at each surface node.
- Developed by George Danko, University of Nevada, Reno.

Code Verification (Benchmarking)

- Analytical solution of transient heat transfer from drift to rock with heat conduction in rock.
- Boundary condition arbitrary function of time.
- Carslaw and Jaeger double integral solution.
- Integrate along drift to give two dimensional transient solution.
- Set parameters to maximize “action”.
- Excellent agreement between model and analytical solution.
- NWRPO-2003-05 Coupled Hydrothermal-Ventilation Studies for Yucca Mountain Annual Report for April 2002 – March 2003, George Danko.

Sensitivity Study

- What factors and parameters are most important?
- Modify: ventilation rate, thermal conductivity (k), heat transfer coefficient (h), heat capacity (ρC_p).
- NWRPO-2003-05 Coupled Hydrothermal-Ventilation Studies for Yucca Mountain Annual Report for April 2002 – March 2003, George Danko.

Sensitivity Study Conclusions

- Thermal loading does not change sensitivities.
- Ventilation rate:
  - Thermal conductivity and thermal diffusivity (density) important at low flow rates (lower than 5 kg/s ~ 0.25 m/s air velocity).
  - Heat transfer coefficient important at high flow rates (higher than 1 kg/s ~ 0.05 m/s air velocity).
- Thermal conductivity important and uncertain in lithophysal areas.

Post Closure Ventilation Simulation

- Simulates current DOE "hot" repository design.
- U-Tube assumption for buoyancy flow:
  - Cold air goes down Solitario Canyon Fault zone.
  - Warm air goes up Ghost Dance Fault Zone.
  - Single drift.
- Flow rates centered on USGS (Gary LeCain) permeability.
- Results for a range of flow rates following 50 years of forced ventilation.
- Highest flow rates illustrate enhanced natural draft ventilation.

Repository

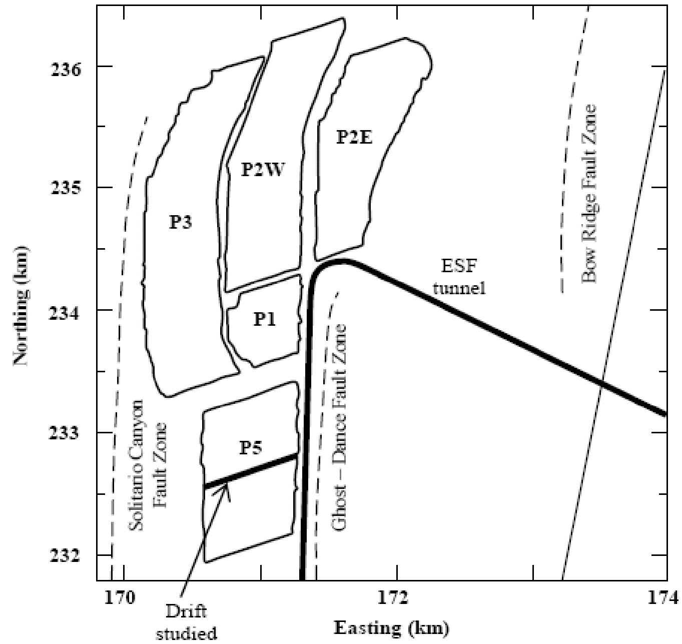

Natural Ventilation Flow System

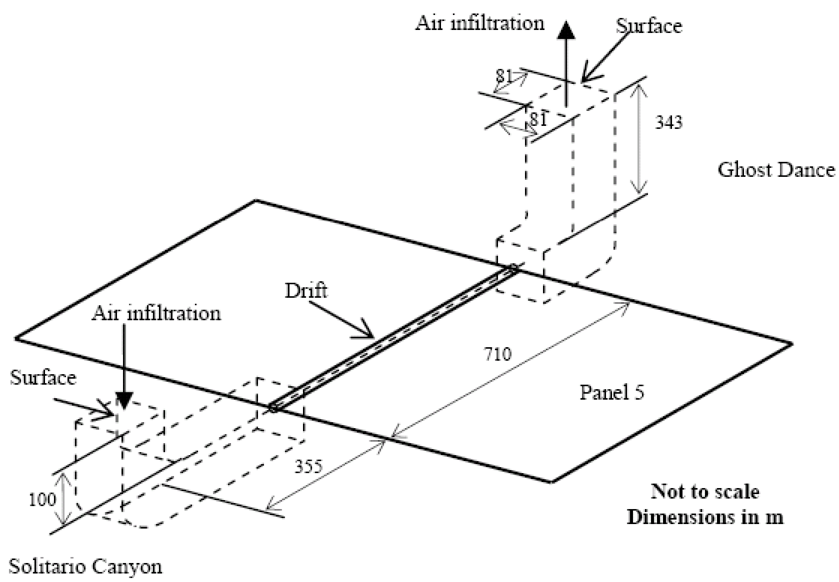

Infiltration Airflow Rates

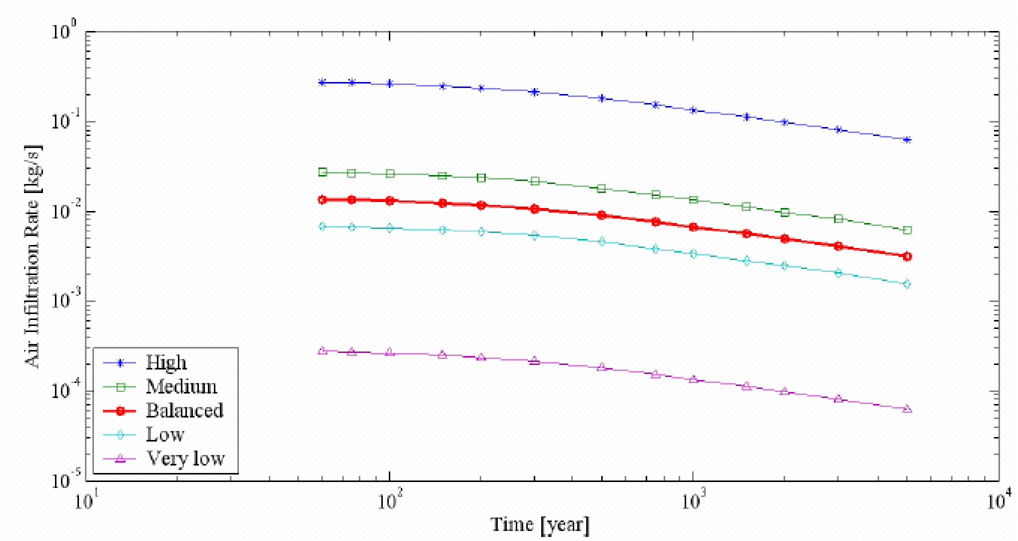

Air Infiltration: Low

Location: WP

In-Drift Model: CFD-Convective

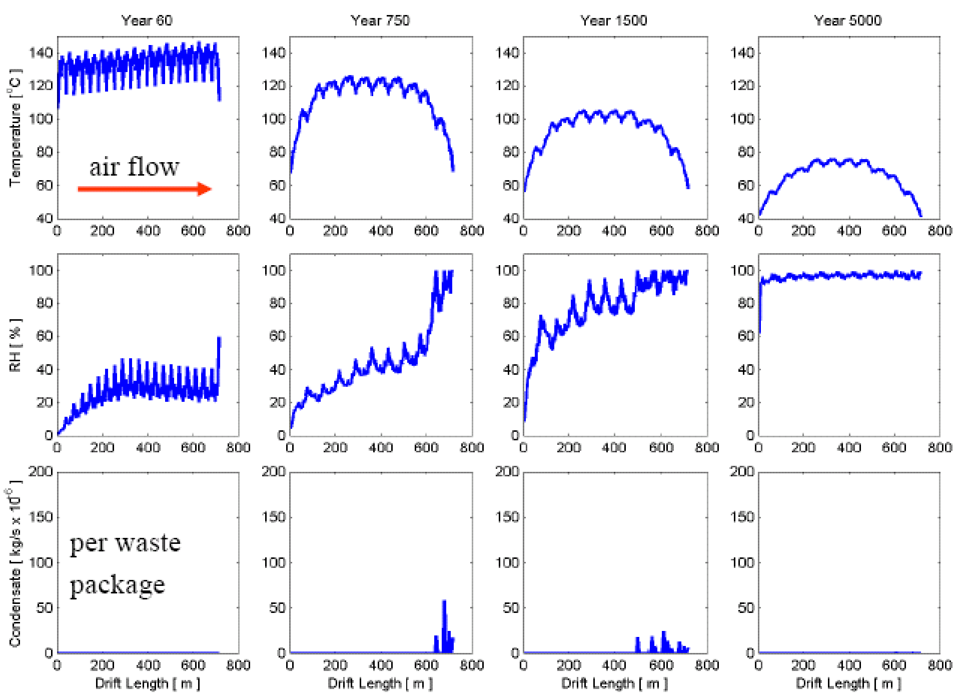

Air Infiltration: Low

Location: WP

In-Drift Model: CFD-Diffusive (Porous Media Emulation)

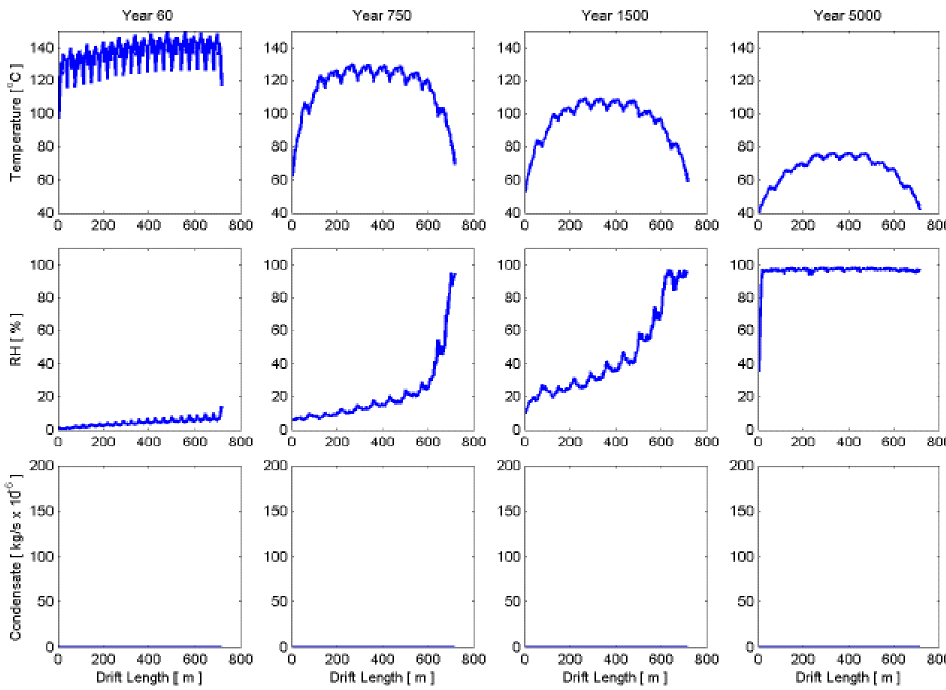

Air Infiltration: Low

Location: Drift wall

In-Drift Model: CFD-Convective

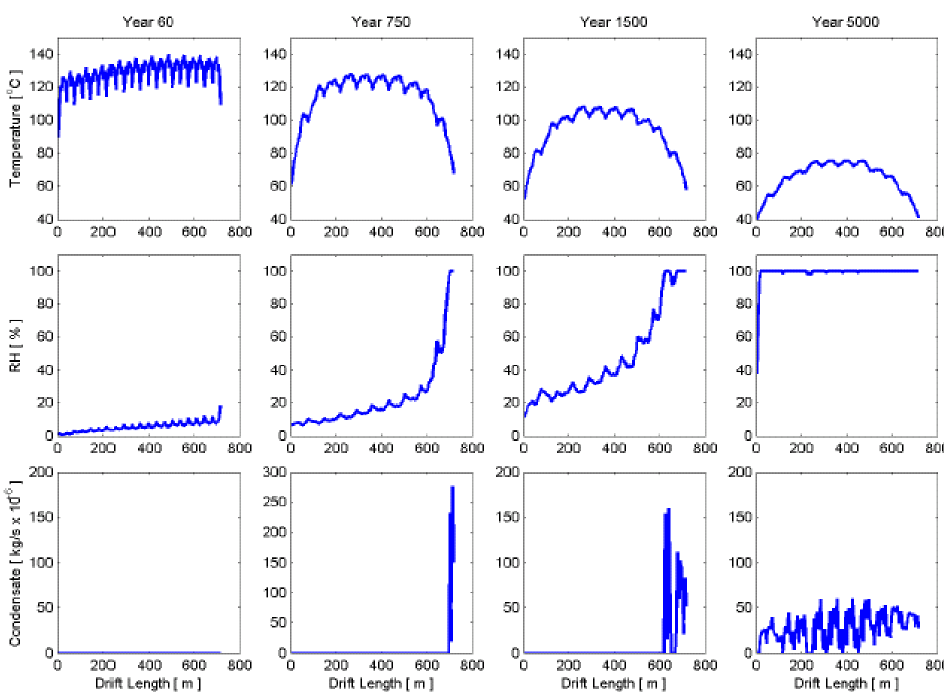

Air Infiltration: Balanced (best estimate of anticipated flow rate)

Location: WP

In-Drift Model: CFD-Convective

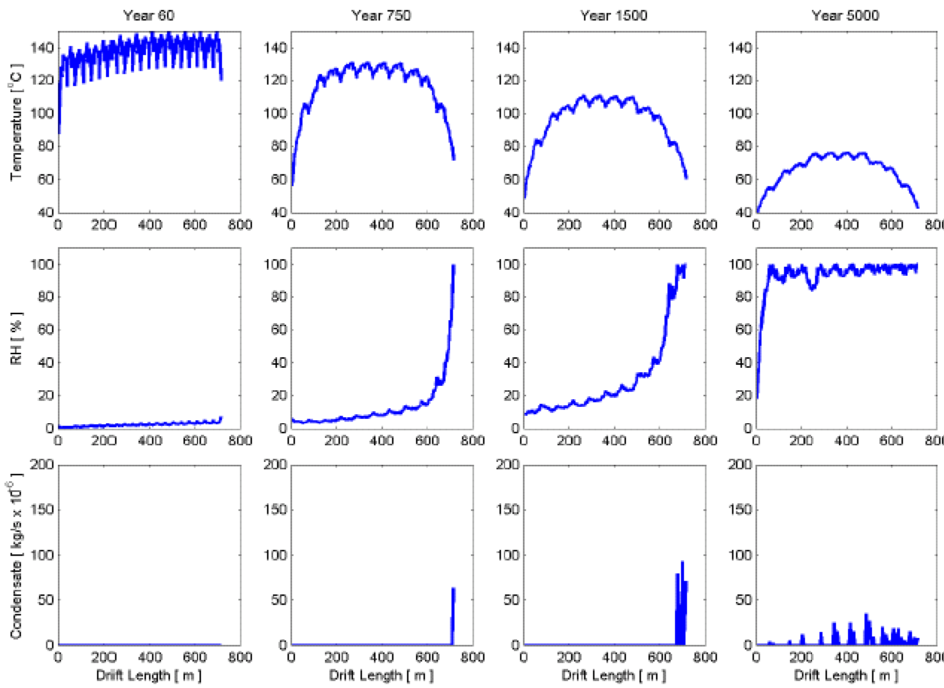

15 *Nye County Department of Natural Resources and Federal Facilities*

Air Infiltration: Balanced

Location: WP

In-Drift Model: CFD-Diffusive (Porous Media Emulation)

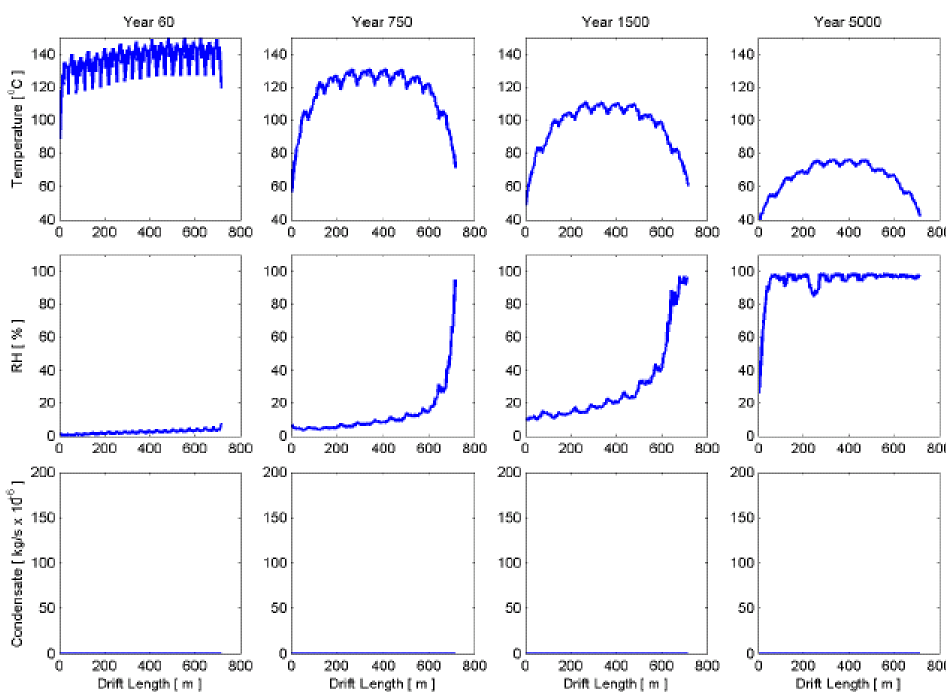

16 *Nye County Department of Natural Resources and Federal Facilities*

Air Infiltration: Balanced

Location: Drift wall

In-Drift Model: CFD-Convective

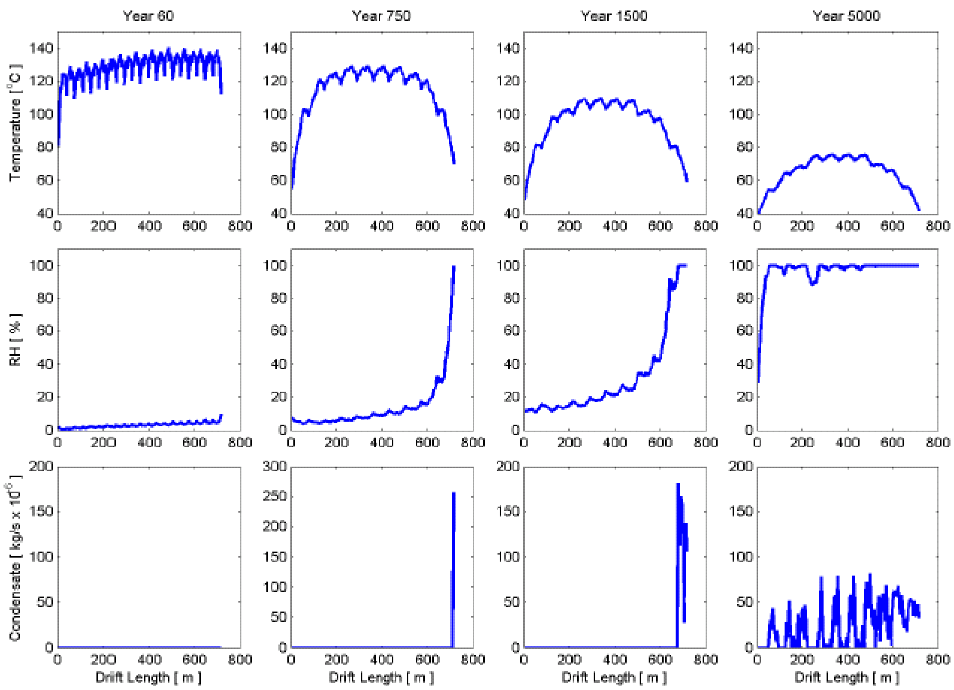

17

Air Infiltration: Medium

Location: WP

In-Drift Model: CFD-Convective

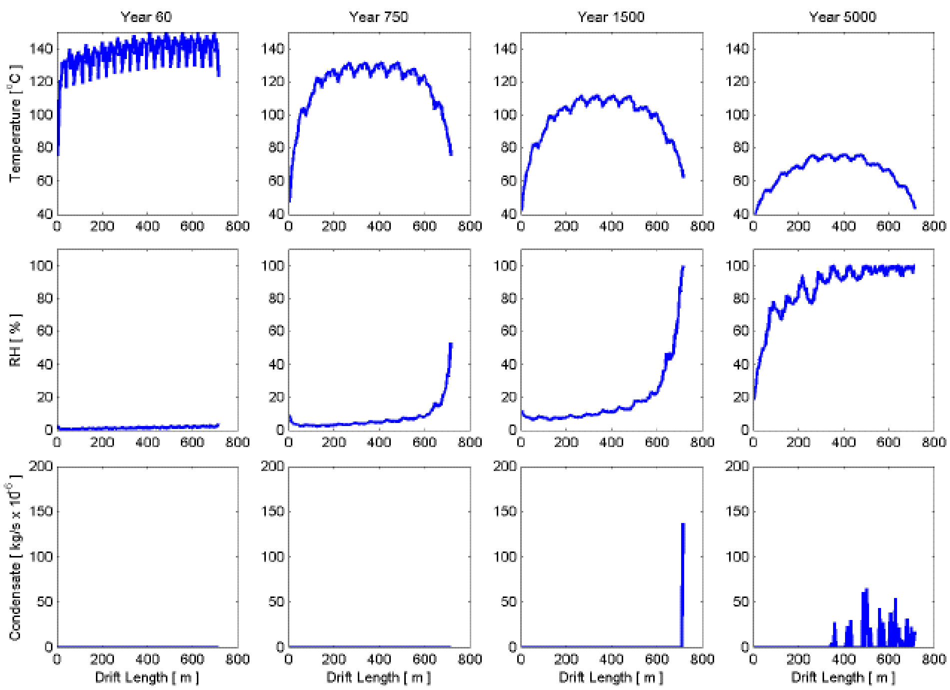

18

Air Infiltration: High

Location: WP In-Drift Model: CFD-Convective

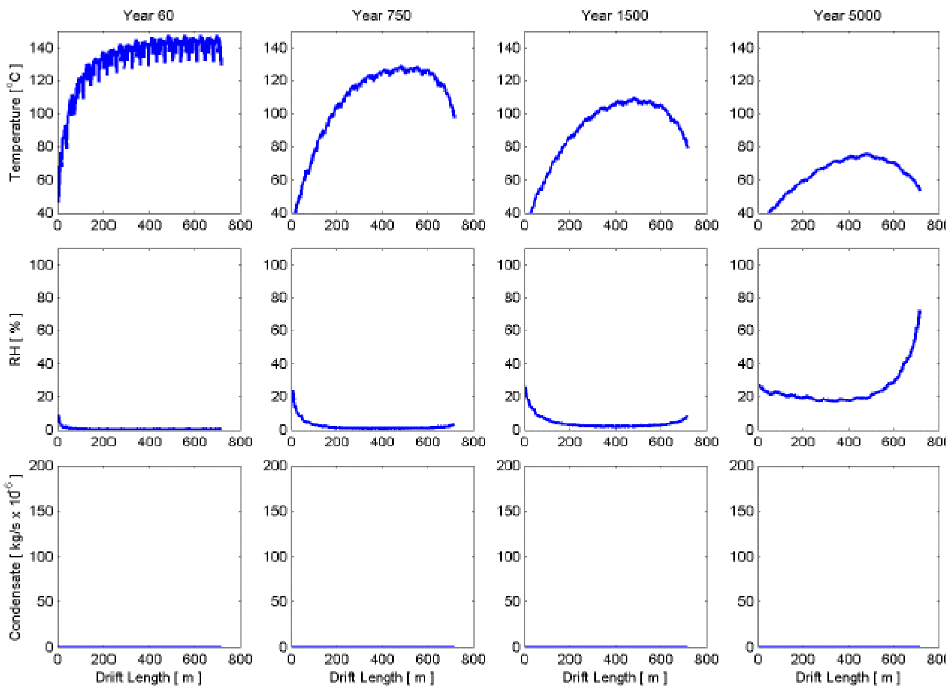

Relative Humidity and Condensate Formation

- Condensation predicted on downstream drift wall and waste packages.
- Condensation disappears at higher flow rates.
- Condensation decreases with decreasing maximum temperatures.
- Refined convective air flow pattern required to see correct condensate formation.
- Best viewed as engineering design challenge.

Summary

- Natural draft ventilation occurs with and without enhancement.
- Design changes will be needed to minimize condensation.
- Active and passive ventilation can be optimized to reduce condensation and lower average temperatures:
  - Run fans longer and/or faster?
  - Enhance natural ventilation?
  - Modify thermal loading?

Future Activities

- We will continue to contribute subject to funding constraints, with Nye County and UNR cooperation.
- Future studies:
  - How to eliminate condensation?
  - Effects of partial roof collapse with air movement above rubble.
  - Effects of cold repository design.
  - Effects of barometric pressure pumping.
  - Will condensate at drift wall drip or imbibe into rock?
  - Can WPs be compartmentalized with alternative emplacement design?
  - We are open to suggestions.